



INVESTMENTS IN EDUCATION DEVELOPMENT

VSB - Technical University of Ostrava



SPECIAL TESTING METHODS

A study support

Karel Matocha

Title: Special testing methods

Author: Karel Matocha

Issue: first, 2014

Number of pages: 160

Number of copies: -

Study documents for the study branch of Material Engineering, Faculty of Metallurgy and Material Engineering

Translation of the study support was funded by project

Operational Programme of Education for Competitiveness

Title: ModIn - Modular Innovation of the Bachelor's and Master's Programs at the Faculty of Metallurgy and Materials Engineering VŠB - TU Ostrava

No. CZ.1.07/2.2.00/28.0304

Implementation: VŠB – Technical University of Ostrava

The project is co-financed by the ESF and the state budget of Czech Republic

Ostrava, 2014

© Karel Matocha

VŠB – Technical University of Ostrava

Study Guide	7
1. Material properties of structural materials and methods for evaluation of mechanical properties	8
1.1 Division of properties of structural materials	8
1.2 Mechanical properties of metallic materials and their division	9
1.3 Types of tests of mechanical properties of metallic materials	10
2. Fundamentals of fracture mechanics	12
2.1 Introduction	12
2.2 Methods of loading of the body with a crack	13
2.3 Linear elastic fracture mechanics	15
2.3.1 Stress in a cracked body	15
2.3.2 Driving force of crack G	17
2.3.3 Crack growth resistance R	19
2.3.4 Plastic zone at the tip of the crack	21
2.3.5 Fracture toughness	24
2.4 Elasto-plastic fracture mechanics	25
2.4.1 Crack tip opening displacement δ (CTOD)	26
2.4.2 J-integral	27
2.4.3 Stable crack growth under uniaxial loading	28
3. Evaluation of fatigue characteristics of metallic materials	31
3.1. Introduction	31
3.2 The cyclic curve of stress – strain $\sigma_a - \epsilon_{apl}$	35
3.2.1 Stage of changes in mechanical properties	35
3.3 Life curve $\epsilon_{at} - N_f$ (Manson-Coffin curve)	36
3.4 Life curve $\sigma_a - N_f$ (Wöhler curve)	40
3.5 Evaluation of the resistance of the material to fatigue crack growth	42
3.5.1 Kinetics of fatigue crack growth in air	42
3.5.2 Effect of a corrosive environment on fatigue crack growth	46
4. Evaluation of fracture behaviour of metallic materials	54
4.1 Introduction	54
4.2 Philosophy of transition temperature	57
4.2.1 Impact bend test	57
4.2.2 Drop-weight test (DWT)	60
4.2.3 Drop-weight tear test (DWTT)	61
4.2.4 Impact bend test for large bodies (DT-dynamic tear)	64
4.3 Philosophy based of fracture mechanics	67
4.3.1 The general temperature dependence of fracture toughness	67
4.3.2 Plane-strain fracture toughness K_{IC}	72
4.3.3 Determination of fracture toughness in the transition region	73
4.3.3.1 Fracture toughness determined from the crack-tip opening displacement	74
4.3.3.2 Fracture toughness determined from J-integral	75
4.3.4 Determination of fracture toughness $\delta_{0,2}$ and $J_{0,2}$ using multi-specimen testing	77

4.3.5 Determination of the reference temperature T_0	80
5. Procedures for determining the creep characteristics of metallic materials	84
5.1 Definition of the concept of creep	84
5.2 Limit temperature T_g	85
5.3 Creep curve ϵ - t	86
5.4 Basic characteristics of the creep resistance of materials	87
5.5 Uniaxial creep testing of metallic materials in tension	88
5.5.1 The shape and dimensions of test specimens	91
5.6 Methods of extrapolating the results of creep testing	93
5.6.1 Graphical method of extrapolating the results of creep testing	93
5.6.2 Parametric methods of extrapolating the results of creep testing	95
5.6.2.1 Larson-Miller (L-M) parametric method	96
5.6.2.2 Sherby-Dorn (S-D) parametric method	98
5.6.2.3 Manson-Haferd (M-H) parametric method	99
5.6.2.4 Seifert method	101
5.6.2.5 SVÚM equation	101
5.7 Practical examples of the evaluation of creep test results using the parametric equations	102
6. Evaluation of resistance of structural steels to stress corrosion cracking in aqueous environments at temperatures from 23 to 300°C	109
6.1 Introduction	109
6.2 Mechanisms of stable crack growth in aqueous environments	112
6.2.1 Mechanism of hydrogen embrittlement	112
6.2.2 Mechanism of anodic dissolution	115
6.3 The procedure for evaluating the resistance of steels to stress corrosion cracking	117
7. Evaluation of resistance of steels to hydrogen embrittlement in environments containing hydrogen sulphide (H_2S)	120
7.1 Introduction	120
7.2 Basic types of degradation mechanisms in hydrogen sulphide environments	121
7.2.1 Hydrogen-induced cracking (HIC)	121
7.2.2 Sulphide stress cracking	123
7.2.3 Stress-oriented hydrogen-induced cracking	124
7.3 Procedures for evaluating the resistance of steels to HIC and against the concurrent action of tensile stress and hydrogen sulphide environment	125
7.3.1 Evaluation of the resistance of steels to hydrogen-induced cracking (HIC)	125
7.3.2 Evaluation of the resistance of steels against concurrent action of tensile stress and hydrogen sulphide environment	133
7.3.2.1 Method A – NACE Standard Tensile test	135

8. Evaluation of mechanical properties of structural steels using penetration

tests	142
8.1 Introduction	142
8.2 Principle of a penetration test	144
8.3 Ball penetration test (Bulge Punch Test)	145
8.4 CWA 15627 Small Punch Test Method for Metallic Materials	151
8.5 Procedure for performing time-independent penetration tests	152
8.6 Determination of mechanical characteristics from the results of penetration tests	158
8.6.1 Determination of the yield strength R_e ($R_{p,0.2}$) and the ultimate strength R_m of steel from the results of penetration tests	158
8.6.2 Determination of the transition behaviour of steel from the results of penetration tests	160
8.6.3 Estimation of the fracture toughness from the results of penetration tests	160
8.6.3.1 The two-stage method to determine K_{IC}	162
8.6.3.2 Direct estimation of the fracture toughness from the results of penetration tests	162
8.6.3.3 EPRI-FAA innovative approach to the estimate of the fracture toughness J_{IC}	167

Foreword

Study support to the subject *Special test methods* is intended for students in the second semester of master's degree combined studies in Advanced Technical Materials. It serves as a compensation for a significantly lower proportion of direct contact teaching, which makes this form of study much more difficult for students. It can, of course, be also used by full-time (daily) students for brushing-up the curriculum presented in lectures during the semester.

The aim of the subject is to broaden the knowledge on the evaluation of special material properties of structural materials and familiarize with the reasons which led to the development and implementation of methods for their evaluation.

After studying this support, a student will be able to characterize standard and non-standard test methods and procedures for determining the special fatigue characteristics of materials, special characteristics of the fracture behaviour of materials, the creep characteristics of the material, characteristics of stress corrosion cracking, characteristics of resistance to hydrogen induced cracking and methods for the assessment of the actual mechanical properties of long-term operating equipment from the results of penetration tests.

This support is divided into eight separate chapters. Most of them are divided into smaller units – subchapters. For the students to be able to easily approach the study of test methods and procedures for determining material characteristics based on linear and elastoplastic fracture mechanics, the second chapter is devoted to the foundations of this discipline.

When writing the text, we tried to maximize clarity in the interpretation of the subject matter. If reading of any of subchapters does not come sufficiently clear, we will appreciate if you notify us, the best thing on the e-mail address karel.matocha@vsb.cz or petr.jonsta@vsb.cz, so we can rearrange it.

An integral part of the support is the *Study Guide*, which describes how to work with the study support.

Study Guide

Basic learning units are chapters and subchapters.

- Read the presentation of the entire chapter.
- Check the summary of terms.
- Look at the questions and try to formulate answers to them.
- Then proceed to tasks to solve.

If you have any problems with which you need help, please contact teachers whose email addresses are listed in the preface.

Within their semester thesis, students will process the results of experiments in special tests in the field of fatigue, fracture behaviour and creep of the structural materials in the form of test reports. Before the exam itself, all students are required to pass a midterm test.

1. Material properties of structural materials and methods for evaluation of mechanical properties



Study time: 0.5 hour



Objective

After reading this chapter, you should be able to:

- **List the properties of structural materials.**
- **Define special mechanical properties.**
- **List the types of tests of mechanical properties of structural materials.**



Presentation

1.1 Division of properties of structural materials

Properties of structural materials can be divided into:

1. mechanical properties,
2. physical properties,
3. chemical properties, and
4. technological properties.

Mechanical properties (yield strength $R_{p,0.2}$ (R_e), ultimate strength R_m , ductility A , contraction Z , fracture toughness K_{IC} , FATT, notch impact strength KCV, creep rupture strength $R_{mT/t/T}$, etc.) are properties of structural materials, which determine their suitability for the intended function and use in practice. Knowledge and improvement of mechanical properties of structural materials is motivated by their optimal use in the manufacture of components.

Among the physical properties belong tensile modulus E , or shear modulus G [MPa], linear and volume expansion, density ρ [kg/m^3], thermal conductivity λ [W/mK], electrical conductivity G [S], electrical resistivity ρ [$\Omega\cdot\text{m}$], permeability $\mu = B/H$ [H/m], where B is the magnetic induction and H is the intensity of the external magnetic field.

Chemical properties reflect the behaviour of structural materials in wet environments, and their resistance to acids and gases. The most important chemical property of metals is the corrosion resistance.

Technological properties of structural materials include formability, weldability, castability, machinability and wear resistance.

1.2 Mechanical properties of metallic materials and their division

Results of the evaluation of mechanical properties of structural materials can be used for:

- 1) Selection of a suitable material at the design stage.
- 2) Control of production.
- 3) Study of the influence of chemical composition, heat treatment, technology of manufacture, temperature and environment on the material properties, therefore, for the purposes of research and development.
- 4) Assessment of degradation of the material properties by long-term operation of the equipment, assessment of defects such as cracks, or estimates of residual life of structures and analysis of the causes of structures failure.

Increasing the useful properties of products requires, inter alia, the dissemination of knowledge about the basic and special mechanical properties of the materials used and the related development and implementation of new test methods. Mechanical properties are divided into basic and special. This division is based on the following reasons.

Basic mechanical properties reflect the general requirements for the material quality and are therefore mostly referred to in data sheets. They are quantitatively expressed by means of material characteristics, such as ultimate (breaking) strength R_m , yield strength R_{eH} , $R_{p0.2}$, ductability A , contraction Z , hardness H , and notch impact strength (toughness) KCV. They do not therefore relate to a specific type of fracture process (limit state of material).

Special mechanical properties are directly related to a specific type of fracture process (limit state of material) and are part of the specific technical conditions. By far the most

common and most important engineered limit state, representing around 80% of operating fractures, is a fatigue fracture, or a fracture caused by corrosion fatigue. Other major limit states include fragile, i.e. sudden unstable fracture, creep fracture and fracture induced by corrosion cracking. The special mechanical properties include fatigue limit σ_c , fracture toughness K_{IC} , corrosion rate and more.

1.3 Types of tests of mechanical properties of metallic materials

In terms of the force applied on a specimen, we divide mechanical tests into:

- 1) Static tests in which the load is constant (creep tests) or the load is increased rather slowly (tensile tests, static fracture toughness tests). It works usually several minutes; in long-term tests days, even years.
- 2) Dynamic impact and cyclic tests, in which a force is applied abruptly during the fraction of a second. During cyclic tests (fatigue tests), the variable load repeats in many cycles per second up to many millions of their total number.

According to the temperatures at which the tests are performed, we divide them into tests at room temperature and testing at elevated and reduced temperatures. To guarantee the reproducibility of results from different test centres and laboratories, the test procedures for determining the mechanical properties are standardized.

In particular, the qualitative changes in design philosophy from design concept of a safe life (safe-life) to the concept of safe construction even in the presence of a damage (damage tolerance) led to the development of many new testing methods especially in the evaluation of stable crack growth and fracture behaviour of steels. These methods will be devoted much attention to in the following chapters.



Summary of terms

After studying the chapter, following terms should be clear to you:

- **Properties of structural materials.**
- **Special mechanical properties.**
- **Static mechanical tests.**
- **Dynamic mechanical tests.**

Questions about the curriculum learnt:

- 1) What properties of structural materials do you know?
- 2) What material properties rank among the physical properties?
- 3) What is expressed by the chemical properties of the material?
- 4) How we divide the mechanical properties of structural materials?
- 5) What are the results of the evaluation of mechanical properties of structural materials used for?
- 6) What are the basic mechanical properties?
- 7) What are the special mechanical properties?
- 8) What kinds of tests of mechanical properties do you know?



Tasks to solve

Try to define, what the difference between basic and special mechanical properties is.

2. Fundamentals of fracture mechanics



Study time: 2 hours



Objective: After reading this chapter, you should be able to:

- Explain the difference between linear and elastoplastic fracture mechanics.
- List the possible ways of loading the body with a crack.
- Define the concept of stress intensity factor K .
- Define the concept of crack driving force G .
- Define the concept of resistance to crack growth R .
- Define the concept of a plastic zone.
- Explain the difference between a state of plane strain and state of plane stress.
- List the parameters used to express the fracture toughness of elastoplastic fracture mechanics.



Presentation

2.1 Introduction

Significant technological advances that occurred in the 19th and 20th centuries were accompanied by a growing number of accidents of huge structures and machinery (steel bridges, gas storage tanks, boilers, etc.) by a sudden unstable failure. A significant increase in the number of these accidents occurred at a time of significant application of large welded structures from the 40's of the last century. During a World War Two about 2,700 ships of Liberty class were produced – first large structures made by welding. Approximately every seventh ship was broken by a sudden unstable (brittle) failure (see Fig. 2.1) outside of combat action. Analysis of the causes of these accidents have shown that sudden unstable (brittle) failures were initiated from crack-like defects in welds and most of the materials have shown

low notch toughness at working temperatures. Generally, the crack-like defects in the equipment may occur as a result of:

- 1) technological operations during production (e.g. by welding). These defects are present in the device before it is put into operation,



Fig. 2.1 Sudden unstable failure of a welded Liberty-class ship

- 2) operational stress and the environment. These defects are initiated during operation mainly on the stress concentrators.

Patters of occurrence of sudden unstable fractures in components with cracks are dealt within the discipline of science, which originated in the 60's of the last century and was called the fracture mechanics. Currently there are two basic concepts:

- 1) LEFM (Linear Elastic Fracture Mechanics) based on the validity of a linear relationship between stress and strain under load. It is used mainly for brittle materials.
- 2) EPFM (Elastoplastic Fracture Mechanics), which is used for materials in which extensive plastic deformation arises when loaded near the defect face.

2. 2. Methods of loading the body with a crack

The crack with length a located in the body (see Fig. 2.2) can be loaded in three different ways (see Fig. 2.3). These three modes marked I, II, and III differ in orientation of the external load acting on the body relative to the plane and face of the crack.

When loading the crack by tensile load (Mode I), the tensile load acts perpendicular to the plane of the crack. When loading the crack by shear load in the plane of the crack (Mode II), the displacement takes place of the fracture surfaces in the plane of the crack and perpendicular to the face of the crack. Crack growth is driven by a shear component of the stress τ_{yx} . Loading the crack by an antiplane shear (Mode III) leads to displacement of the fracture surfaces in the plane of the crack, but parallel with the face of the crack. Crack growth is driven by a shear component of the stress τ_{yz} . In terms of common engineering practice, the tensile mode I is the most important.

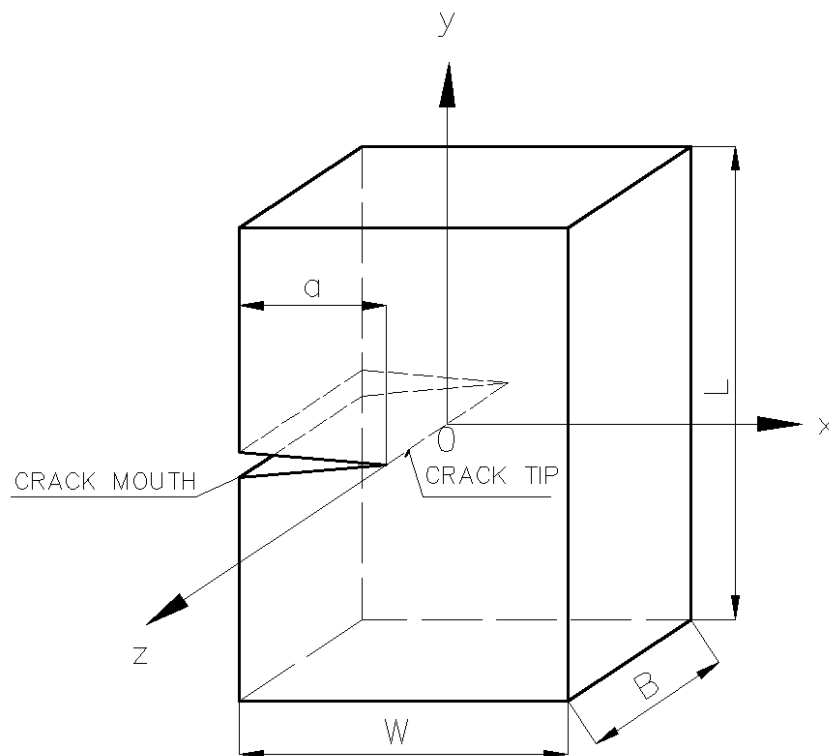


Fig. 2.2 Body of width W , thickness B , with a crack of length a

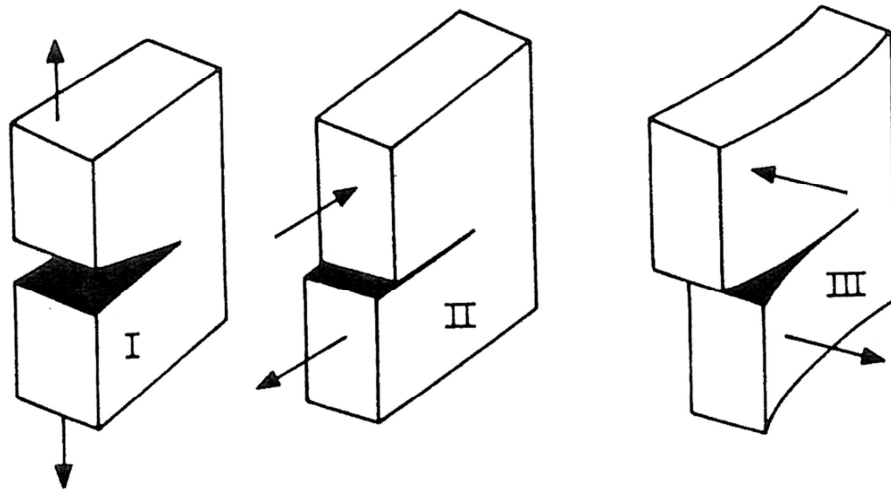


Fig. 2.3 Three types of load, or failure of a cracked body

2.3 Linear elastic fracture mechanics

2.3.1 Stress in a cracked body

Consider an infinitely wide plate with a crack of length $2a$ loaded by uniaxial tension (Mode I) (see Fig. 2.4). The element of surface of the plate $dx \cdot dy$ is loaded at a distance r from the tip of the crack, tilted by an angle θ from the plane of the crack, by normal stresses σ_x and σ_y , and by shear stress τ_{xy} that can be expressed in the form:

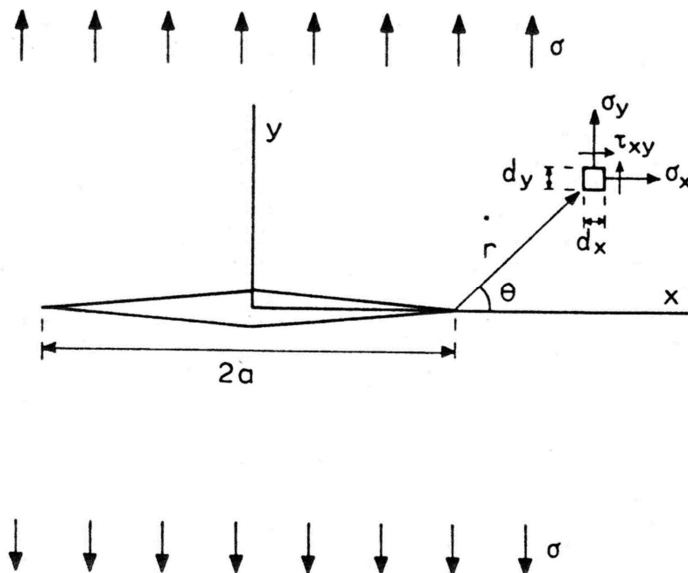


Fig. 2.4 Crack of length $2a$ in an infinitely wide plate under tensile stress σ

$$\sigma_x = \sigma \sqrt{\frac{a}{2r}} \cos \frac{\theta}{2} \left[1 - \sin \frac{\theta}{2} \sin \frac{3\theta}{2} \right]$$

$$\sigma_y = \sigma \sqrt{\frac{a}{2r}} \cos \frac{\theta}{2} \left[1 + \sin \frac{\theta}{2} \sin \frac{3\theta}{2} \right] \quad (2.1)$$

$$\tau_{xy} = \sigma \sqrt{\frac{a}{2r}} \sin \frac{\theta}{2} \cos \frac{\theta}{2} \cos \frac{3\theta}{2}$$

$\sigma_z = 0$ for the state of plane stress

$\sigma_z = \nu \cdot (\sigma_x + \sigma_y)$ for the state of plane strain

Stress components σ_x , σ_y , τ_{xy} are proportional to the external tensile stress σ and the square root of crack length a . Their size around the tip of the crack is approaching infinity. Figure 2.5 shows the dependence of stress σ_y on r for $\theta = 0$. Since for large r the stress $\sigma_y \rightarrow 0$ instead of $\sigma_y = \sigma$, the above equations are valid only near the tip of the crack. The equations for individual components of the elastic stress can be rewritten as:

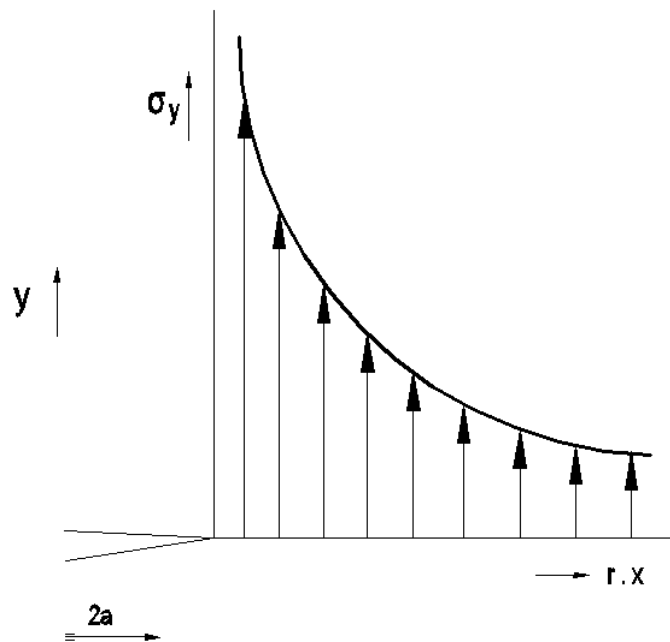


Fig. 2.5 Dependence of stress σ_y on the distance from the tip of the crack

$$\sigma_{ij} = \frac{K}{\sqrt{2\pi r}} \cdot f_{ij}(\theta) \quad (2.2)$$

Where
$$K = \sigma \cdot \sqrt{\pi \cdot a} \quad (3.2)$$

The parameter K is the so-called “stress intensity factor” [MPa]. Stress intensity factor K describes the state of stress at the crack tip. For finite-width bodies then apply

$$K = \sigma \cdot \sqrt{\pi \cdot a} \cdot f\left(\frac{a}{W}\right) \quad (4.2)$$

The dependence between the stress intensity factor K, body dimension W and crack length a is called K-calibration. Two cracks, the first of size 4a and the second of size a have the same stress field at the tip of the crack, when the first crack is under tensile stress σ and the second crack is under tensile stress 2σ . In this case, the stress intensity factor K is the same for both cracks.

2.3.2 Crack driving force G

When loading an ideal elastic body with a crack, the dependence between the applied force and displacement is rectilinear on the basis of Hooke's law (see Fig. 2.6).

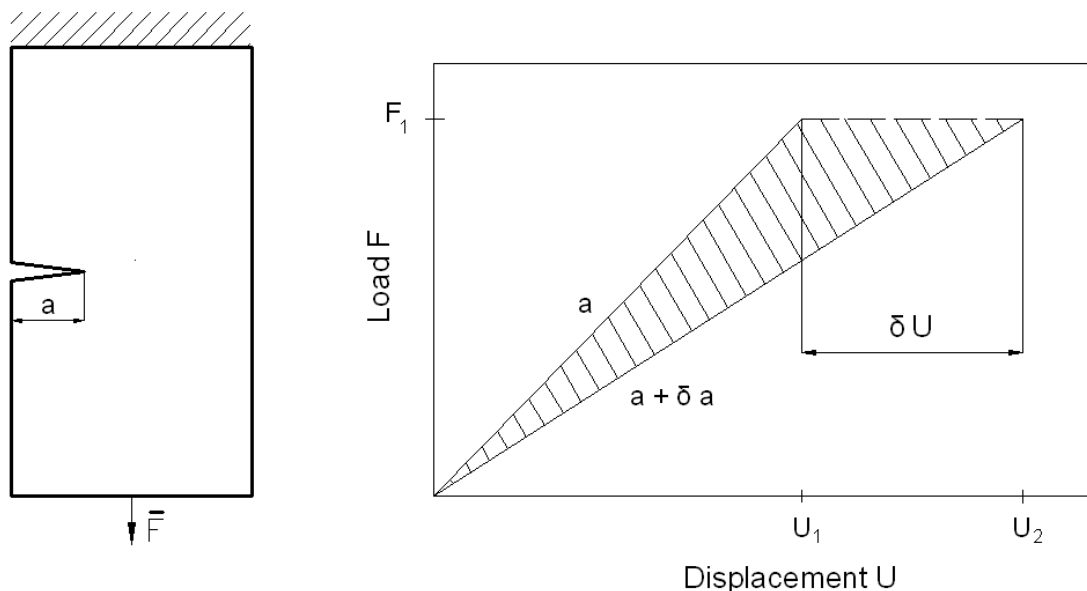


Fig. 2.6 Dependence of load - displacement of the body with a crack for the increase of the crack length at a constant force (soft loading mode)

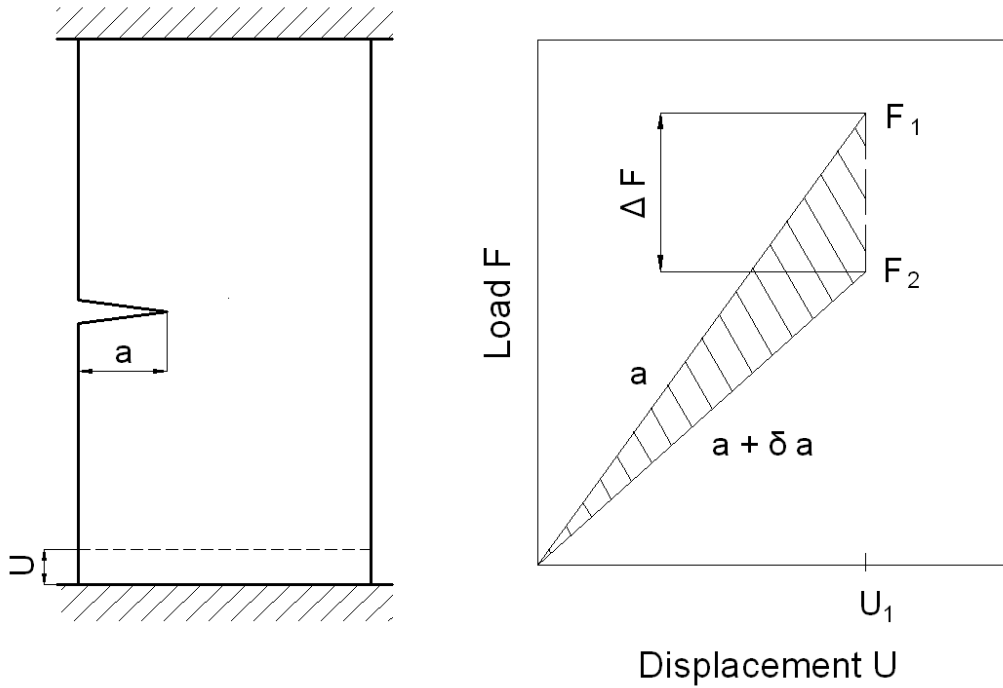


Fig. 2.6b Dependence of load – displacement of the body with a crack for the increase of the crack length at a constant displacement (hard loading mode)

The slope of the line may be defined by introduction of the so-called “compliance” C , which is defined as a displacement corresponding to the unit of force. It is therefore the inverse of the stiffness of the body. Generally, it is therefore possible to write

$$U = C \cdot F \quad (5.2)$$

Due to the change of crack length a by δa to $a + \delta a$ at a constant force, elastic energy dE is released

$$dE = \frac{1}{2} \cdot F_1 \cdot \delta U \quad (6.2)$$

Because

$$\delta U = F_1 \cdot \left(\frac{dC}{da} \right) \cdot da \quad (7.2)$$

$$dE = \frac{1}{2} \cdot F_1^2 \cdot \left(\frac{dC}{da} \right) \cdot da \quad (8.2)$$

and the rate of energy release, i.e. the crack driving force is equal to

$$\left(\frac{dE}{da} \right)_{F=\text{konst.}} G = \frac{1}{2} \cdot F_1^2 \cdot \left(\frac{dC}{da} \right) \quad (9.2)$$

For body with thickness B then applies that

$$(G)_{F=konst.} = \frac{1}{2} \cdot \left(\frac{F_1^2}{B} \right) \cdot \left(\frac{dC}{da} \right) \quad (10.2)$$

Also in the case of hard loading mode (constant position of clamping jaws $U = \text{constant}$) the change of crack length by δa leads to the elastic energy release dE

$$dE = \frac{1}{2} \cdot U_1 \cdot dF \quad (11.2)$$

Whereas, in this case

$$dU = 0 = dC \cdot F_1 + \left(\frac{U}{F_1} \right) \cdot dF \quad (12.2)$$

$$\left(\frac{dE}{da} \right)_{U=konst.} \cdot G = \frac{1}{2} F_1^2 \cdot \left(\frac{dC}{da} \right) \quad (13.2)$$

The crack driving force is thus alike for both loading cases.

From the stress and displacement at the crack face, Irwin derived the relationship between the crack driving force G and the stress intensity factor K for the state of plane stress in the form

$$G = \frac{K^2}{E} \quad (14.2)$$

For the state of plane strain it applies that

$$G = (1 - \nu^2) \cdot \frac{K^2}{E} \quad (15.2)$$

2.3.3 Crack growth resistance R

The crack growth occurs when the following condition is met

$$G = R \quad (16.2)$$

For the case of an ideal brittle material and in cases where it is possible to speak about the state of plane strain, the crack growth resistance can be considered to be constant (see Fig. 2.7). Crack driving force increases linearly with the length of the crack (see equations (14), (15)). If the stress is at level σ_1 , no sudden unstable crack growth occurs, because for a crack of length a_0 the crack driving force G at this stress level is less than the crack growth

resistance R . The sudden unstable crack growth occurs only at stress σ_2 , when the crack driving force reaches the level of resistance to crack growth R .

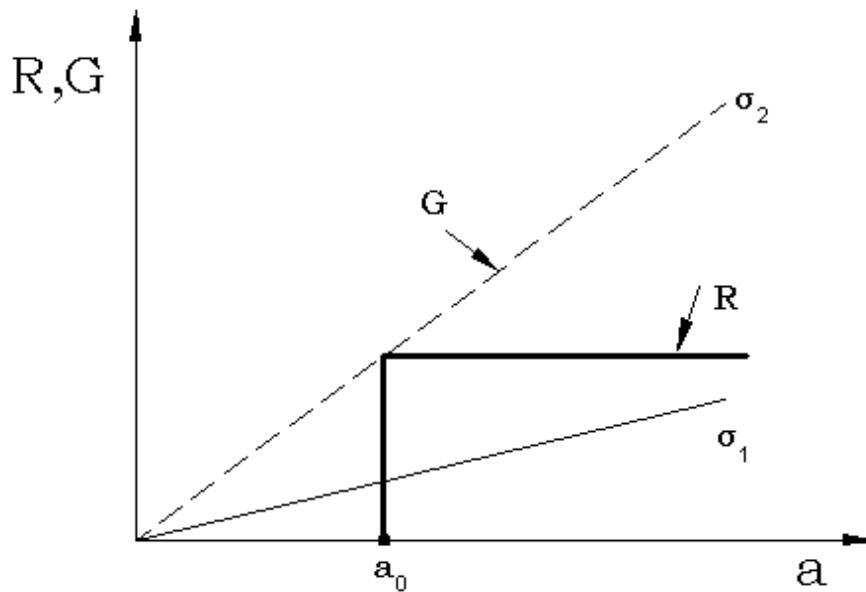


Fig. 2.7 Dependence of the crack growth resistance R on the length of crack a for brittle material and state of plane strain

For the cases of plane stress or large plastic deformation at the tip of the crack, the resistance to crack growth increases with the crack length (see Fig. 2.8).

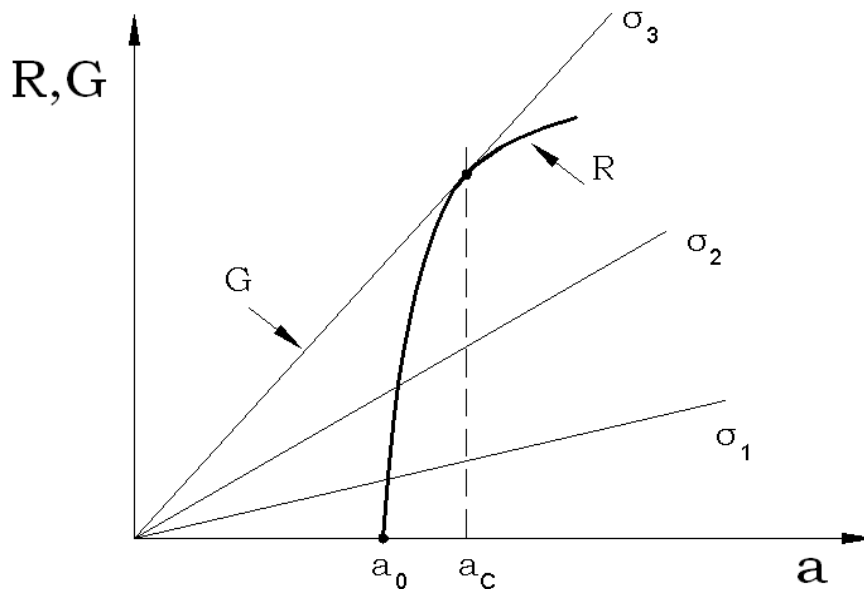


Fig. 2.8 Dependence of the crack growth resistance R on the length of crack a for the state of plane stress and for cases of large plastic deformation at the tip of the crack

Stable ductile crack growth occurs when the crack driving force reaches the threshold. Stable crack growth occurs at stress σ_2 , since $G = R$ and at the same time

$$\frac{dG}{da} \leq \frac{dR}{da} \quad (17.2)$$

In the moment when the line of the crack driving force becomes tangent to the curve of crack growth resistance R , a sudden unstable crack growth occurs, because

$$\frac{dG}{da} \geq \frac{dR}{da} \quad (18.2)$$

2.3.4 Plastic zone at the tip of the crack

Equation (2) assumes a linear relationship between the stress and strain. In fact, there is a plastic deformation at the tip of the crack, which results in a stress drop to the level of yield strength $R_{p,0,2}$ (see Fig. 2.9).

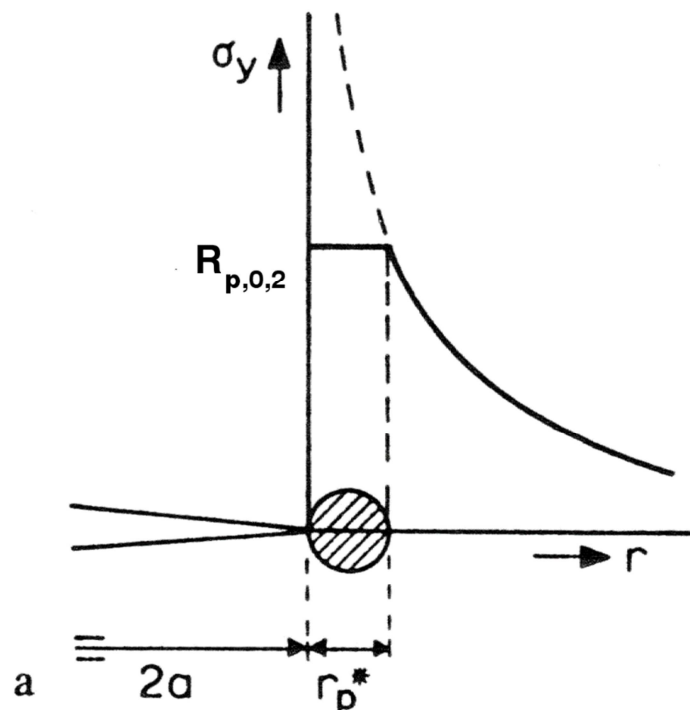


Fig. 2.9 Size of the plastic zone in the plane of the crack based on the assumption of a linear relationship between the stress and strain

Size of plastic zone r_p^* in the plane of the crack for the state of plane stress can then be expressed as

$$r_p^* = \frac{K_I^2}{2 \cdot \pi \cdot (R_{p0,2})^2} = \frac{\sigma^2 \cdot a}{2 \cdot R_{p0,2}^2} \quad (19.2)$$

For the state of plane strain we get the size of the plastic zone in the plane of the crack from the elastic stress distribution ahead of crack face in the form

$$r_p^* = \frac{K_I^2}{2 \cdot \pi \cdot (R_{p0,2})^2} \cdot (1 - 2\nu)^2 \quad (20.2)$$

The estimated size of the plastic zone is not completely correct. Due to the plastic deformation of the material in the area around the crack tip, the stress redistribution takes place (see Fig. 2.10).

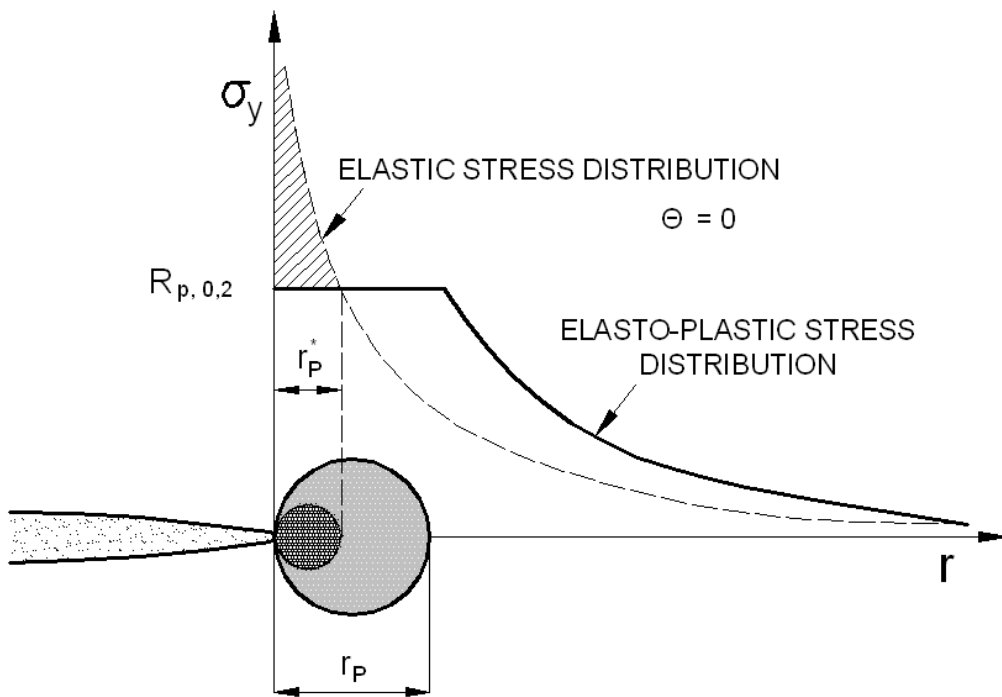


Fig. 2.10 Size of the plastic deformation in the plane of the crack considering the stress redistribution due to plastic deformation

The size of the plastic zone in the plane of the crack is in this case for the state of the plane stress equal to

$$r_p = \frac{K_I^2}{\pi \cdot (R_{p0,2})^2} \quad (21.2)$$

For the state of plane strain it is equal to

$$r_p = \frac{K_I^2}{6\pi \cdot (R_{p0,2})^2} \quad (22.2)$$

Until now it was assumed for simplicity reasons that the plastic zone has a circular shape. A more accurate expression of the shape of the plastic zone can be obtained by analysing the conditions of the beginning of plastic deformation for angles $\theta \neq 0$. For the beginning of plastic deformation we use either Treska (plastic deformation occurs when $\tau_{\max.} = R_{p0,2}/2$) or Von Mises criterion, which defines the beginning of plastic deformation by following relationship

$$(\sigma_1 - \sigma_2)^2 + (\sigma_2 - \sigma_3)^2 + (\sigma_3 - \sigma_1)^2 = 2 \cdot R_{p0,2}^2 \quad (23.2)$$

where $\sigma_1, \sigma_2, \sigma_3$ are normal stresses. As stated above, the size of the plastic zone depends on the state of stress. On the surface of the body, there is always the state of plane stress and towards the centre of the body the size of the plastic zone decreases from the size corresponding to the state of plane stress to the size corresponding to the state of plane strain (see Fig. 2.11).

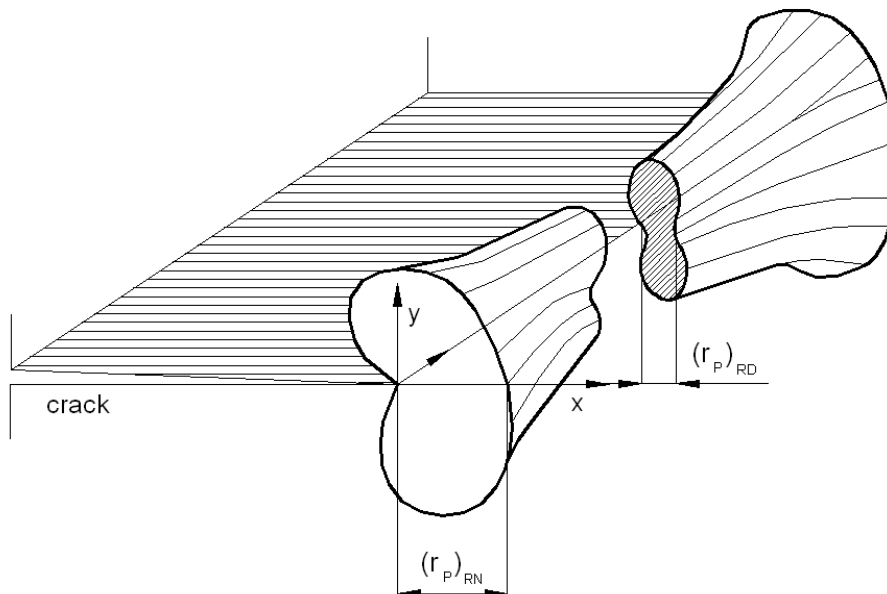


Fig. 2.11 The shape of the plastic zone in a cracked body

2.3.5 Fracture toughness

The crack becomes unstable when the stress intensity factor reaches its critical value K_C . If the assumptions for linear elastic fracture mechanics are to be met, the size of plastic zone at the tip of the crack must be small (<2% of the size of the body thickness) in the moment of the fracture occurrence.

The critical value of the stress intensity factor K_C depends on the thickness of the body. It decreases with increasing thickness of the body, and with sufficiently large thicknesses of the body it is approaching the limit value marked K_{IC} - plane strain fracture toughness (see Fig. 2.12).

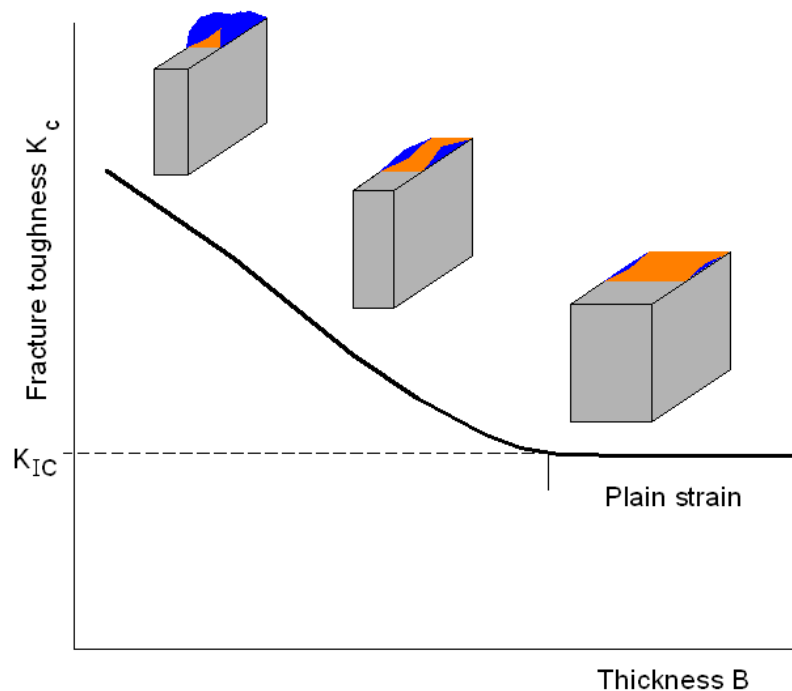


Fig. 2.12 Effect of the body thickness on the fracture toughness K_C

The value of K_C can be considered as $K_C = K_{IC}$, if the condition

$$B \geq 2,5 \left(\frac{K_C}{R_{p0,2}} \right)^2 \quad (24.2)$$

is met.

Fracture toughness of a material depends on:

- 1) Temperature
- 2) Rate of deformation
- 3) Environment

The lower the yield strength $R_{p0,2}$ of the material, the higher the fracture toughness. With decreasing temperature the fracture toughness of steel with BCC (body-centered cubic) lattice structure decreases.

2.4 Elastoplastic fracture mechanics

To determine the fracture toughness of ductile materials, it is usually not possible (with the exception of very low temperatures, respectively high strain rates) to use linear fracture mechanics and therefore valid values of K_{IC} cannot be determined. To describe the fracture behaviour of materials, in which a time-independent plastic deformation occurs before the breach, the elastoplastic fracture mechanics is used. When loading the body, the crack faces separate before the fracture occurs and the initially sharp crack tip becomes blunt (see Fig. 2.13).

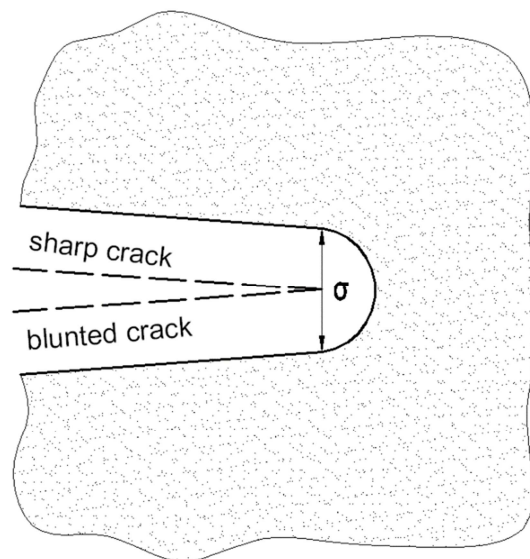


Fig. 2.13 Blunting of the initially sharp crack during loading the body made of a ductile material

The crack opening size δ increases proportionally with the ductility of the material. Two parameters are currently used to express the fracture toughness in elastoplastic fracture mechanics:

1. crack tip opening displacement δ (CTOD)
2. J-integral

These parameters each describe the conditions at the crack tip in elastoplastic material and can be used as fracture criteria. Fracture toughness is expressed through a critical crack opening δ and critical value of J-integral J_c .

2.4.1 Crack tip opening displacement δ (CTOD)

The principle of this concept is based on the assumption that an unstable crack growth occurs when the crack opening at its tip reaches (at a selected temperature, thickness of the body and rate of loading) critical value δ_c . CTOD value in the linear elastic fracture mechanics can be expressed as

$$\delta = \left(\frac{K^2}{m \cdot R_{p0,2} \cdot E} \right) \quad (25.2)$$

where m is a dimensionless constant approximately equal to $m = 1.0$ for the state of plane stress and $m = 2.0$ for the state of plane strain. The concept of crack opening is however intended primarily for cases where the conditions of linear elastic fracture mechanics are not met at the crack tip (SSY – small scale yielding). In the elastoplastic fracture mechanics the crack opening δ can be expressed as

$$\delta = \delta_{le} + \delta_{pl} = \frac{(1 - \nu^2)}{2 \cdot E \cdot R_{p0,2}} \cdot K^2 + \frac{V_p \cdot r_p (W - a)}{r_p (W - a) + a} \quad (26.2)$$

where

V_p is a plastic component of the notch opening measured by a clip gage at the loading axis

r_p is a rotation factor whose value depends on the type of specimen.

Stress intensity factor corresponding to the critical size δ_c can be expressed in the form

$$K_{\delta_c} = \sqrt{\frac{2 \cdot E \cdot R_{p0,2}}{1 - \nu^2}} \cdot \delta_c \quad (27.2)$$

2.4.2 J- integral

The potential energy of a body with a crack is generally the difference between the impact of external forces acting on the body and the elastic strain energy of the body. Rice has demonstrated that J-integral represents the change in the potential energy of a body depending on the length of the crack a (see Fig. 2. 14).

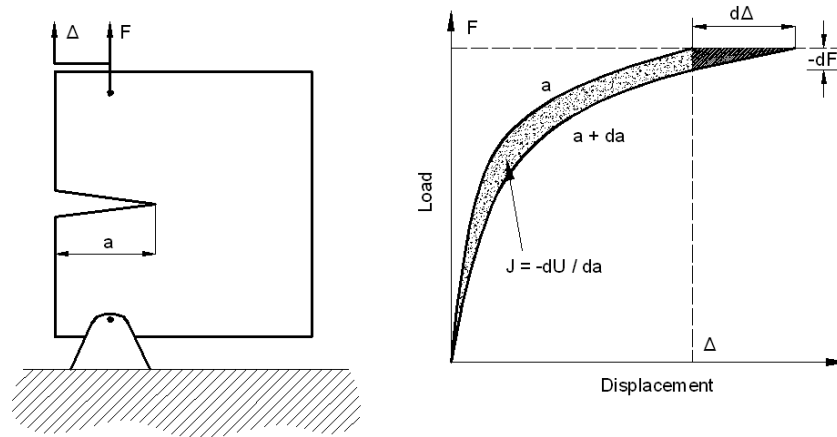


Fig. 2.14 Change in the potential energy when the crack length changes by da

$$J = - \frac{dU}{da} \quad (28.2)$$

This relationship is formally the same as that for the crack driving force G (strain energy release rate) (see equation (9)). In the field of linear elastic fracture mechanics, J-integral can be expressed as

$$J = \frac{K^2}{E} \quad (29.2)$$

for the state of plane stress and as

$$J = \frac{(1 - \nu^2)}{E} \cdot K^2 \quad (30.2)$$

for the state of plane strain. The relationship between J-integral and crack opening can then be described by the equation

$$J = m \cdot R_e \cdot \delta \quad (31.2)$$

where $m = 1$ for the state of plain stress and $1 < m < 3$ for the state of plane strain.

2.4.3 Stable crack growth under uniaxial loading

The previous chapters were devoted to the conditions of initiation of an unstable fracture in terms of linear and elastoplastic fracture mechanics. For a material with high toughness no sudden unstable fracture occurs, but the initiation and growth of a ductile crack. In this case, the fracture behaviour is characterized by J - R curve (J - Δa dependence) or δ - R curve (see Fig. 2.15)

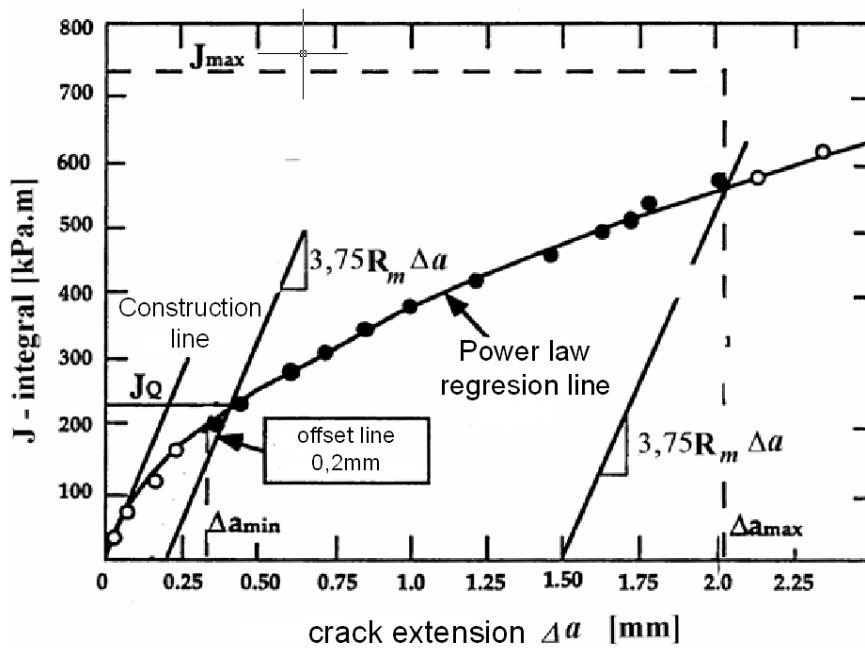


Fig. 2.15 J – R curve determined by a multi-specimen method



Summary of terms: After studying the chapter, following terms should be clear to you:

- Linear elastic fracture mechanics.
- Elastoplastic fracture mechanics.
- Mode I, II, III of loading the body with a crack.
- Crack driving forces.
- Plastic zone.
- State of plane stress.

- State of plane strain.
- Fracture toughness K_{IC}
- Crack opening δ
- J–integral
- J – R curve

Questions

- 1) What is the linear elastic fracture mechanics based on?
- 2) What materials is the elastoplastic fracture mechanics used for?
- 3) Which of the modes of loading is the most important for practice?
- 4) What does the stress intensity factor K express?
- 5) What do we mean by the crack driving force?
- 6) What do we mean by resistance to crack growth R ?
- 7) When the sudden unstable crack growth occurs?

- 8) What determines the size of a plastic zone?
- 9) What determines the fracture toughness K_{IC} of the material?
- 10) What parameters expressing the fracture toughness of the material in the elastoplastic fracture mechanics do you know?
- 11) What is J - R curve?



Tasks to solve

- Calculate the critical length of crack a_c for an infinitely wide plate under tensile stress $\sigma = 100$ MPa and made of a material having fracture toughness $K_C = 60$ MPa.m^{1/2}.
- Calculate the critical stress for the formation of a sudden unstable fracture of an infinitely wide plate with a crack length of $2a = 20$ mm made of a material having fracture toughness $K_C = 80$ MPa.m^{1/2}.
- Calculate the size of a plastic zone in cases of plane stress and plane strain for the stress intensity factor $K_I = 60$ MPa.m^{1/2} and material yield strength $R_{p,0.2} = 900$ MPa for the case where there is the redistribution of stress in the area around the crack tip.
-



References

- [1] BROEK, David: Elementary engineering fracture mechanics. 3rd revised edition 1982, 2nd printing 1983, Martinus Nijhoff Publishers, The Hague, ISBN 90-247-2656-5.
- [2] VLK, Miloš-FLORIAN, Zdeněk: Mezní stavy a spolehlivost. VÚT Brno, Fakulta strojního inženýrství, Ústav mechaniky těles, mechatroniky a biomechaniky, Brno 2007.
- [3] HOLZMANN, Miroslav- KLESNIL, Mirko: Křehký a únavový lom

materiálů a konstrukcí. 1. vydání. Praha, SNTL, 1972. 208s.

- [4] KUNZ, Jiří: Aplikovaná mechanika kontinua II. Základy lomové mechaniky. 1. vydání. Praha, ČVUT Praha, 1991, 110s.

3. Evaluation of fatigue characteristics of metallic materials



Study time: 2 hours



Objective: After reading this chapter, you should be able to:

- Define the concept of fatigue of materials.
- List the various stages of fatigue process.
- Define the term of cyclic stress-strain curve.
- Explain the difference between life curves $\sigma_a - N_f$ and $\epsilon_t - N_f$.
- Describe the types of testing machines for fatigue tests.
- Describe the procedure for determining the curves of long crack growth rate.
- Describe the procedure for determining the thresholds for the growth of long cracks.



Presentation

3.1 Introduction

When a component or structure is subjected to the effect of varying external forces, a fracture may occur after some time, although the maximum level of stress is substantially lower than the yield strength of the material. The process of gradual weakening of the material, the so called fatigue of material takes place. Fatigue fracture, respectively a fracture caused by corrosion fatigue is, by far, the most common and most important operating limit state as far as engineering is concerned (around 80% of operating fractures).

If you change the sense of external forces that have an equally largest rate in both directions, we are talking about alternating stress. If only the size is changing with time, but not the sense of forces, it is the area of repeated or pulsating stresses. The general case with force amplitudes of different sizes and different character of their temporal variability is

called the oscillating stress. If the variability of forces is settled to the same highest and lowest limits at the same frequency of changes, it is a simple cyclic stress, which is a special case of oscillating stress.

Simple cyclic stress can have a varying nature of the cycle based on the ratio of maximum and minimum stress (see Fig. 3.1). Medium stress of the cycle σ_m and the stress amplitude σ_a can be expressed as

$$\sigma_m = \frac{\sigma_h + \sigma_d}{2}, \sigma_a = \frac{\sigma_u - \sigma_d}{2} \quad (3.1)$$

Cycle asymmetry can then be expressed as

$$R = \frac{\sigma_d}{\sigma_h} \quad (3.2)$$

or

$$P = \frac{\sigma_h}{\sigma_a} \quad (3.3)$$

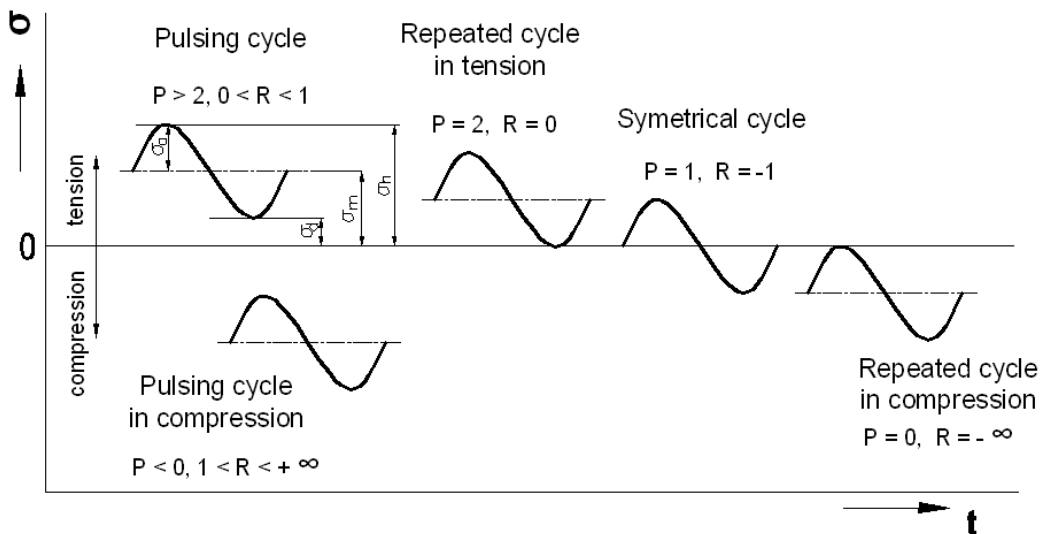


Fig. 3.1 Schematic representation of the cyclic stress

Existence of metal fatigue is conditioned upon and determined by a cyclic plastic deformation. The cause of alternating plastic deformations can be mechanical or thermal loading, or a combination thereof. For example, amplitude of the cyclic plastic deformation at the fatigue limit is of 10^{-5} regardless of the type of material. Uniaxial, non-repetitive strain of such order does not lead to any major changes in the material structure or its characteristics. Only multiple repetitions of plastic deformation, though so small that in terms

of current concepts we speak about elastic loading, leads to a cumulative damage ending in fatigue fracture. If the number of cycles to failure is 10^5 and above, we're talking about high-cycle fatigue, if the number of cycles to failure is 10^4 or less, we're talking about low-cycle fatigue. This division can be considered a convention, even if it has no deeper foundation.

Fatigue fracture surface has mostly smooth surface, worn, usually of shell appearance. For dynamic loads and at higher tensions, the appearance of fracture is more complex and fatigue fracture surfaces may alternate with areas corresponding to stages of a brittle fracture (see Fig. 3.2).



Fig. 3.2 Fatigue fracture of the shaft of the wheel of giant machine K 10000

The ratio of the definite brittle fracture surface to the size of the surface affected by a gradual growth of fatigue crack points at the amount of rated stress (see Fig. 3. 3). The smaller the static fracture surface compared to the whole cross section, the smaller cross-sectional area could resist the working load before the fracture occurred, i.e. the smaller the initial nominal stress was. The origin of the fatigue crack in these cases was caused by a large notch effect or very unfavourable local effect of the component's surface. The smaller the relative size of the amplitude of the operating stress as compared to the static component (pre-stress), the relatively larger the area of the definite brittle fracture. Also the curvature of the

lines dividing the shell-like fracture surface points at a minimum stress level and relative size of the notch effect. It should be noted that the fatigue cracks usually start from the point of maximum tensile stress and grow, macroscopically contemplated, perpendicular to the largest tensile stress. Gradual breaking of material thus proceeds through a nucleation of micro-defects and their growth.

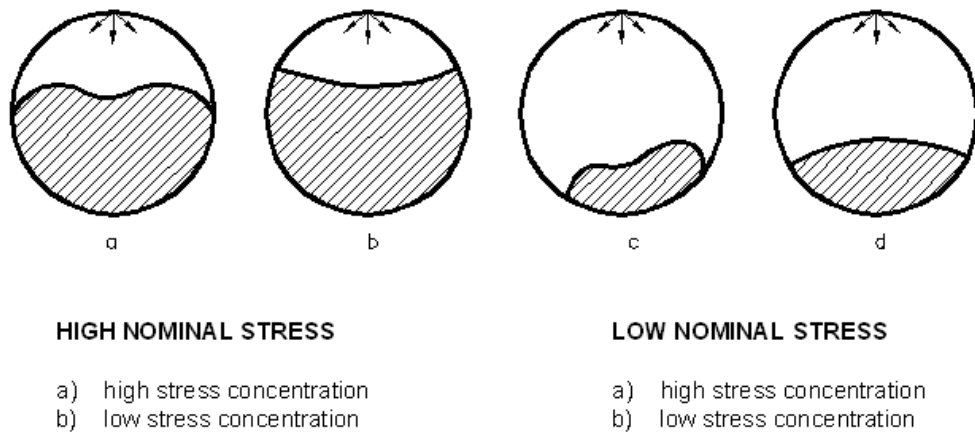


Fig. 3.3 The importance of the proportion of surfaces of fatigue and definite brittle fractures (definite fracture indicated by hatching) and the curvature of the dividing line

The chronology of individual stages of the fatigue process in a body without technological defects is evident from Fig 3.4.

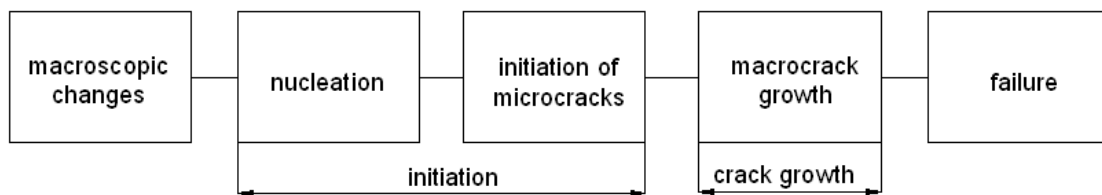


Fig. 3.4 Chronology of individual stages of the fatigue process in a body without technological defects

From this chronology, fatigue characteristics used in the design are derived, as well as assessment of residual life, respectively assessment of integrity of structures under cyclic loading. These characteristics include:

- 1) cyclic stress-strain curve,
- 2) fatigue strength and life curve $\sigma_a - N_f$ (Wöhler curve) determined on smooth cylindrical bodies,
- 3) life curve $\epsilon_{ac} - N_f$ determined on smooth cylindrical bodies under tension-pressure,

- 4) threshold of stress intensity factor amplitude ΔK_{th} for the fatigue crack growth and the dependence of the fatigue crack growth rate da/dN on ΔK .

3.2 The cyclic stress-strain curve $\sigma_a - \epsilon_{apl}$

3.2.1 Stage of changes in mechanical properties

This stage is characterized by changes in the entire volume of the loaded metal. Under cyclic loading, at first the changes in the mechanical properties of the material occur due to changes in the density and spatial arrangement of lattice defects. In this case, the term of mechanical properties refers to those properties that characterize the resistance of material to deformation caused by external forces (yield strength, ultimate strength, and dependence of the stress amplitude on the amplitude of deformation during cyclic loading).

The resistance of material against cyclic deformation can increase (cyclic hardening) or decrease (cyclic softening) during the process of fatigue, depending on the type of material, loading conditions and temperature. Significant changes, however, end after a certain number of cycles - saturation of mechanical properties occurs. The best way to detect changes in mechanical properties is a direct measurement of the parameters of hysteresis loops - dependences of the stress amplitude σ_a on the amplitude of total strain ϵ_{at} measured during cyclic loading (see Fig. 3.5).

Cyclic hardening is typical for annealed materials. In contrast, cyclic softening is typical of materials reinforced by

- strain hardening,
- precipitation hardening,
- hardening through martensitic transformation, and
- dispersion hardening by adding foreign particles into the matrix.

If the ratio of ultimate strength R_m to yield strength ($R_e, R_{p0.2}$) is higher than 1.4, there will be a cyclical stabilization. If this ratio is less than 1.2, there will be a cyclic softening. Once the stage of changes in mechanical properties is completed, both the stress amplitude and strain amplitude reach their saturated values and a stable hysteresis loop is formed. If we plot a curve through the peak points of stable hysteresis loops, we obtain the dependence between the stress amplitude and the plastic strain amplitude in a steady state, which is referred to in the literature as a cyclic stress-strain curve. This is a very important material characteristic, as

it describes the plastic response of metal throughout most of its life. All experimental data in both the low-cycle and high-cycle area agree that the cyclic curve of stress-strain can be expressed as (3.4)

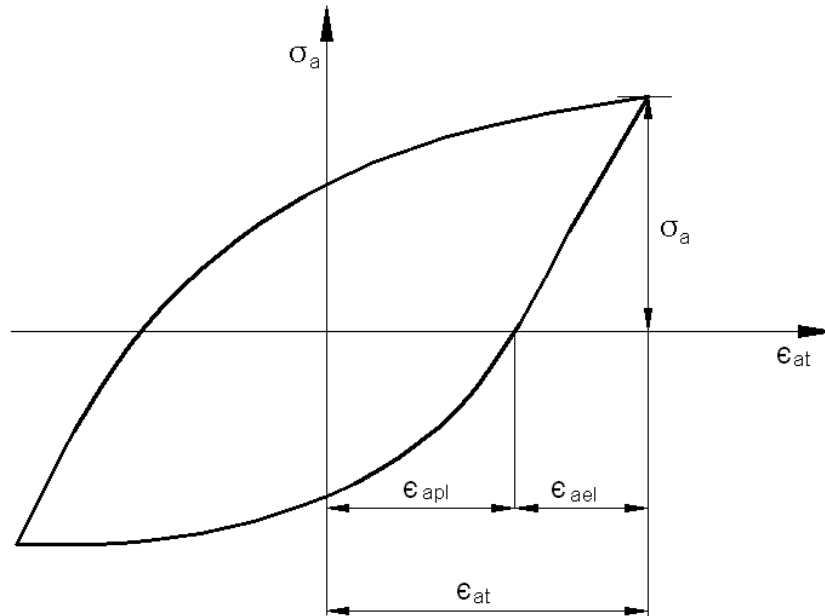


Fig. 3.5 Schematic representation of a hysteresis loop

$$\sigma_a = K \cdot (\epsilon_{apl})^n \quad (3.4)$$

where K is the cyclic strength coefficient
 n' is the fatigue hardening exponent

Tension diagram represents the dependence of stress on the strain in the first quarter of the cycle, cyclic stress-strain curve represents the same dependence after hardening and softening. Figure 3.6 illustrates the cyclic and static stress-strain curve for 08CH18N10T grade steel determined at room temperature.

3.3 Life curve $\epsilon_{at} - N_f$ (Manson-Coffin curve)

There are a number of experimental evidence that in low-cycle fatigue metals exhibit varying resistance to cyclic stress and cyclic strain. Interpretation of the fatigue process using the total strain amplitude, which is composed of elastic and plastic components of strain, occurs only in the last thirty years. This approach has its practical merit, as for example in construction notches the material is subjected to the total cyclic strain. Manson suggested the

dependence of the number of cycles to failure on the total strain amplitude in the form of (see Fig. 3.7)

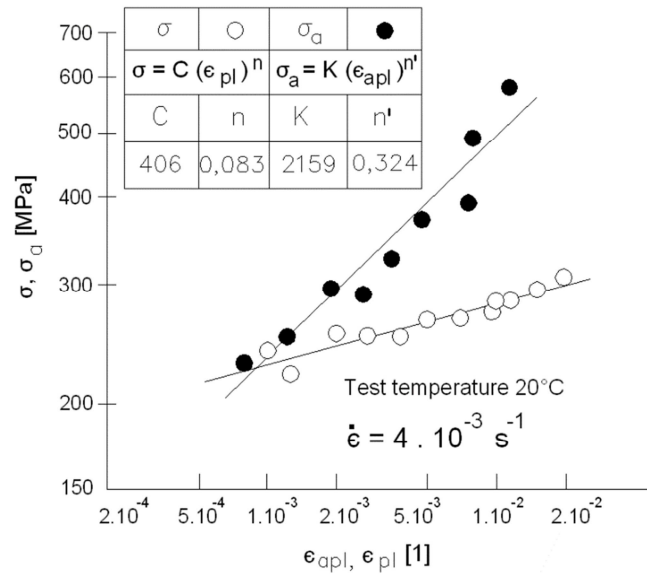


Fig. 3.6 Static and cyclic stress strain curve determined at room temperature for steel 08CH18N10T

$$\epsilon_{at} = \epsilon_{at} + \epsilon_{ap} = \frac{\sigma_f'}{E} (2N_f)^b + \epsilon_f' (2N_f)^c \quad (3.5)$$

- where E is the tensile modulus
- σ_f' is the fatigue strength coefficient
- ϵ_f' is the fatigue ductility coefficient
- b is the fatigue strength exponent
- c is the fatigue life exponent

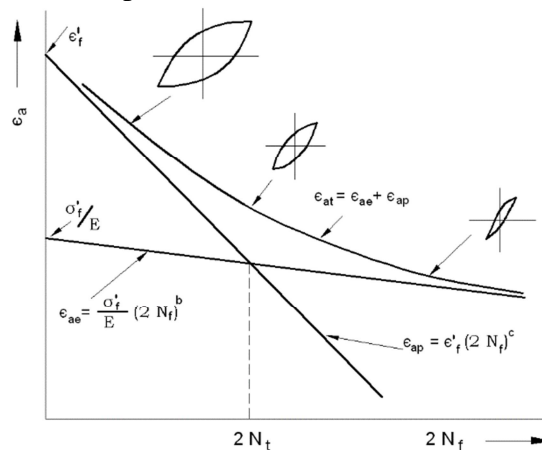


Fig. 3.7 Schematic running of curves $\epsilon_{ae1} - N_f$ and $\epsilon_{apl} - N_f$

Life curves $\epsilon_{at} = f(N_f)$ and cyclic stress-strain curves $\sigma_a = f(\epsilon_{apl})$ are determined under cyclic load with the constant total strain amplitude ϵ_{at} under tension - pressure (hard loading mode) on a series of smooth cylindrical test specimens (see Fig. 3.8). Total strain amplitudes are chosen so that the number of cycles to failure N_f covered the interval of $10^2 \div 10^5$ cycles. During the test, hysteresis loops are recorded at selected time intervals that are used to determine the elastic and plastic components of the total strain amplitude (see Fig. 3.9).



Fig. 3.8 Smooth cylindrical test body with a longitudinal strain sensor

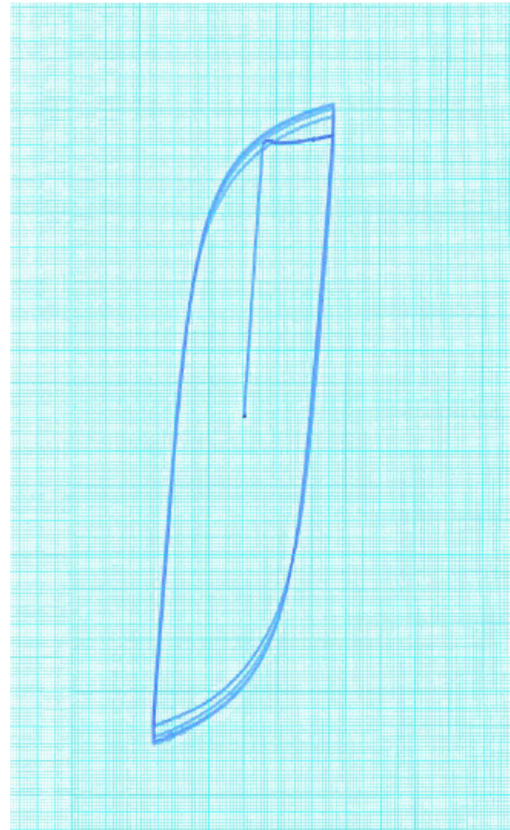


Fig. 3.9 Hysteresis loops captured during the test with $\epsilon_{at} = 0.01$.

To determine the life curve $\epsilon_{at} = f(N_f)$, it is recommended to test at least 10 specimens that are loaded at least at 6 levels of total strain amplitude ϵ_{at} .

For the experimental determination of the cyclic stress-strain curve and Manson-Coffin dependence, the test device must be equipped with a suitable strain gage and appropriate electronics. The strain is measured as the change in elongation of the gage specific length, which is usually around 10 mm.

The procedure for carrying out tests of low-cycle fatigue and subsequent determination of cyclic stress-strain curve and life curve $\epsilon_{at} = f(N_f)$ is described in ISO 12106 Metallic materials - Fatigue testing – Axial-strain - controlled method and ASTM

Standard E 606-92 Standard Practice for Strain Controlled Fatigue Testing. Figures 3.10 and 3.11 show dependences $\epsilon_{apl} - N_f$ and $\epsilon_{ael} - N_f$ determined for 08CH18N10T grade steel at 20°C and 350°C.

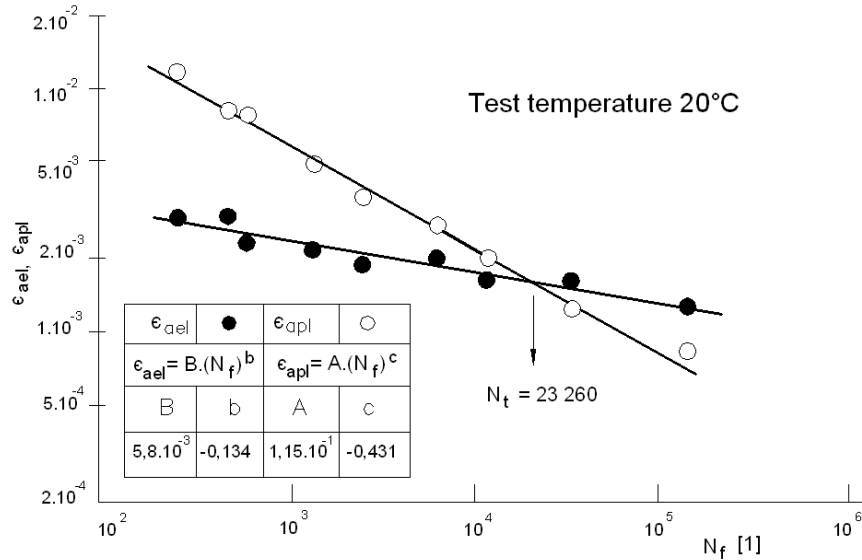


Fig. 3.10 Life curves $\epsilon_{ael} - N_f$ and $\epsilon_{apl} - N_f$ determined for 08Ch18N10T grade steel at room temperature

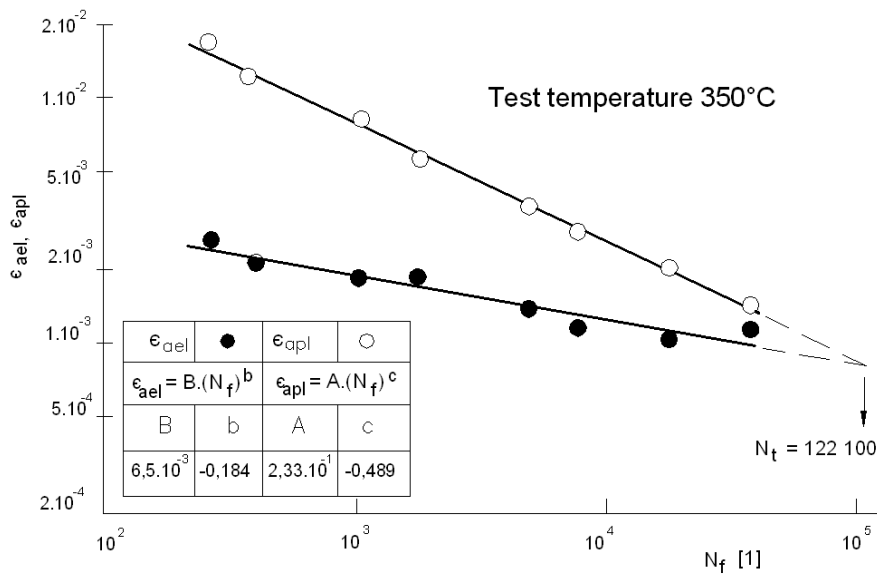


Fig. 3.11 Life curves $\epsilon_{ael} - N_f$ and $\epsilon_{apl} - N_f$ determined for 08Ch18N10T grade steel at 350°C

It is evident from Figures 3.10 and 3.11 that change in test temperature from 20°C to 350°C significantly influenced the transition number of cycles to failure N_t , for which the plastic strain amplitude ϵ_{apl} is equal to the elastic strain amplitude ϵ_{ael} during the loading cycle.

3.4 Life curve $\sigma_a - N_f$ (Wöhler curve)

Wöhler curve is named after its author who judged the fatigue strength of vehicle axles on the basis of rotating bending test more than 130 years ago. It provides information about the dependence of the stress amplitude σ_a on the number of cycles to failure N_f . Most often, smooth cylindrical test specimens are subjected to a homogeneous stress in tension-pressure ($R = -1$) or repeated tension ($R = 0$), and in some cases alternating or rotating bending is used. Course of Wöhler curve is characterized by growth of the number of cycles to failure with a decrease in the stress amplitude. Its characteristic shape in $\log \sigma_a - \log N_f$ coordinates is schematically illustrated in Figure 3.12.

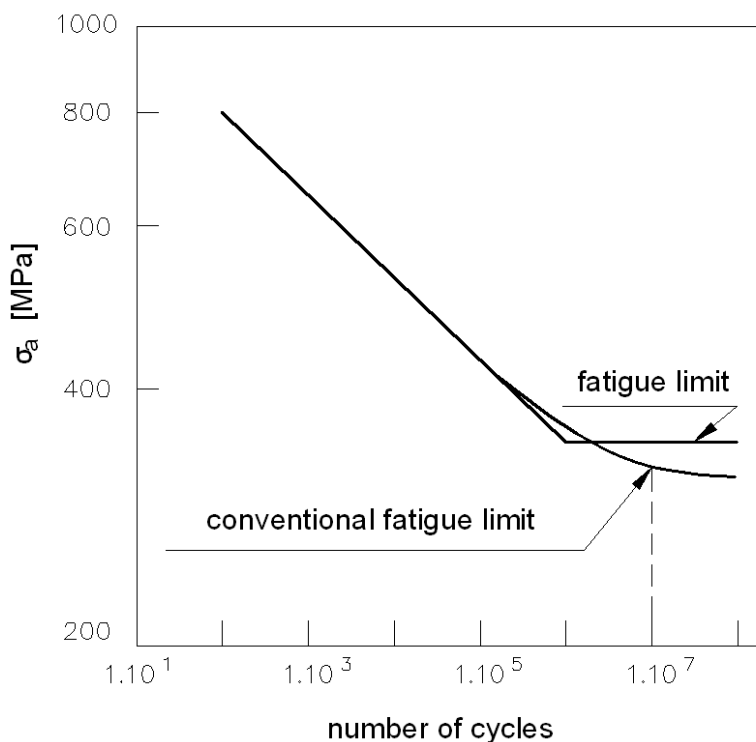


Fig. 3.12 Schematic representation of the life curve

The amplitude of stress, below which there is no failure by fatigue fracture is called a fatigue limit. Fatigue limit in alternating tension - pressure ($R = -1$) is denoted σ_c , while the fatigue limit in repeated tension ($R = 0$) is denoted σ_{hc} . The occurrence of fatigue limit is typical of steel and some other interstitial alloys. For metals and alloys having a face-centered cubic (FCC) lattice (austenitic steels, Al-based alloys), the incidence of fatigue is not observed, even after application of 10^7 to 10^9 cycles and the stress amplitude decreases with increasing number of cycles to failure. In these cases, we use the conventional fatigue limit, which is

determined by the stress amplitude at which the fatigue fracture occurs after a predetermined number of cycles. The standard number of cycles to determine the fatigue strength of steel, cast iron, copper and its alloys is $N_c = 10^7$. To determine the slant branch of the fatigue curve, the group consist of at least 8 test bars. Dependences in $\log \sigma_a - \log N_f$ or $\sigma_a - \log$ coordinates in the area of timed strength are interleaved by values measured on the bars of one group. These dependences represent the regression curves with a survival probability of 50%.

Course of Wöhler (SN) curve and fatigue limit level is influenced, in addition to cycle asymmetry R, also by the temperature, existence of corrosive environment and metallurgical parameters of the material. Figure 3.13 shows the effect of the degree of peening on the slant branch of Wöhler curve and on the fatigue limit for $N = 1 \cdot 10^7$ cycles for 16540.6 grade steel.

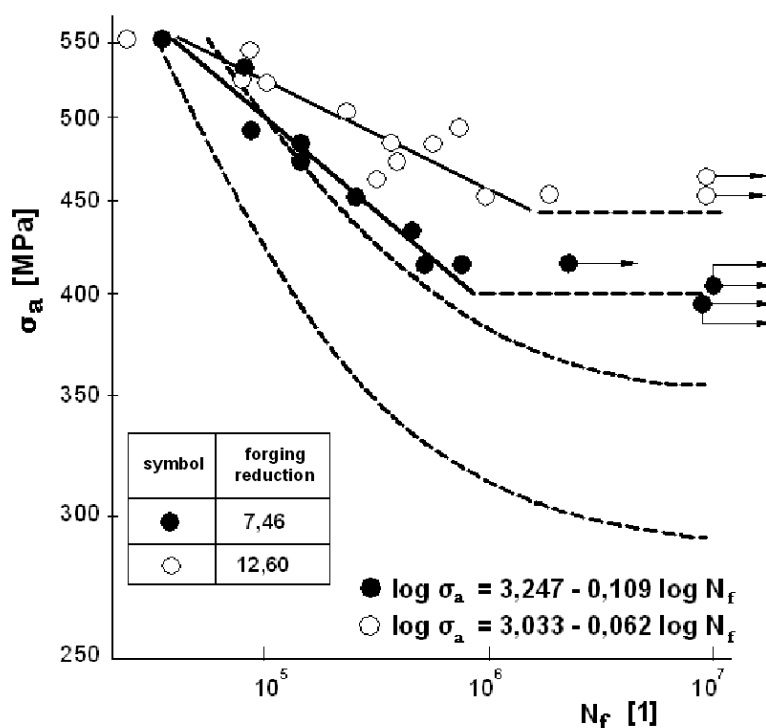


Fig. 3.13 Effect of the forging reduction on the Wöhler curve and on the fatigue limit for $N = 1 \cdot 10^7$ cycles for 16540.6 grade steel.

The procedure for determining the fatigue limit and slant branch of Wöhle curve is described in ČSN 420363 Fatigue Testing of Metals - Methodology of Testing, ISO 1143 Metallic materials - Rotating Bar Bending Fatigue Testing, ČSN ISO 1099 Metallic materials - Fatigue testing - Axial force - controlled method, and ASTM Standard E466-07 Conducting Force Controlled Constant Amplitude Axial Fatigue Tests of Metallic Materials. Basic terms and symbols are given in ČSN 420362 Fatigue Testing of Metals – Terms, Definitions and Symbols. Determination of regression curves and other statistical characteristics is described

in ISO 12107 - Metallic materials - Fatigue testing - Statistical planning and analysis of data and ASTM Standard E468-90 (2004) Presentation of Constant Amplitude Fatigue Test Results of Metallic Materials.

3.5 Evaluation of the resistance of the material to fatigue crack growth

Stable crack growth can be induced by cyclic loading, simultaneous application of static loads and corrosive environment, or is a hallmark of fracture behaviour of structural materials in a certain temperature interval. In the case of cyclic loading, we are talking about fatigue crack growth; in the case of simultaneous application of static loads and corrosive environment about the so called “stress corrosion cracking”.

Evaluation of resistance to fatigue crack growth is based on the principles of linear elastic fracture mechanics. The resistance to crack growth is assessed on the basis of the experimentally determined threshold ΔK_p for the fatigue crack growth and dependence of crack growth rate da/dN on the amplitude of the stress intensity factor ΔK .

3.5.1 Kinetics of fatigue crack growth in air

The dependence of the rate of growth of fatigue cracks on the amplitude of the stress intensity factor ΔK and the threshold for fatigue crack growth ΔK_p are material characteristics important for calculating the lifetime of defect structures exposed to cyclic loading.

The results of experimental measurements of the fatigue crack growth rate in the absence of a corrosive environment are schematically and in the most general form shown in Figure 3.14. As shown in this figure, it is possible to divide the whole dependence da/dN vs $\log \Delta K$ into 3 areas (A, B, and C) with respect to the scope of the fatigue crack propagation velocity. In the area of small fatigue crack growth rates ($10^{-8} \div 10^{-6}$ mm/cycle) and accordingly in the area of small values of the amplitude of the stress intensity factor ΔK (area A), the dependence da/dN vs. ΔK asymptotically approaches the threshold value ΔK_p , below which fatigue cracks do not propagate.

In this area, the fatigue crack growth rate is strongly dependent on the microstructure of the material and cycle asymmetry R . For medium rates (area B), where the fatigue crack propagation velocity lies approximately in the interval of 10^{-6} - 10^{-4} mm/cycle, the curve is linear in log-log coordinates and the fatigue crack growth rate can be expressed by the Paris-Erdogan power law relationship:

$$\frac{da}{dN} = C(\Delta K)^m \quad (3.6)$$

where C and m are material constants.

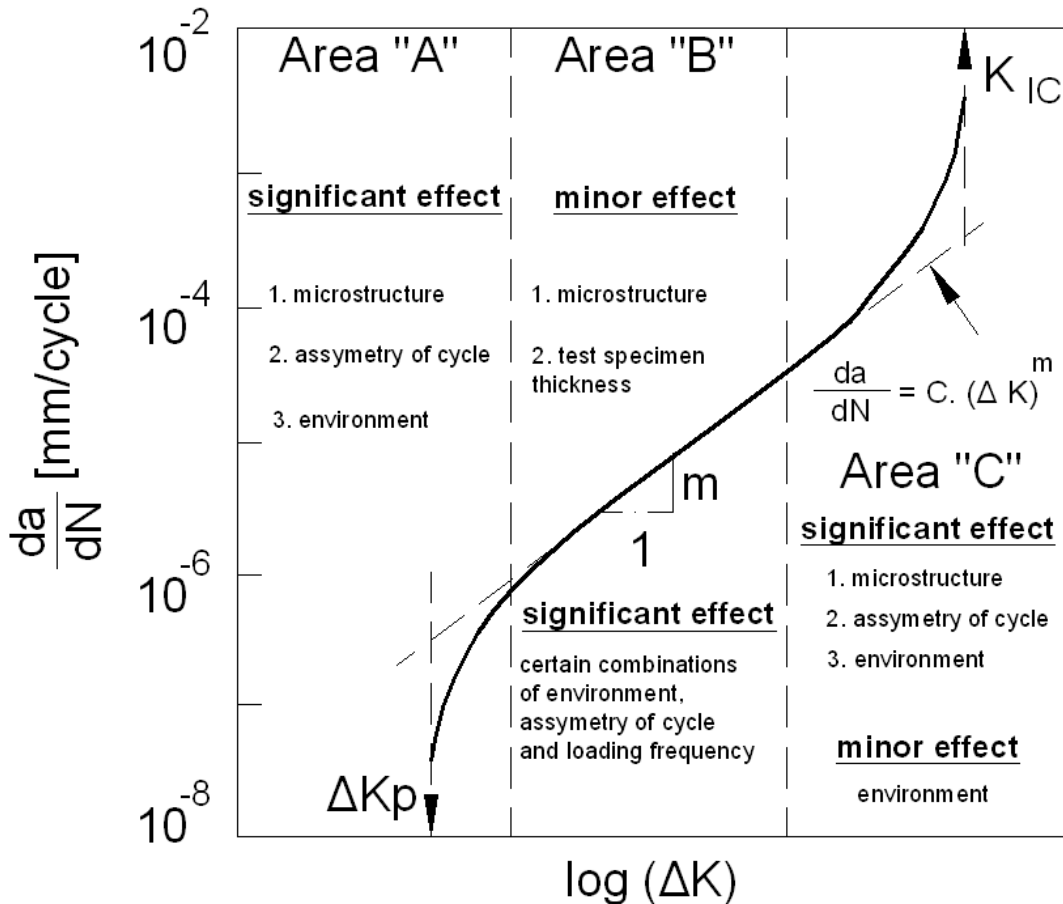


Fig. 3.14 Schematic representation of the general form of dependence of da/dN vs. ΔK in the absence of a corrosive environment

The crack growth rate in this area is little sensitive to the microstructure of the material and thickness of the specimen. At high crack growth rates (area C), when the maximum value of the stress intensity factor during the loading cycle K_{max} approaches the fracture toughness K_{IC} , also other micromechanisms of failure, typical of static fracture, are increasingly involved in the growth of cracks (transcrystalline ductile or cleavage fracture, intercrystalline decohesion) and the crack growth becomes sensitive to microstructure and cycle asymmetry R. This area is of little importance in practical terms, because it is a matter of only a relatively small proportion of the total number of load cycles.

Kinetics of fatigue crack growth is evaluated according to ČSN ISO 12108 Metallic materials - Fatigue testing - Method of fatigue crack growth or ASTM Standard E 647-08 Method for Measurements of Fatigue Crack Growth Rates.

To determine \underline{C} and \underline{m} constants in equation 3.6, it is necessary to experimentally determine the dependence of crack length \underline{a} on the number of cycles \underline{N} and know the parameters of loading and formula for calculating ΔK for the selected shape of the specimen. This dependence is determined by the constant force method, when constant amplitude of force ΔF is maintained during the test and the amplitude of the stress intensity factor ΔK and fatigue crack growth rate da/dN increase with the increasing length of the crack. Fatigue crack growth rate da/dN is determined from the recorded pairs of crack length \underline{a}_i and corresponding number of load cycles N_i . It is calculated as the slope of the line connecting two consecutive measurements of crack length \underline{a} according to the relation

$$\left(\frac{da}{dN} \right)_{\bar{a}} = \frac{a_{i+1} - a_i}{N_{i+1} - N_i} \quad (3.7)$$

Since the calculated rate of crack growth is the average speed in the interval $i \div i + 1$, the average value $\bar{a} = \frac{1}{2}(a_{i+1} + a_i)$ is considered to calculate ΔK , which corresponds to this crack growth rate. If possible, the lengths of the fatigue cracks are optically measured on both sides of the specimen using a microscope with a measuring accuracy of 0.01 mm. It is also possible to use indirect methods to measure the crack length, such as the method of potential or compliance involving a change in the electrical resistance or stiffness of the body as a result of the crack growth. They are mainly used in assessing the impact of environment on the resistance to fatigue crack growth.

Threshold fatigue crack growth ΔK_p generally corresponds to ΔK , for which the corresponding da/dN approaches zero. It is usually defined as ΔK value corresponding to the crack growth rate, which is equal to 10^{-8} mm/cycle. The common way to determine the threshold is to interleave the line by at least five approximately equally distant pairs of data of $\log da/dN$ versus $\log \Delta K$ between 10^{-7} mm/cycle and 10^{-8} mm/cycle established through a procedure with decreasing K . Test with decreasing K can be controlled through a stepwise reduction of the stress intensity factor after the chosen crack growth is reached at constant ΔF (see Fig. 3.15). The threshold ΔK_p is then considered to be ΔK value corresponding to the crack growth rate of 10^{-8} mm/cycle.

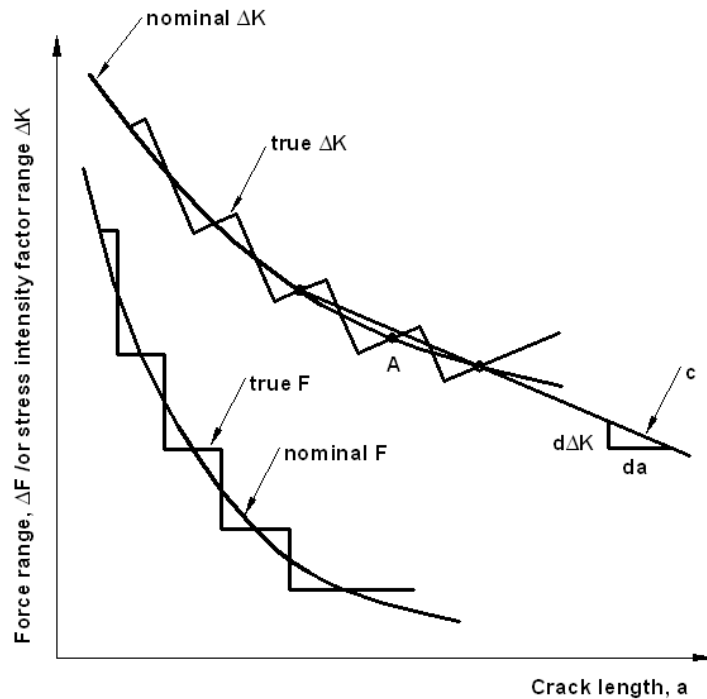


Fig. 3.15 Typical test with decreasing K using the method of a stepwise decrease in the loading force

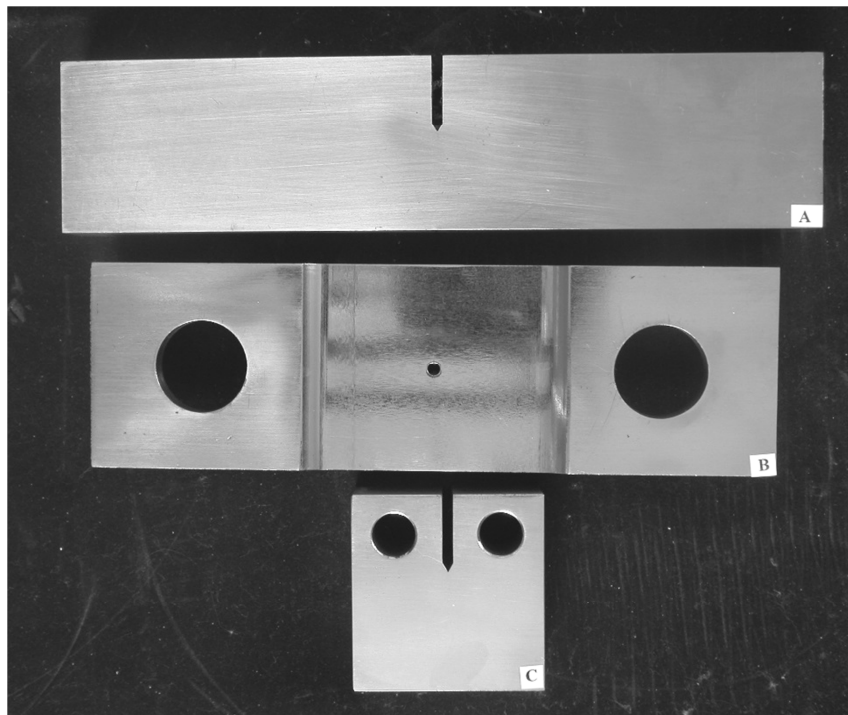


Fig. 3.16 Shapes of specimens used to evaluate the kinetics of fatigue crack growth

- A – Specimen with a unilateral notch loaded in three-point bending (SENT B3)
- B – Specimen with a central crack under tensile loading (Center Cracked Tension – CCT specimen)

C – Compact specimen under tensile loading (Compact Tension – CT specimen)

Figure 3.16 shows the shapes of specimens, which are typically used to assess the kinetics of the fatigue crack growth in air, respectively in corrosive environments. The amplitude of the stress intensity factor for all standard types of specimens is calculated using the following equation:

$$\Delta K = \frac{\Delta P}{BW^{1/2}} \cdot f(a/W) \quad (3.8)$$

where $f(a/W)$ is the so called compliance function depending on the type of specimen.

For SENT B3 specimen, it applies that

$$f(a/W) = 6 \cdot (a/W)^{1/2} \cdot \frac{[1,99 - (a/W)(1-a/W)(2,15 - 3,93(a/W) + 2,7 \cdot (a/W)^2)]}{(1 + 2a/W)(1-a/W)^{3/2}} \quad (3.9)$$

For CT specimen, it applies that

$$f\left(\frac{a}{W}\right) = \frac{\left(2 + \frac{a}{W}\right) \left(0,886 + 4,64 \cdot \frac{a}{W} - 13,3 \left(\frac{a}{W}\right)^2 + 14,72 \left(\frac{a}{W}\right)^3 - 5,6 \left(\frac{a}{W}\right)^4\right)}{\left(1 - \frac{a}{W}\right)^{3/2}} \quad (3.10)$$

For CCT specimen with a central crack of length $2a$ it applies for the compliance function that

$$f(a/W) = 1,77 \cdot (a/W)^{1/2} + 0,45 \cdot (a/W)^{3/2} - 2,04 \cdot (a/W)^{5/2} + 21,6 \cdot (a/W)^{7/2} \quad (3.11)$$

or it is possible to use the following relationship for this type of specimen

$$\Delta K = \frac{\Delta P}{B \cdot W} (\pi \cdot a)^{1/2} \frac{1 - 0,5 \frac{2a}{W} + 0,326 \left(\frac{2a}{W}\right)^2}{\sqrt{1 - \frac{2a}{W}}} \quad (3.10)$$

Figure 3.17 then shows the dependence da/dN vs. ΔK determined for cycle asymmetry $R = 0$ for low-alloy 10GN2MFA grade steel used for the production of PG VVER 1000 components.

3.5.2 Effect of a corrosive environment on fatigue crack growth

Simultaneous action of cyclic stress and aggressive environment that is generally called the corrosion fatigue, often results in increasing the fatigue crack growth rate relative to the growth rate determined in air, respectively in inert environments. The rate increase

depends on the type of environment, mechanical and metallurgical parameters of the material, method of stress (R, f frequency, shape of the load cycle), or their interaction. However, generally it can be stated that gaseous environments are usually milder and liquid environments generally more aggressive in terms of their impact on the fatigue crack propagation velocity.

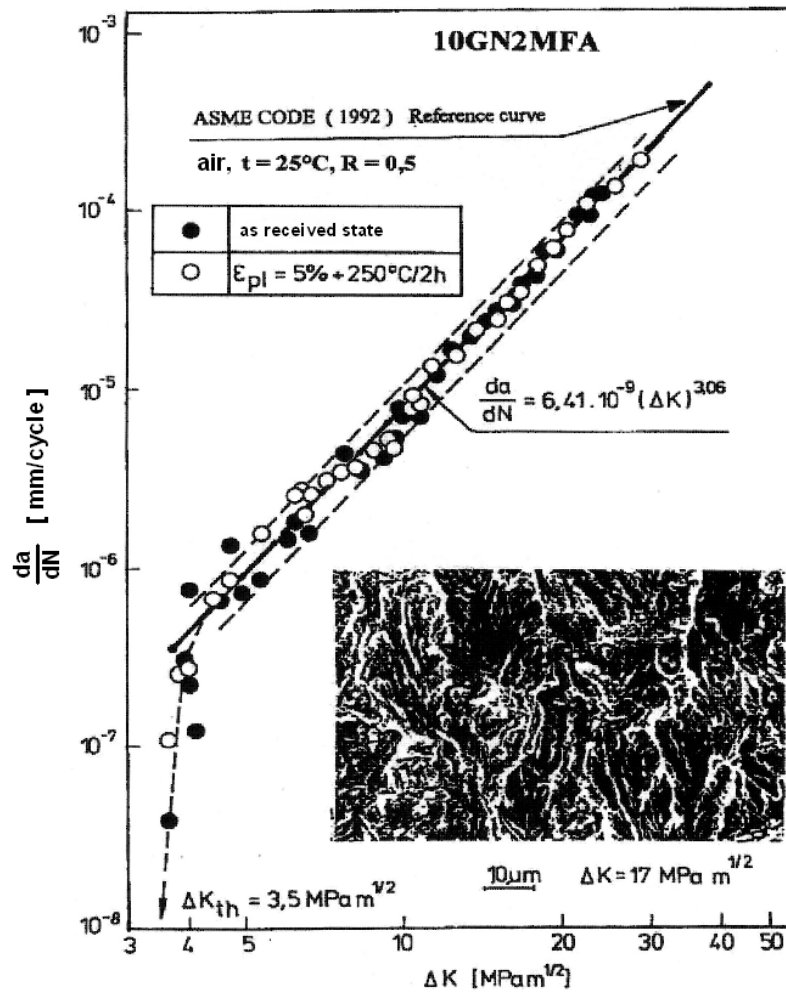


Fig. 3.17 Kinetics of the fatigue crack growth in air in 10GN2MFA grade steel (room temperature)

The dependence of da/dN vs. ΔK may be modified by the existence of a corrosive environment in essentially two ways which correspond to the basic types of corrosion fatigue termed as (see Fig. 3.15):

1. true corrosion fatigue, and
2. stress corrosion cracking under cyclic loading.

True corrosion fatigue refers to the situation when the rate of fatigue crack growth is enhanced by the simultaneous action of an aggressive environment and cyclic loading, while

the increase in crack growth rate occurs throughout the range of the amplitude of the stress intensity factor ΔK . Another characteristic of true corrosion fatigue is the reduction of threshold ΔK_p . Stress corrosion cracking under cyclic loading is characterized by the existence of threshold $K_{ISCC(f)}$ in the area of Paris-Erdogan relationship. For $\Delta K > K_{ISCC(f)}$, there is an increase in the rate

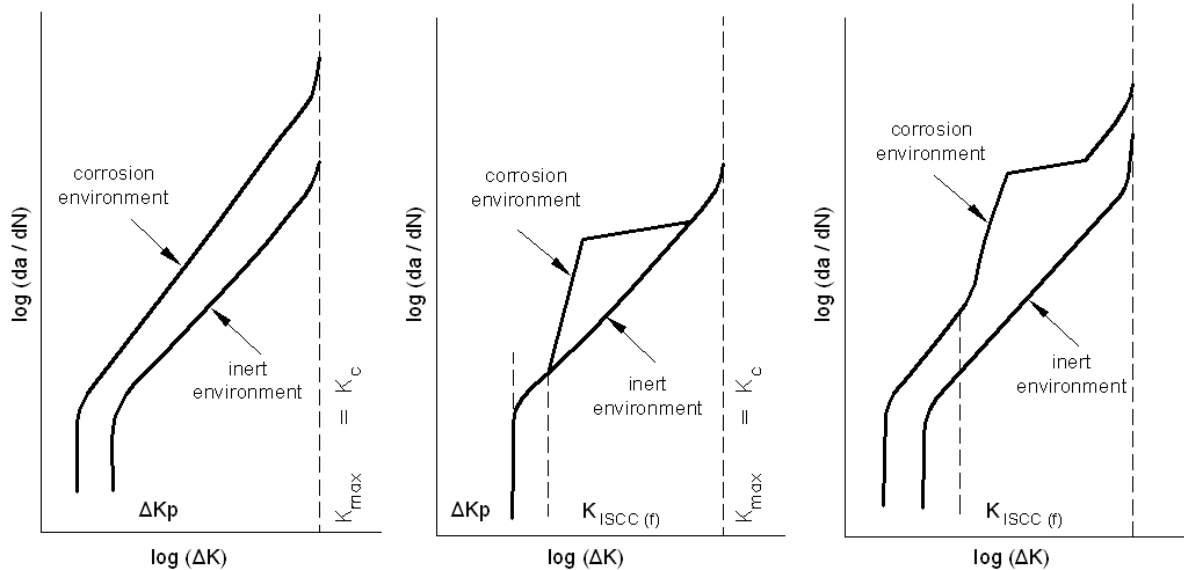


Fig. 3.18 Schematic representation of basic types of corrosion fatigue

of fatigue crack growth compared to the growth in air, but for $\Delta K < K_{ISCC(f)}$ the rate of fatigue crack growth is not influenced by the existence of a corrosive environment. Stress corrosion cracking under cyclic loading is further characterized by the emergence of a "hump", which implies that the growth rate cannot be described by Paris-Erdogan relationship. Most generally, the influence of the environment on the kinetics of fatigue crack growth can be expressed by combination of true corrosion fatigue and stress corrosion cracking under cyclic loading.

For many types of steels either true corrosion fatigue or stress corrosion cracking under cyclic loading arises under fatigue loading in corrosive environments. The transformation of the true corrosion fatigue to stress corrosion cracking under cyclic loading and vice versa can be caused by change in the parameters of loading, namely by change in the cycle asymmetry R and loading frequency f (see Fig. 3.19). Figure 3.20 shows the dependence of the effect of aqueous environment and the frequency of cycling on the kinetics of fatigue crack growth in high-strength low-alloy 38Cr2Ni2SiMo grade steel with

martensitic structure. In both cases, kinetics of the reference steel failure in distilled water is equivalent to the process of stress corrosion under cyclic loading, and is characterized by

1. the existence of a threshold stress corrosion cracking under cyclic loading $K_{ISCC(f)}$, and
2. the existence of two stages depending on $d2a/dN = f(\Delta K)$, which differ in the strength of relationship of the crack growth rate on ΔK

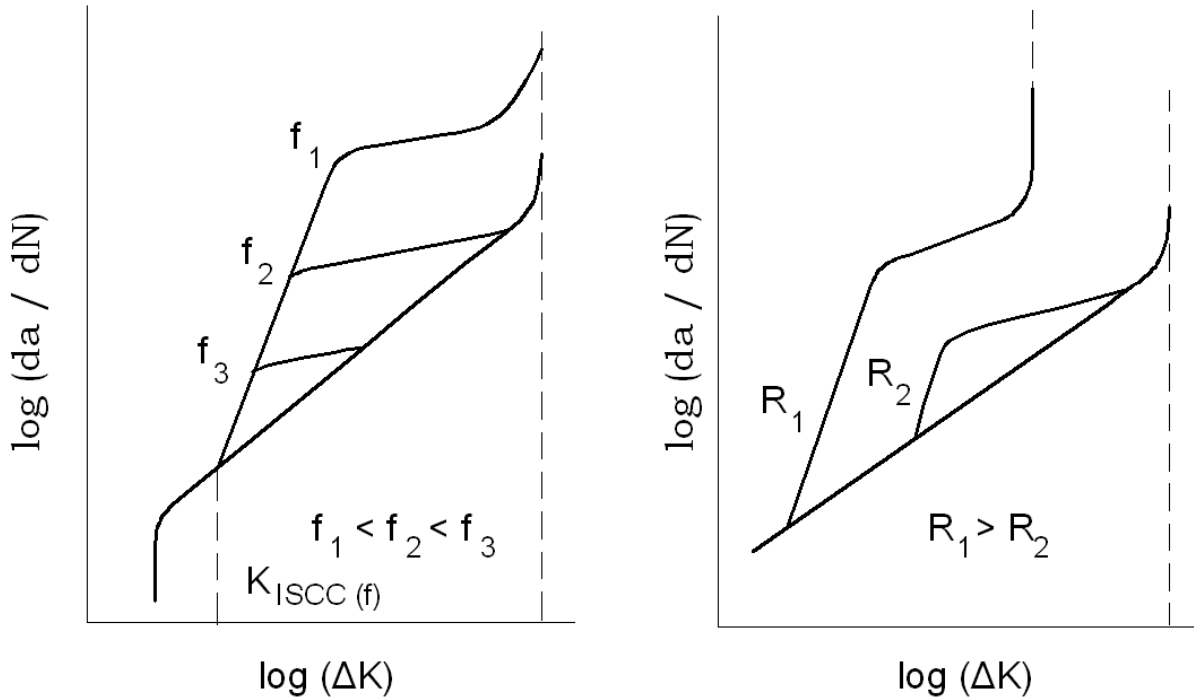


Fig. 3.19 Schematic representation of the effect of frequency and cycle asymmetry on the fatigue crack growth in corrosive environments

The rate of fatigue crack growth is in the first stage (after a threshold $K_{ISCC(f)}$ has been reached) strongly dependent only on ΔK and independent of the water temperature and frequency of cycling. In the second stage, the rate of fatigue crack growth becomes particularly heavily dependent on the water temperature or cycling frequency. This experimentally proven fact can be interpreted as the effect of time, over which the exposed surfaces of the crack tip are in contact with corrosive environments during the loading cycle.

38Cr2Ni2SiMo
 Tempering temperature 200°C
 0,009% S; 0,012%P

loading mode: $\Delta P = \text{const.}$
 assymetry of cycle: $R = 0$
 shape of loading cycle: sin
 environment: water

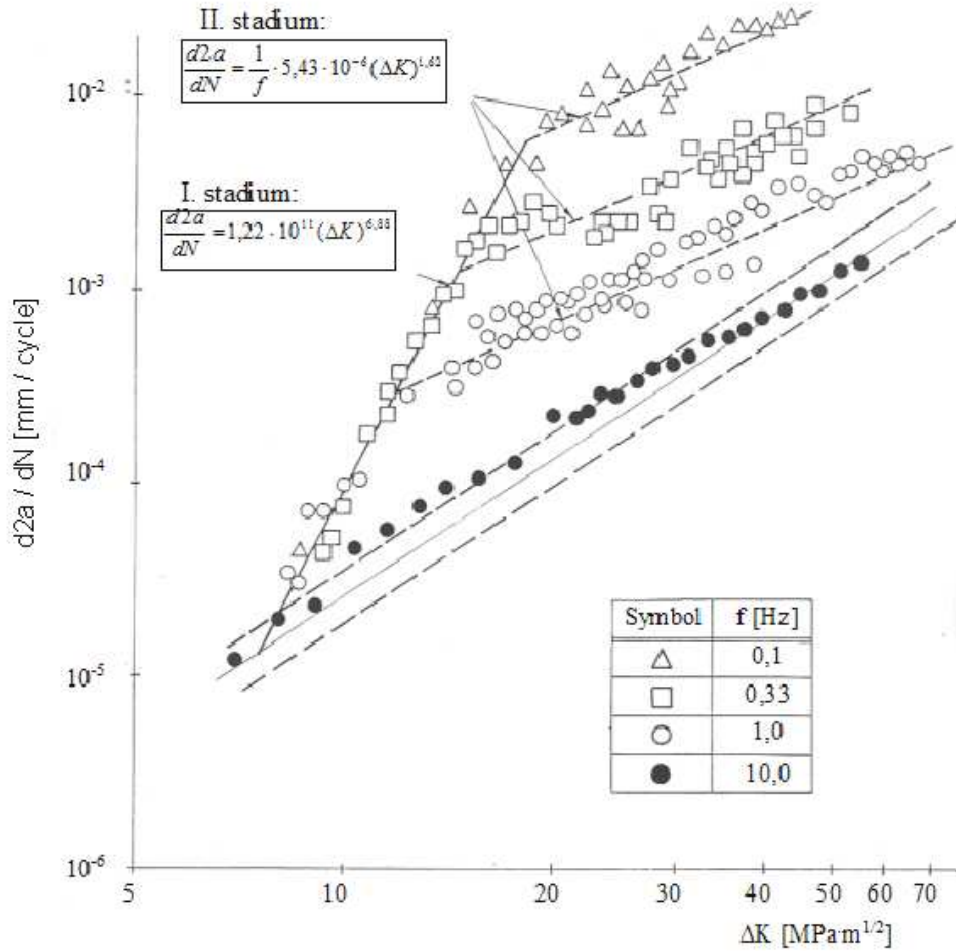


Fig. 3.20 Effect of ΔK and frequency of cycling on the kinetics of fatigue crack growth in distilled water at room temperature



Summary of terms

After studying the chapter, following terms should be clear to you:

- Fatigue of materials.
- Cyclic stress and oscillating stress.
- Cycle asymmetry R .
- Low-cycle and high-cycle fatigue.
- Stage of macroscopic changes.
- Cyclic stress-strain curve $\sigma_a - \epsilon_{apl}$.
- Life curve $\epsilon_{at} - N_f$.
- Life curve $\sigma_a - N_f$.
- Three areas of fatigue crack growth in air.
- Threshold amplitude of stress intensity factor ΔK_p .
- True corrosion fatigue.
- Stress corrosion cracking under cyclic loading.

Questions

- 1) What is meant by fatigue ?
- 2) What is asymmetry of cycle and how can be expressed ?
- 3) What are the stages of fatigue ?
- 4) What describes cyclic stress – strain curve and how is determined ?
- 5) What does the Manson – Coffin curve express ?
- 6) What the Wohler curve is ?
- 7) What does the threshold value for fatigue crack growth express ?
- 8) What basic types of corrosion fatigue do you know ?
- 9) What the kinetics of fatigue crack growth in water environment is

dependent on ?



Tasks to solve

Results of low cycle fatigue tests of austenitic stainless steel 08Ch18N10T at laboratory temperature. Are listed in tab. 3.1 Calculate

σ_f' fatigue strength coefficient
 ϵ_f'' fatigue ductility coefficient
 b fatigue strength exponent
 c fatigue ductility exponent
 and cyclic stress strain curve $\sigma_a - \epsilon_{apl}$

Tab. 3.1

$\epsilon_{ac} \cdot 10^2$ [1]	$\epsilon_{apl} \cdot 10^2$ [1]	$\epsilon_{ae} \cdot 10^2$ [1]	σ_a [MPa]	N_f [1]
1,46	1,20	0,26	454	399
1,24	0,97	0,27	435	531
0,98	0,76	0,22	403	1093
0,74	0,54	0,20	351	1630
0,50	0,34	0,16	292	4520
0,40	0,25	0,15	287	7270
0,35	0,20	0,15	274	14080
0,30	0,17	0,13	249	27720
0,25	0,12	0,13	252	68260



References

- [1] KLESNIL, Mirko-LUKÁŠ, Petr: Únava kovových materiálů při mechanickém namáhání. 1. vydání. ACADEMIA Praha 1975, 224s.
- [2] HOLZMANN, Miroslav-KLESNIL, Mirko: Křehký a únavový lom materiálů a konstrukcí. 1. vydání. Praha, SNTL, 1972. 208s.
- [3] KUNZ, Ludvík: Experimentální stanovení únavových charakteristik materiálů. 1. Vydání. Žilinská univerzita v Žilině, 2003, 81s., ISBN 80-8070-069-9.
- [4] NĚMEC, Jaroslav - PUCHNER, Ondřej: Tvarová pevnost kovových těles, SNTL Praha 1971.

- [5] BARSOM, John M. – ROLFE, Stanley T.: Fracture and Fatigue Control in Structures. ASTM *Applications of Fracture Mechanics*, third edition, ISBN 0-8031-2082-6.
- [6] ČSN ISO 12108 Kovové materiály – Zkoušení únavy – Metoda růstu únavové trhliny. UNMZ, druhé vydání, 2012 – 08 – 15

4. Evaluation of fracture behaviour of metallic materials



Study time: 3 hours.



Objective: After reading this chapter, you should be able to:

- **Define the concept of brittle fracture.**
- **List the factors that affect the toughness.**
- **Describe two philosophies of evaluation of material resistance against brittle fracture.**
- **Describe test procedures and material characteristics of both philosophies.**
- **Describe the general temperature dependence of fracture toughness.**
- **Define the concept of reference temperature and MASTER curve.**
- **Describe what is the difference between the impact bend test and DWT (drop weight test) and DWTT (drop weight tear test) respectively.**



Presentation

4.1 Introduction

High demands on safety and reliability of large structures give rise to increased demands on the resistance of material to a sudden unstable fracture. Upon sudden (unstable) failure, the separation of particles of metal is sudden and uncontrollable and occurs under the effect of elastic energy accumulated in the body, without the need for any additional energy supply from outside. The difference between stable and unstable failure of metal is given by the relationship between the elastic energy released during fracture propagation and the work that must be done against the resistance of the material to fracture propagation.

Brittle fracture of steels of low and medium strength is an unstable fracture occurring during nominal stress, which is smaller than the macroscopic yield strength. From a microscopic point of view, the fracture is of cleavage nature (see Fig. 4.1).

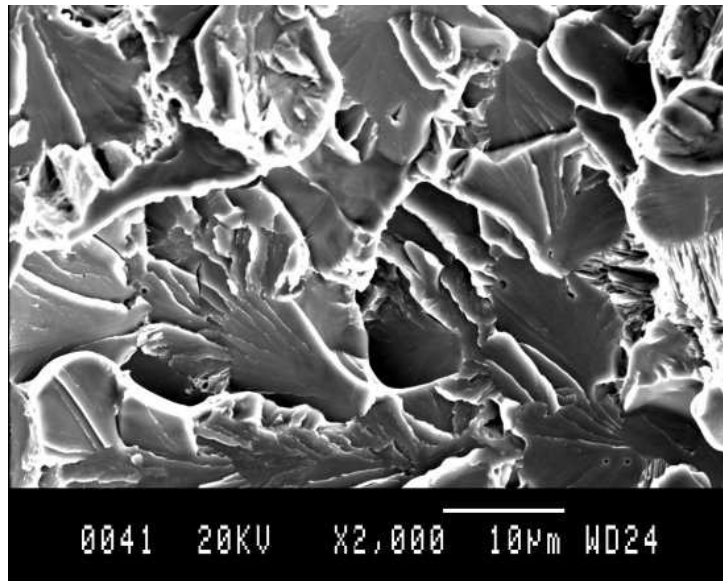


Fig. 4.1 Transcrystalline cleavage fracture

Brittle fracture of steels of high and very high strength is an unstable fracture occurring under stress that is lower than the yield strength. From a microscopic point of view, the fracture occurs either through quasi-cleavage, in an intercrystalline manner (see Fig. 4.2), or by ductile separation of metal particles (see Fig. 4.3).

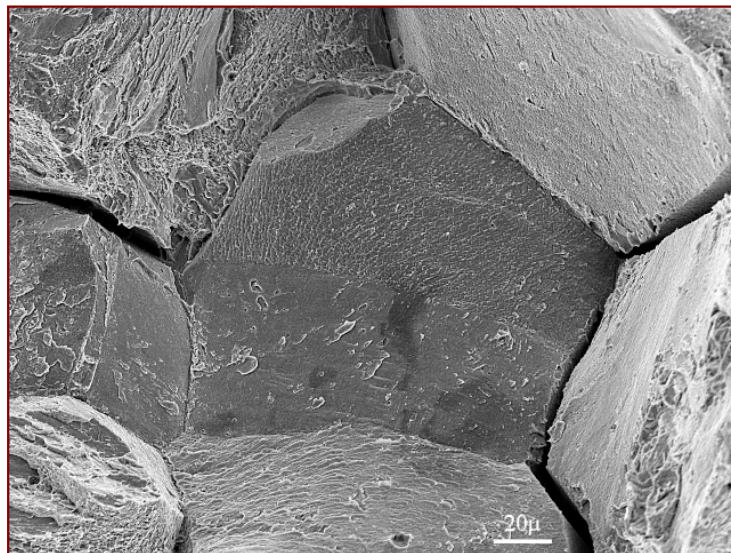


Fig. 4.2 Intercrystalline failure

Resistance of any material to brittle fracture is given by the level of its toughness. Toughness is defined as the ability of a material to deform plastically and absorb energy before and during the failure. It depends on:

1. metallurgic characteristics of material,

2. rate of loading,

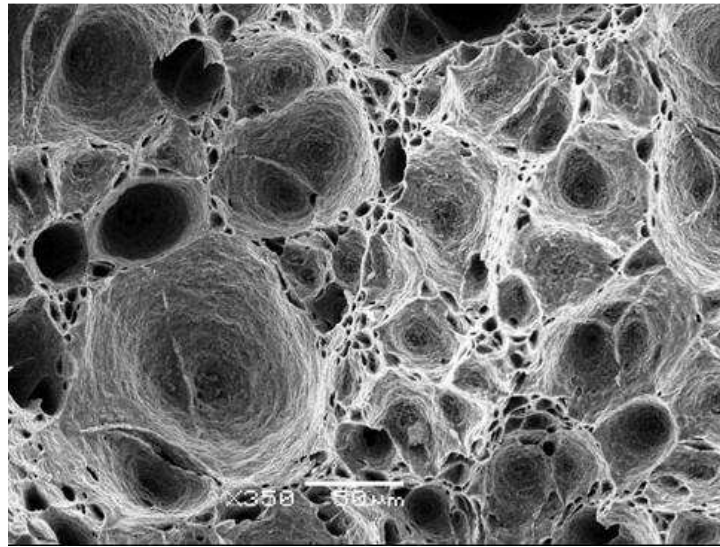


Fig. 4.3 Ductile failure

3. temperature,
4. component thickness, and
5. the presence of notches, either shaped or strength.

There are two fundamentally different philosophies of evaluation of resistance of materials to brittle fracture, and thus two groups of material properties used in the design of a structure resistant to brittle fracture or in assessing the residual life of the long-term operating equipment.

- 1) Philosophy of transition temperature. It has validity only for materials that exhibit transition fracture behaviour. Material property is the transition temperature.
- 2) Philosophy based on fracture mechanics. It has validity for materials that exhibit unstable fracture and/or stable ductile crack growth. Their material characteristic is the fracture toughness and reference temperature T_0 , respectively.

4.2 Philosophy of transition temperature

The basis of this philosophy is to evaluate the temperature at which there is a change in toughness associated with a change in fracture mechanism from ductile to cleavage. Different types of tests classify a given range of steels generally in the same order with

respect to susceptibility to brittle fracture. For a different type of test, however, the curve can be shifted to the right or left, the transition area may be narrower or wider. The most important tests include:

- Impact bend test using Charpy method,
- **DWT (drop weight test),**
- **DWTT (drop weight tear test)**
- Impact bend test of larger bodies

4.2.1. Impact bend test

It is the most widely used test evaluating transition behaviour of materials. The test consists in loading notched specimens by impact bending (see Fig. 4.4).

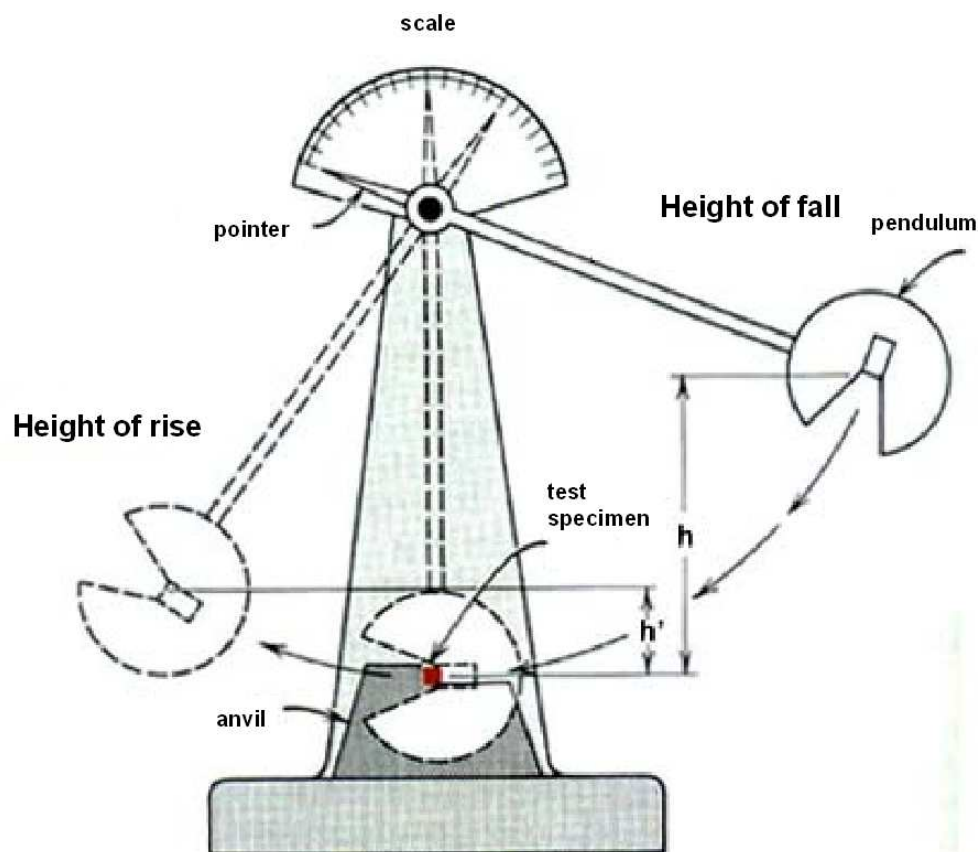


Fig. 4.5 Schematic representation of the impact bend test

The results allow comparing the resistance of materials to brittle fracture by the shift of the transition curve in the direction of the axis of temperatures. However, they do not provide a basis for dimensioning structural parts. The energy needed to fracture a specimen

contains both the component exerted on the crack initiation and the component needed for its growth. Initiation energy is relatively extensive with respect to rounding of the "V" notch tip.

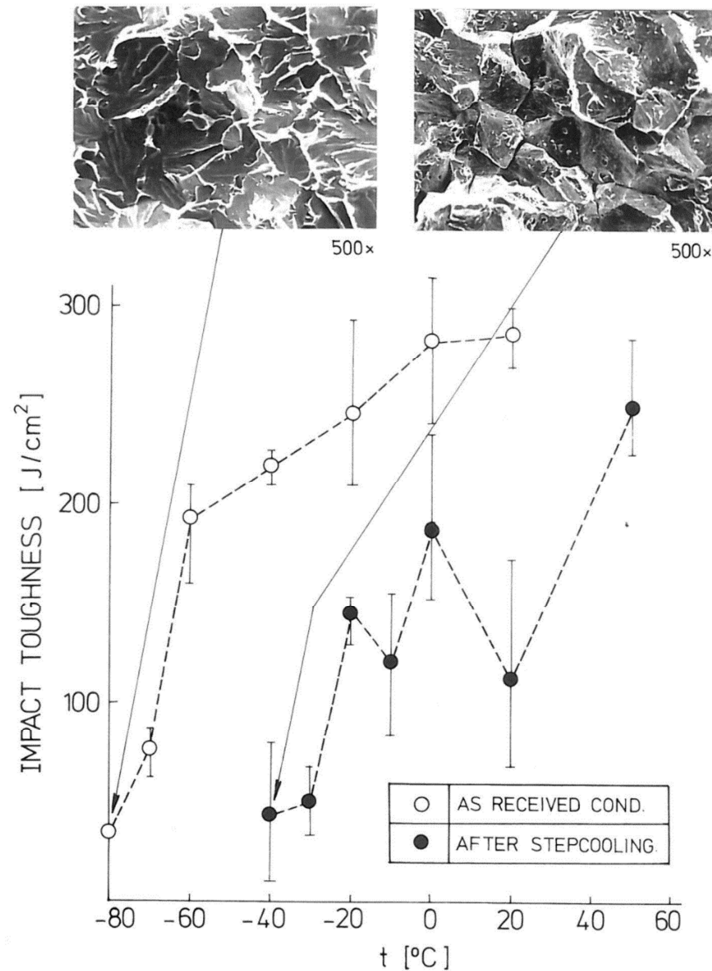


Fig. 4.5 Temperature dependence of notch toughness of 10GN2MFA grade steel as supplied and after being slowly cooled down from the temperature of 595°C (step-cooling).

Test procedures are described in the following standards:

- ČSN ISO 148-1 (420381) Metallic materials – Charpy impact bend test - Part 1: Test method
- ČSN 420382 Testing of metals. Impact bend test at low temperatures
- ČSN 420383 Testing of metals. Impact bend test at high temperatures
- ČSN 420350 Testing of metals. Determination of embrittlement temperature of structural steels by impact bend test.

Impact bend test can detect the following: size of impact energy consumed to fracture, notch toughness, fracture appearance (the proportion of ductile fracture) and side extension. By

plotting the dependence of these values on test temperature, transition curves are obtained, from which transition temperatures are taken (see Fig. 4.6).

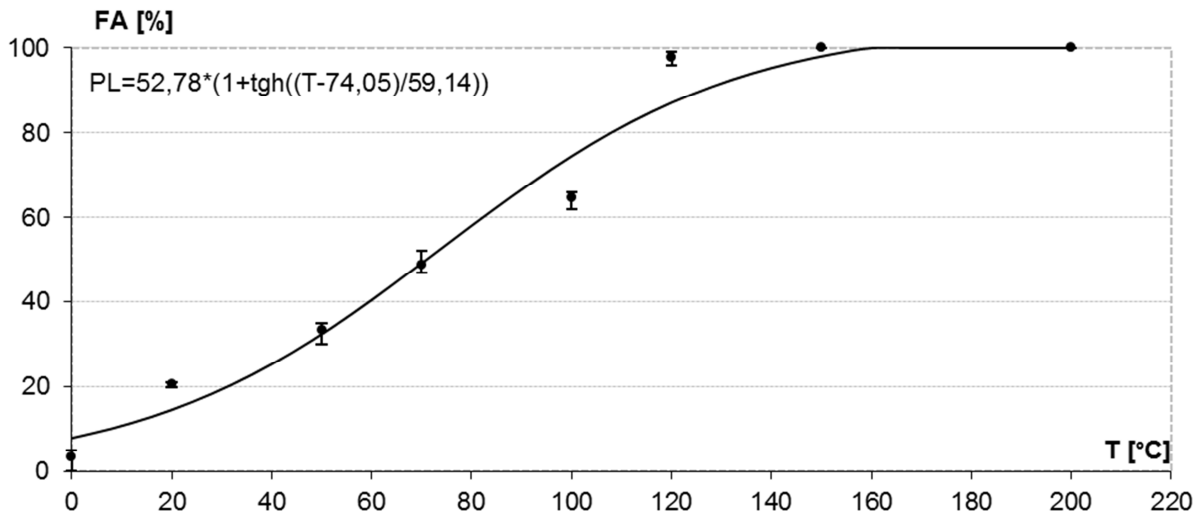


Fig. 4.6 Temperature dependence of the ductile fracture proportion; the low alloy 15 128.5 grade steel after 90,000 hours of operation at temperature of 540°C

They are defined by different criteria, such as:

- ❖ selected value of notch toughness (e.g. 35 Jcm^{-2}),
- ❖ mean value of max and min notch toughness,
- ❖ conventional value of notch toughness, which depends on the yield strength of the material (critical temperature of brittleness),
- ❖ transition temperature for 50% of ductile fracture (FATT), and
- ❖ side extension 0.9 mm.

From the level of transition temperature we can deduce the resistance of steel to brittle fracture, or the evaluation of metallurgical and technological factors on the change in the resistance of steel to brittle fracture.

The effort to determine the amount of energy needed for crack growth led to the draft test procedures using test specimens of larger dimensions with notches that reduce to the minimum the energy needed to initiate a crack. These tests include DWT test, DWTT test and impact bend test of large bodies. These tests are increasingly being part of the technical conditions of business cases.

4.2.2. Drop-weight test (DWT)

Drop-weight test (DWT) consists in stressing the specimen equipped with a brittle weld deposit with a notch (see Fig 4.7) by one impact bend at limited deformation. Testing takes place at various temperatures of test specimen. According to ČSN 420349, test specimens with dimensions 16x50x130 mm, 19x50x130 mm and 25x90x360 mm are used for DWT tests.



Fig. 4.7 Specimen with dimensions 16 x 50 x 130 mm used for DWT

The aim of the test is to determine the temperature of zero toughness t_{NDT} – a characteristic expressing the resistance of materials against unstable crack growth. It is the limit temperature above which no unstable fracture occurs from a small defect initiated from the weld metal into the base material under dynamic stress around the yield point. The specimen is considered broken when the fracture extends to one or both edges of the specimen on the surface with weld deposit, or its side walls (see Fig. 4.8).



Fig. 4.8 Specimen intact during the drop-weight test. Fracture in the base material did not extend to either one or both edges of the specimen.

Zero temperature toughness t_{NDT} is the highest temperature at which the fracture occurs in the specimen (determined with an accuracy of $\pm 5^\circ\text{C}$). It is thus the temperature, at which the brittle crack initiated in hardfacing metal weld deposit extends by effect of stress around the yield strength over the cross-section of the specimen. The sudden transition from cracked specimens to intact ones is the result of growth of plastic deformation necessary for the fracture propagation at temperatures above t_{NDT} . Zero toughness temperature t_{NDT} is determined using drop-weight testers with a potential energy of the hammerhead up to 1900 J, while the minimum height of the fall of the hammerhead must be at least 1 m. The hammerhead weight must be in the range from 25 to 135 kg. The test is not valid when:

- a) the weld deposit with notch is not visibly broken,
- b) the body is not sufficiently bent after the test to touch the stops of the jig, or
- c) the weld deposit breaks outside the notch.

4.2.3 Drop-weight tear test (DWTT)

This test is normally used to evaluate the resistance of metal plates or seamless pipes, with an outside diameter greater than 300 mm and wall thickness greater than 6 mm of ferritic steels for the manufacture of pipelines, against unstable crack growth. During the drop-weight tear test, a specimen measuring 76 x T x 305 mm and provided with a cold-pressed notch is being broken. The specimen is supported at both ends, while the impact acts against the notch (see Fig. 4.9).

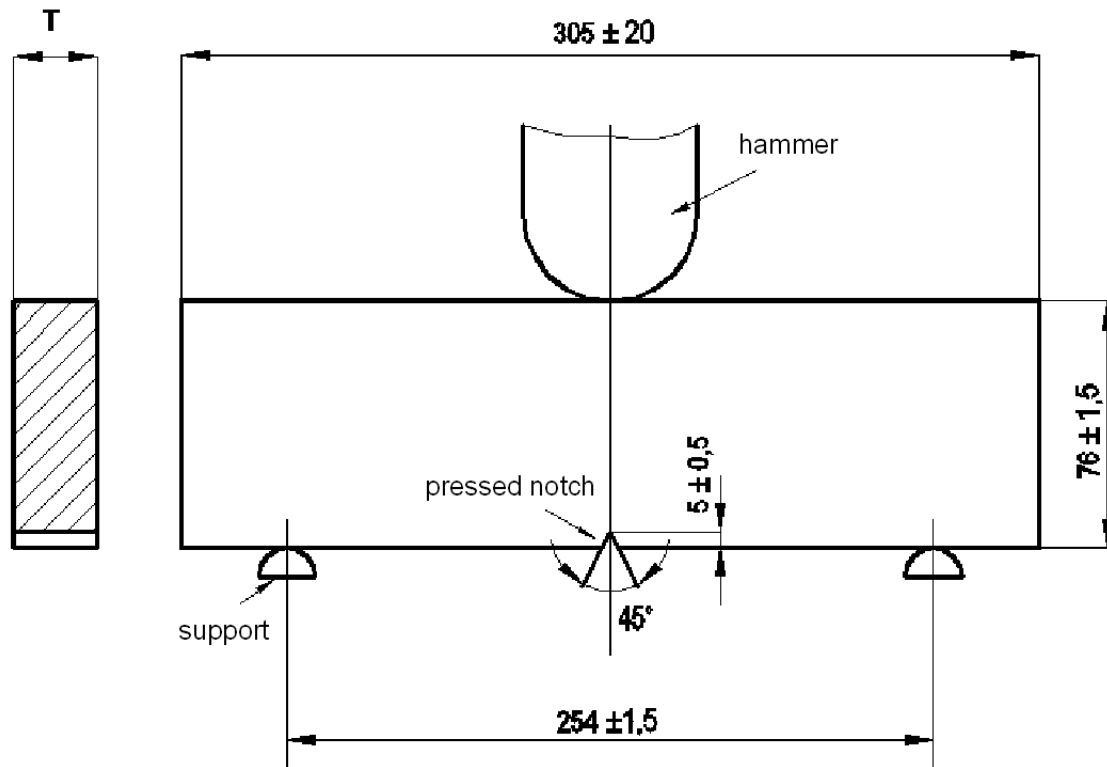


Fig. 4.9 Geometry of a specimen for DWTT

The test specimen shall have up to 19 mm full thickness of the tube wall or plate thickness. At thicknesses above 19 mm, the specimen may have either the full thickness of the wall or plate, or the thickness of the specimen may be reduced to 19 mm. Testing device may be either a weight-dropping device or a pendulum-type machine. DWTT proceeds according to the European standard ČSN EN 10 274 Metallic materials – Pendulum impact test. It sets out the procedure for evaluating the appearance of the fracture surfaces of specimens made of ferritic steels.

The test results are usually expressed as fracture appearance transition temperature (FATT) or as a percentage of ductile fracture at a temperature prescribed for product by the standard. E.g. FATT (fracture appearance transition temperature) for 85% of ductile fracture at -30°C is expressed as follows: $\text{FATT}(85) = -30^{\circ}\text{C}$.

For test specimens with a thickness of 19 mm or less, the percentage of ductile fracture at the fracture surface is evaluated so that it does not take into account the fracture surface at a distance of one specimen thickness T from the notch tip and at a distance of one specimen thickness from the side opposite the notch (see Fig. 4.10).

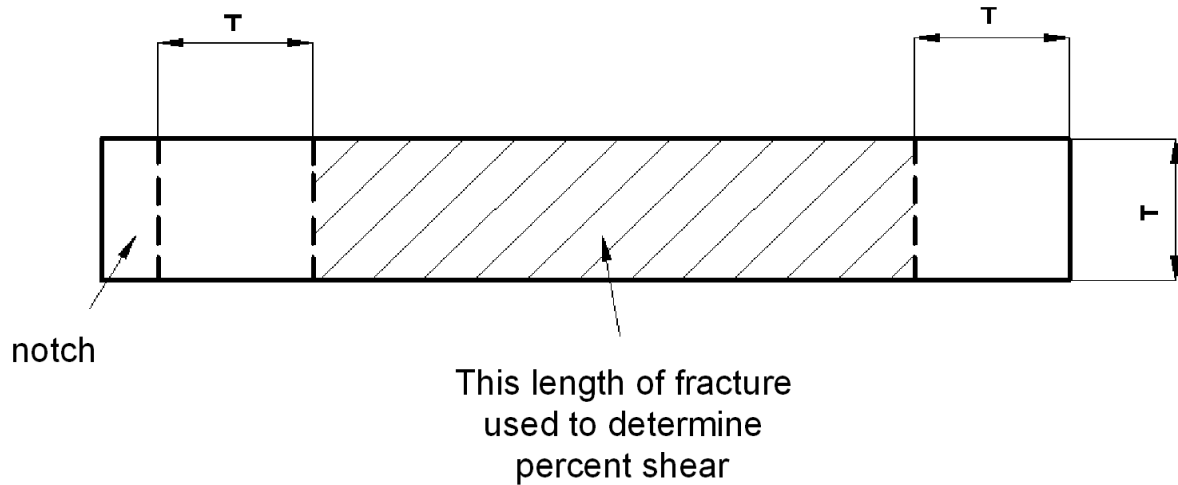


Fig. 4.10 Determination of percentage of ductile fracture on the fracture surface

Assessment may also be based on the absorbed energy consumed during the test, especially for materials other than ferritic steel.

Figures 4.11, 4.12 and 4.13 are examples of fracture surfaces of specimens broken during DWTT at a selected temperature, along with the assessed share of ductile fracture according to ČSN EN 10 274. Figure 4.14 shows the temperature dependences of the proportion of ductile fracture set visually on the fracture surfaces of specimens taken from X70 steel sheets of thickness 9.3 and 14 mm and broken in the temperature range $-70^{\circ}\text{C} \div -10^{\circ}\text{C}$.



Fig. 4.11 Room temperature, proportion of ductile fracture 100%



Fig. 4.12 Test temperature -40°C , proportion of ductile fracture 45%



Fig. 4.13 Test temperature -60°C , proportion of ductile fracture 10%

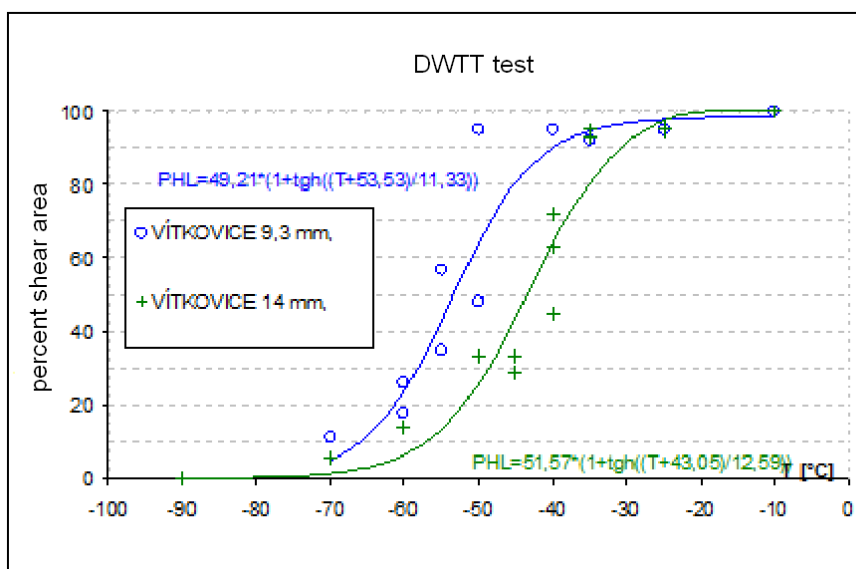


Fig. 4.14 Temperature dependences of the proportion of ductile fracture set visually on the fracture surfaces of specimens taken from X70 steel sheets of thickness 9.3 and 14 mm

4.2.4 Impact bend test of large bodies (DT- dynamic tear)

The test consists in breaking the test specimen by a pendulum hammer or drop-weight tester with a variable drop height and weight of the hammerhead. Test equipment must allow determination of the impact energy. Impact energy is determined using test specimens measuring $16 \times 40 \times 180$ mm and/or $25 \times 120 \times 460$ mm. Preferably, and for decision making purposes, test specimens with 16 mm thickness are selected, which are marked "Specimen 16 CSN 420340". The shape and dimensions of the notch for Specimen 16 are shown in Figure 4.15. The notch is fabricated by chip machining. Sharp notch tip is formed by pressing using a punch made of tool steel with a hardness of at least 60 HRC.

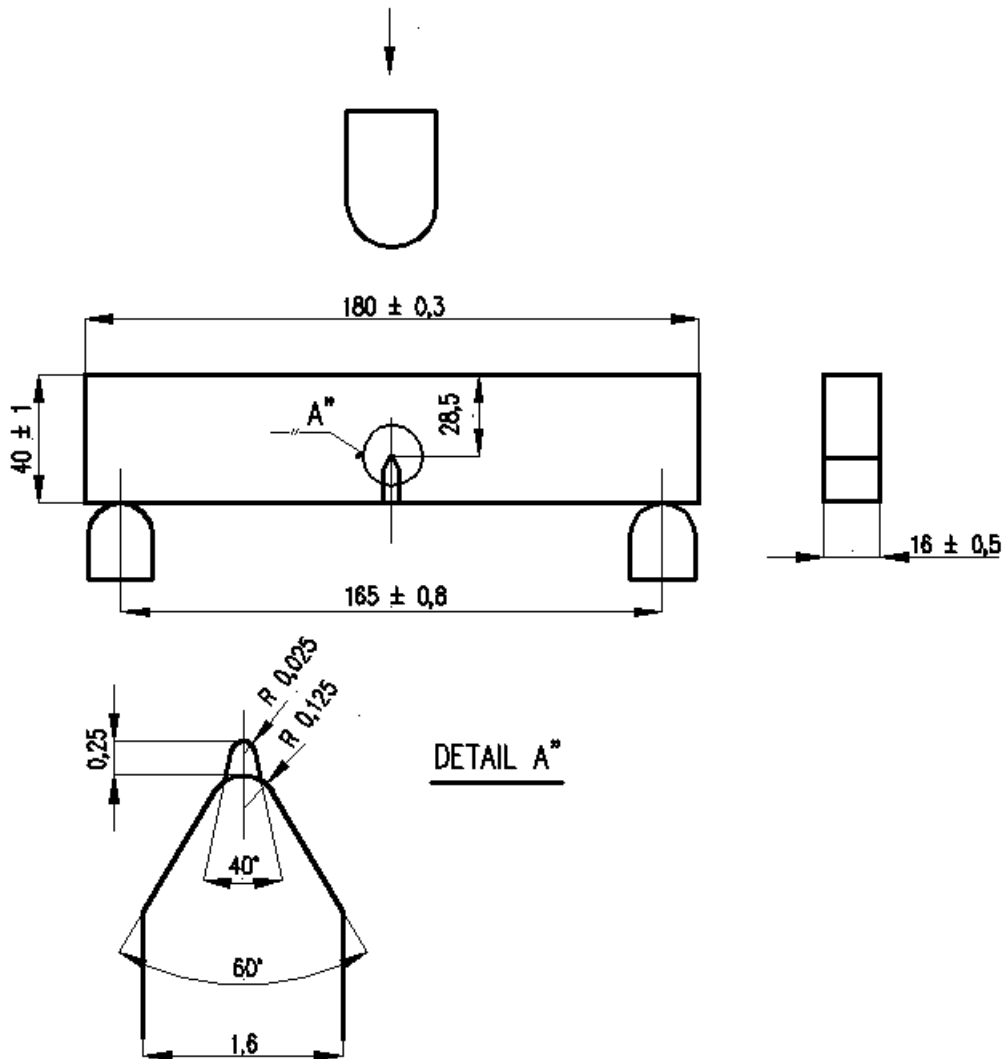


Fig. 4.15 A schematic of DT test for Specimen 16.

The test procedure is described in ČSN 420340 Impact bend test for large bodies or in ASTM Standard E 604-83 Standard Test Method for Dynamic Tear Testing of Metallic Materials. This test is performed at different temperatures of the specimen. Dependence of energy E_{DT} on temperature determines for each temperature the energy needed for crack growth to fracture. Because in these tests the component of energy to initiate a crack by embrittled notch is suppressed (hardening due to a cold-pressed notch), the results can be used after some adjustments to construct the crack arrest temperature (CAT) curve or the entire fracture analysis diagram (FAD) proposed to examine the admissibility of sharp crack-like defects. To obtain the CAT curve, test results must be transformed from the coordinate system of energy -

temperature to the system of nominal stress - temperature. Figure 4.16 shows the diagram of the transition curve of DT energy - temperature.

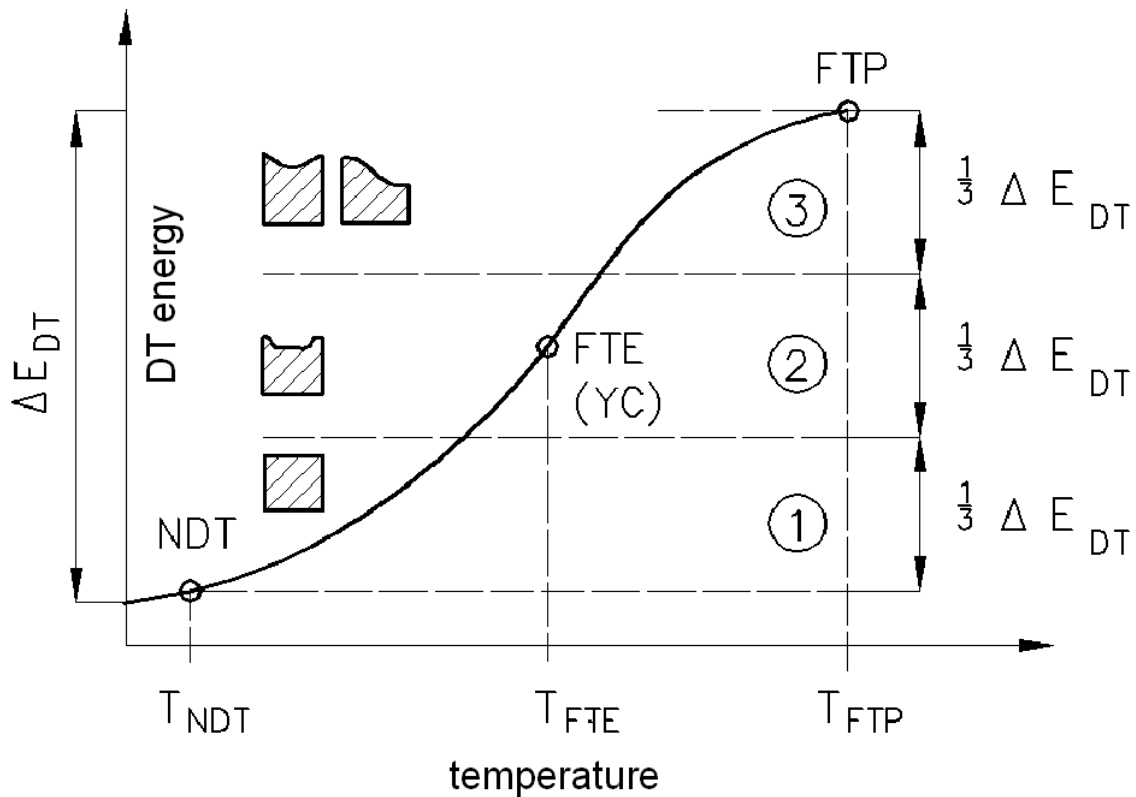


Fig. 4.16 Diagram of transition curve of DT energy – temperature

At the lower part of the diagram numbered (1) and extending into 1/3 range between the lower and upper energy level, the temperature t_{NDT} is situated. With the temperature t_{NDT} the nominal stress $\sigma = 45 \div 55$ MPa is associated, below which unstable cracks do not propagate. In the middle third (numbered (2)), there is the temperature t_{FTE} (transition temperature of elastic fracture) - the highest temperature at which an unstable crack growth can occur at stress below the yield strength. While there exists a standardized procedure for determination of t_{NDT} , position of FTE point is put by estimate to the middle of the middle third (see Fig. 4.16). Because the transition curve is very steep here, this option does not lead to any larger error in determining the temperature t_{FTE} . In the last third of the diagram, FTP point and the corresponding temperature t_{FTP} - transit temperature of plastic fracture are situated. If the operating temperature exceeds t_{FTP} , then the structure may only fail by a ductile fracture. Figure 4.17 shows the temperature dependence E_{DT} for S355J2H grade steel determined on Specimens 16 ČSN420340.

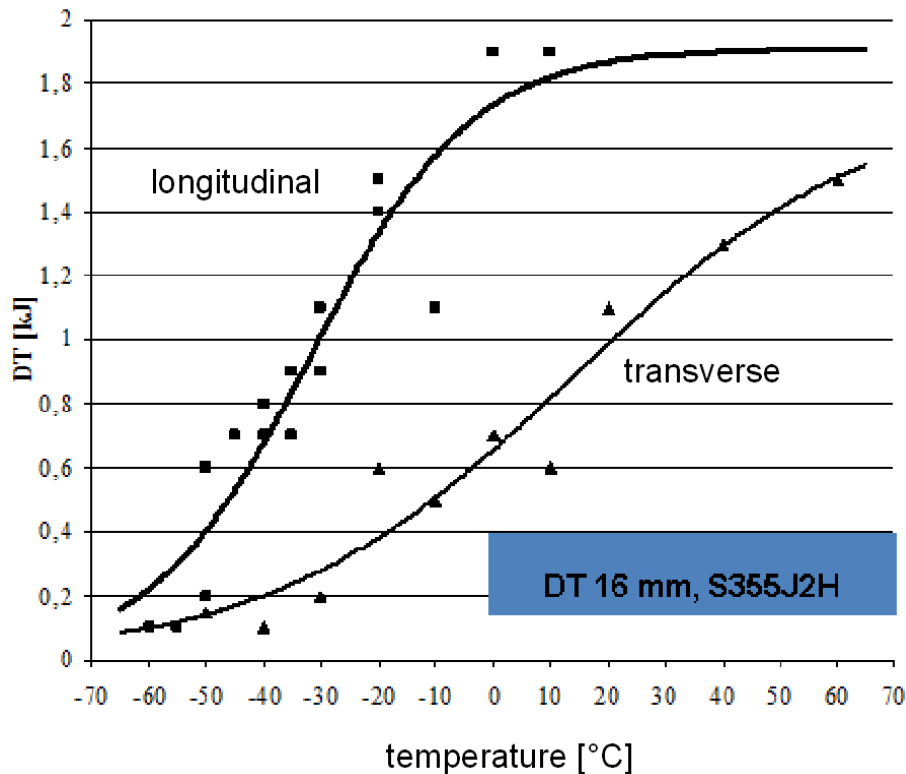


Fig. 4.17 Temperature dependence E_{DT} pro S355J2H grade steel determined on Specimen 16 ČSN 420340.

4.3 Philosophy based of fracture mechanics

4.3.1 The general temperature dependence of fracture toughness

Also the fracture toughness determining the resistance of materials against crack initiation and growth shows a transition behaviour due to changes in temperature or strain rate. With increasing temperature the yield strength declines and thus at the same value of applied stress the plastic zone at the crack tip gets larger and consequently the crack driving force and thereby also the fracture toughness increases. Fracture toughness can be characterized either by a single value of relevant parameter (K_{IC} , δ_c , J_{IC}) or the dependence of the corresponding parameter on the increment in crack length Δa (the so called J-R curves or $\delta - R$ curves).

The general scheme of the temperature dependence of static fracture toughness was compiled in the Institute of Physics of Materials (IPM) Brno based on the analysis of specimens of C(T) and SENT(B3) types, 23 mm thick (see Fig. 4.18). It can be assumed that

it will represent the temperature dependence of fracture toughness also for other thicknesses and other shapes of specimens.

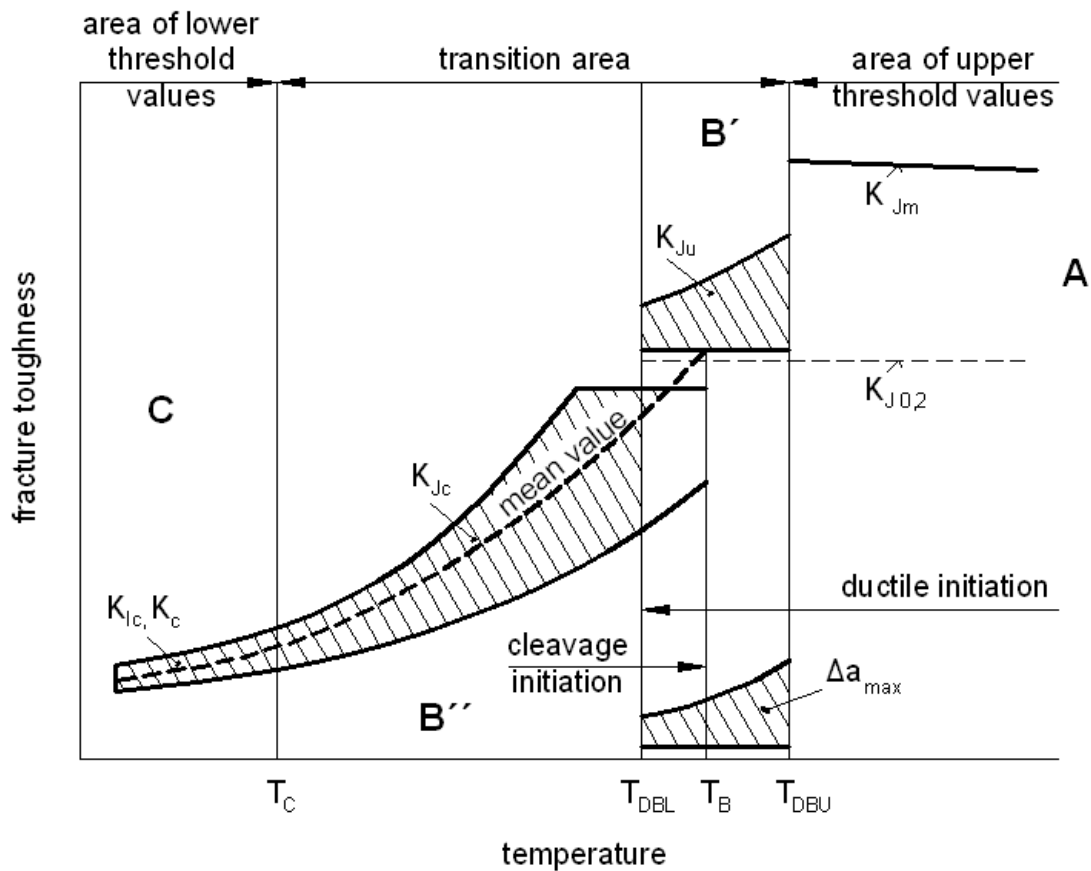


Fig. 4.18 The general scheme of the temperature dependence of fracture toughness

Temperature dependence of fracture toughness is divided into three parts.

Zone C is the area of lower threshold values of fracture toughness characterized by a critical value of the stress intensity factor K_{IC} , if the conditions of plane strain are met, and K_C when not.

Zone A is the area of upper threshold values of fracture toughness. The value $K_{J,0.2}$, converted from the value $J_{i,0.2}$ using the relationship (30.2), characterizes the initiation of the ductile stable crack growth.

In Zone B, the transition temperature T_B indicates such temperature, below which unstable fractures occur (after a certain blunting of the tip of pre-prepared fatigue crack) by cleavage initiation. In this case, the measured fracture toughness lies in the scattered field marked K_{JC} in Figure 4.18. Above T_B , unstable fractures occur after a stable growth of ductile

crack with length Δa . It results from Figure 4.18 that stable growth of ductile crack prior to an unstable fracture can take place in the temperature range from T_{DBL} to T_{DBU} . The corresponding values of fracture toughness then lie in the scattered field marked K_{J_u} . In terms of engineering practice, the course of fracture toughness K_{J_C} from the temperature T_C to the temperature T_B is important. Fracture toughness in this area is characterized by parameters J_{IC} or δ that are determined by standardized procedures of elastoplastic fracture mechanics.

Procedures for determining the fracture toughness are based on loading a specimen provided with a notch and fatigue crack performed by cycling and loaded by a slowly increasing force that opens the crack by a constant speed of movement of the cross-arm of an electromechanical testing machine or constant speed of movement of the piston rod of a servohydraulic testing machine and scanning the force - crack opening displacement (COD) dependence or force – force displacement dependence. Two types of specimens are most often used for fracture toughness testing.

- 1) Compact tension specimen, known as C (T) in Anglo-Saxon literature, is a specimen with thickness B and width W (see Fig. 4.19) subjected to tensile load. The width of the specimen $W = 2 \cdot B$
- 2) Bend test specimen, known as SE (B) in Anglo-Saxon literature, where B is the thickness of the specimen and W is the width (see Fig. 4.20) subjected to three-point bending. The width of the specimen $W = 2 \cdot B$ and/or $W = B$. Spacing of supports is equal to $S = 4 \cdot W$.

To measure the crack opening in SE(B) specimen, or crack opening and/or force displacement in C(T) specimen, clip gages are used (see Fig. 4.21 and 4.22).

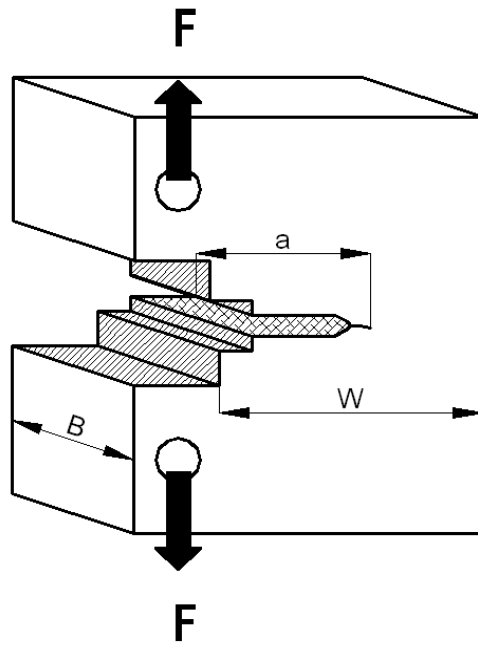


Fig. 4.19 Compact specimen of width W and thickness B

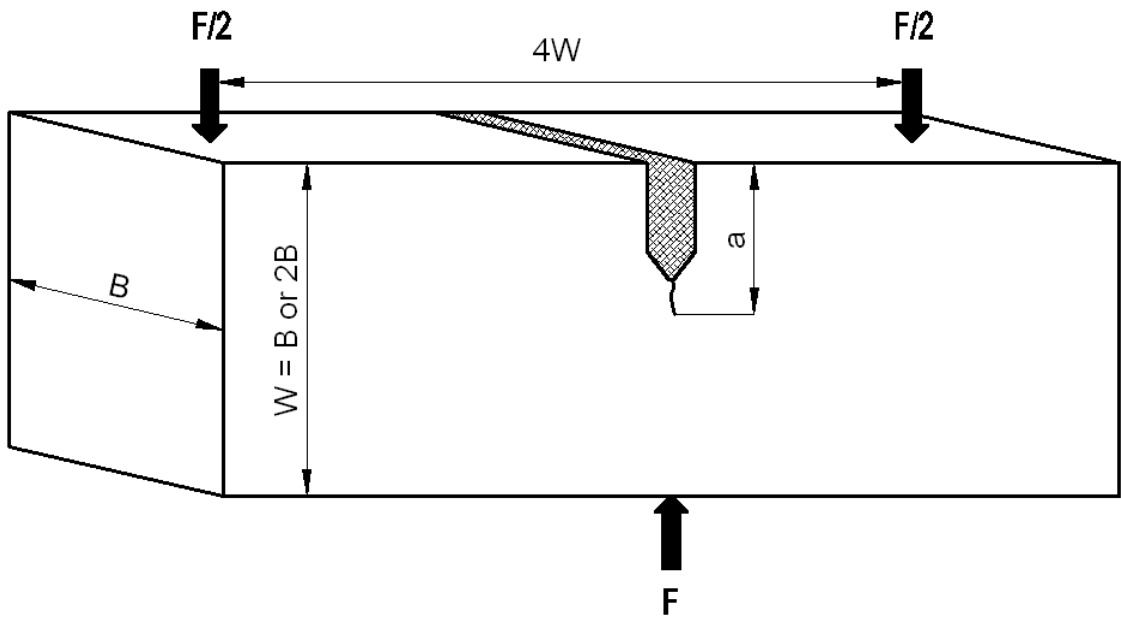


Fig. 4.20 Bend specimen of width W and thickness B



Fig. 4.21 Experimental test of fracture toughness at room temperature using the compact tension specimen

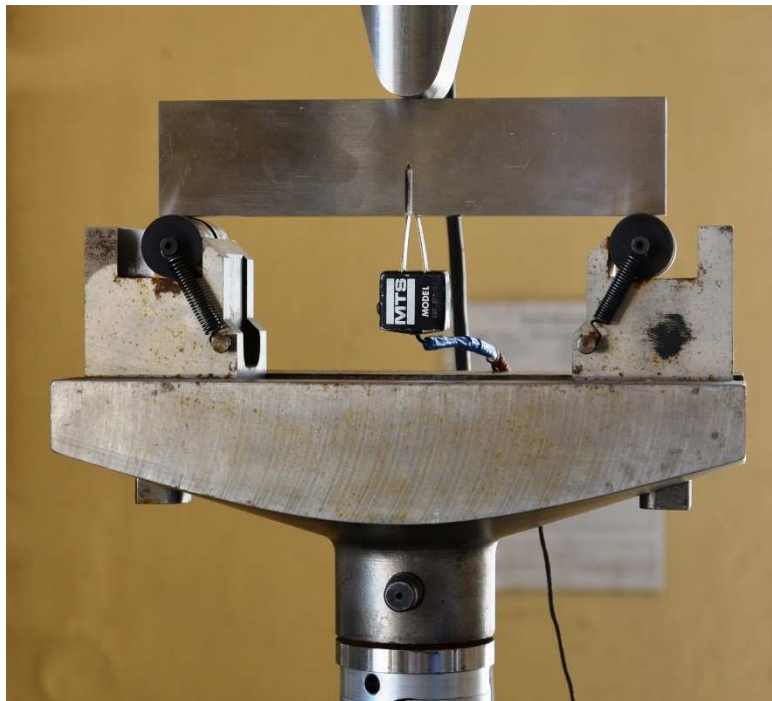


Fig. 4.22 Experimental test of fracture toughness at room temperature using the bend test

4.3.2 Plane-strain fracture toughness K_{IC}

The test procedure is described in ČSN EN ISO 12737 Metallic materials - Determination of plane-strain fracture toughness. Figure 4.23 shows three basic types of dependence of force - crack opening corresponding to a sudden fracture in the area where the linear elastic fracture mechanics applies.

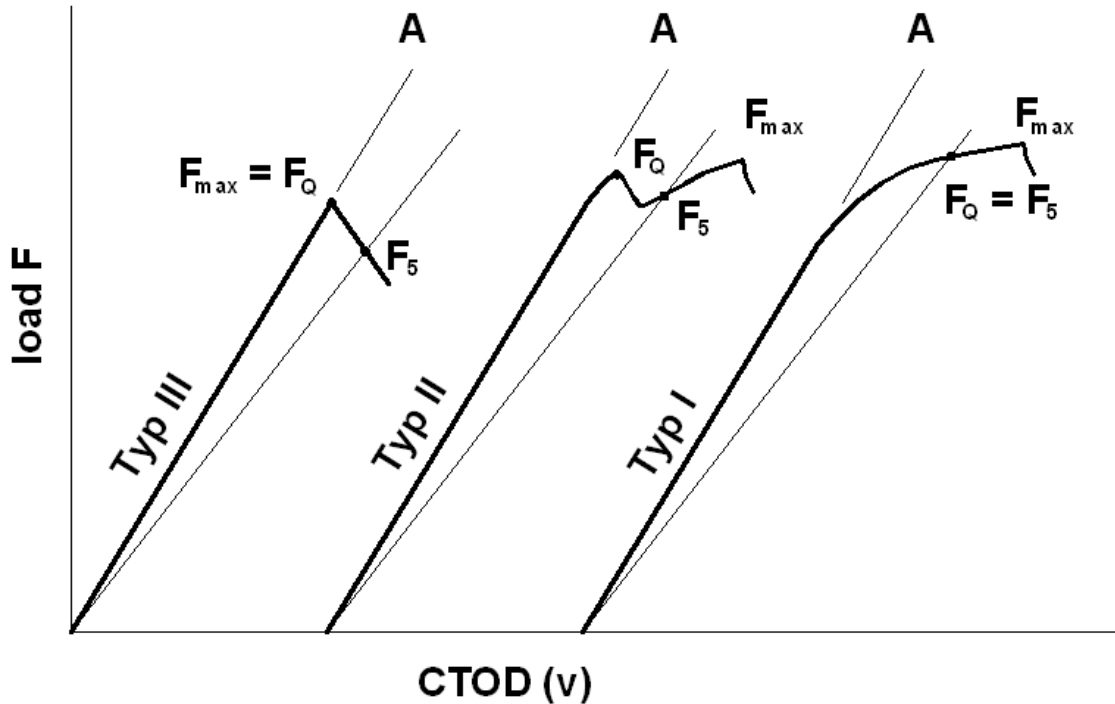


Fig. 4.23 Three types of dependence of force - CTOD corresponding to a sudden fracture in the area where the linear elastic fracture mechanics applies

From the record obtained during the test, the value of force F_Q is determined by constructing a secant $0F_5$ from point 0 with slope $(F/V)_5 = 0.95 \cdot (F/V)_0$, where $(F/V)_0$ is the slope of a tangent line of the linear part of record $0A$. For the selected type of a specimen, the value of K_Q is determined in $\text{MPa}\cdot\text{m}^{1/2}$. K_Q value for the bend test specimen is calculated from equation

$$K_Q = F_Q \frac{S}{BW^{3/2}} f(a/W) \quad (4.1)$$

where S is the spacing of supports and $f(a/W)$ is

$$f(a/W) = 3(a/W)^{1/2} \cdot \frac{1,99 - (a/W)(1 - a/W) [2,15 - 3,93(a/W) + 2,7(a/W)^2]}{2(1 + 2a/W)(1 - a/W)^{3/2}} \quad (4.2)$$

K_Q value for the compact tensile specimen is calculated from equation

$$K_Q = \frac{F_Q}{BW^{1/2}} \cdot f(a/W) \quad (4.3)$$

For $f(a/W)$ it applies that

$$f(a/W) = (2 + a/W) \cdot \frac{0,886 + 4,64(a/W) - 13,32(a/W)^2 + 14,72(a/W)^3 - 5,6(a/W)^4}{(1 - a/W)^{3/2}} \quad (4.4)$$

K_Q value may be considered a valid K_{IC} value provided that

$$a, (W - a), B \geq 2,5 \left(\frac{K_Q}{R_{p0,2}} \right)^2 \quad (4.4)$$

where $R_{p0,2}$ is the conventional yield strength of the material in the environment and at test temperature.

4.3.3 Determination of fracture toughness in the transition region

In the transition area, an unstable fracture occurs either after the tip of the crack is blunted by plastic deformation and/or after the stable ductile crack growth.

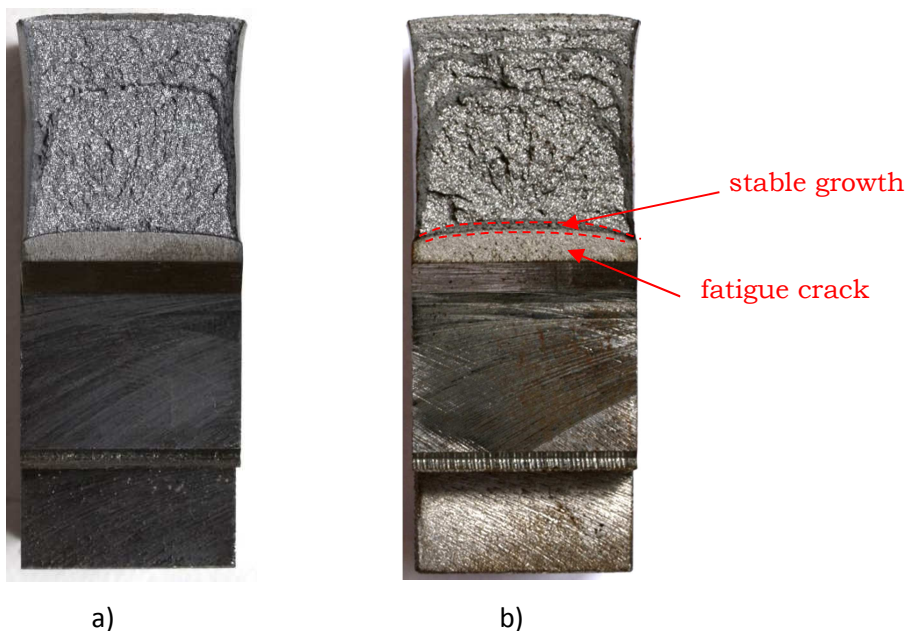


Fig. 4.24 Fracture surfaces of specimens broken by a sudden unstable fracture
a) after tip blunting by plastic deformation
b) after stable ductile crack growth.

The fracture behaviour in this area, given the extent of plastic deformation at the tip of the crack, is described by parameters of elastoplastic fracture mechanics. Fracture toughness is then characterized by a critical value of crack opening δ_c or critical value of the J-integral J_{IC} . The test procedure is described in ČSN 420347 Fracture toughness of metals on static loading.

4.3.3.1 Fracture toughness determined from crack-tip opening displacement

Dependence of the force F – notch opening displacement v is monitored during the test (see Fig 4.25). From the obtained record, the plastic notch opening displacement v_{CP} is subtracted.

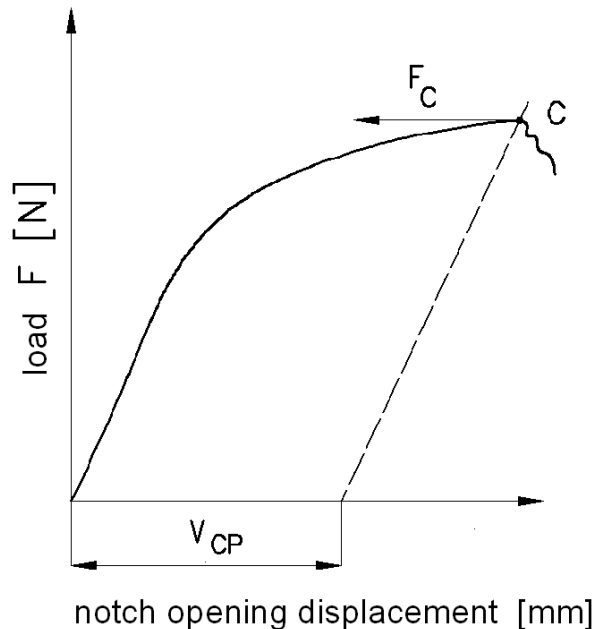


Fig. 4.25 Dependence of the force F on the notch opening displacement v monitored during the test to determine δ_c

Critical crack tip opening is calculated from the relationship

$$\delta_C = \delta_{el} + \delta_{pl} = \frac{(1-\nu^2)K_C^2}{2R_e E} + \frac{r_p(W-a)V_p}{r_p(W-a)+a} \quad (4.5)$$

where

K_C is calculated from equation (4.1) or (4.3) (according to the type of specimen used). Force F_Q is substituted by the value of force F_C ,

V_{CP} is a plastic component of the notch opening

r_p is the rotational factor in the plastic range. It is calculated from the relationship

$$r_p = 0,4(1 + \alpha) \frac{a S_n}{W R_e} \quad (4.6)$$

where

R_e is the yield strength of material

S_n is the nominal stress calculated for the bend test specimen from equation

$$S_n = \frac{1,5.F_C.L}{B(W - a)^2} \quad (4.7)$$

For the compact tension specimen, the nominal stress S_n is calculated from equation

$$S_n = \frac{2.F_C.(2W + a)}{B(W - a)^2} \quad (4.8)$$

The coefficient α is equal to $\alpha = 0.1$ for bend test specimen. For the compact tension specimen, the coefficient α is calculated from equation

$$\alpha = 2 \left[\left(\frac{a}{b} \right)^2 + \frac{a}{b} + \frac{1}{2} \right]^{\frac{1}{2}} - 2 \left(\frac{a}{b} + \frac{1}{2} \right) \quad (4.9)$$

where $b = W - a$

The calculated value of δ_C is the fracture toughness δ_{IC} determined from the crack tip opening displacement, if the condition

$$a, (W - a) \leq 50.\delta_C \quad (4.10)$$

is met.

For comparability of fracture toughness, the critical crack opening displacement δ_C can be expressed as the stress intensity factor K_{δ_C} using the relationship

$$K_{\delta_C} = \sqrt{\frac{R_{p,0,2} \cdot E}{1 - \nu^2}} \cdot \delta_C \quad (4.11)$$

4.3.3.2 Fracture toughness determined from J-integral

Dependence of force F on displacement of force f to the point of instability is monitored during the test (see Fig 4.26), from which the area of diagram under the load curve is determined. The area of A_{CP} is determined by planimetry or other equivalent method. Critical value of J_C is calculated from the relationship

$$J_C = J_{CE} + J_{CP} = \frac{1-\nu^2}{E} \cdot K_C^2 + \frac{X_i \cdot A_{CP}}{B(W-a)^2} \quad (4.12)$$

where

K_C is calculated from equation (4.1) or (4.3) (according to the type of specimen used). Force F_Q is substituted by the value of force F_C ,

The coefficient X_i is equal to $X_i = 2$ for bend test specimen and $X_i = 2 + 0,522(1 - a/W)$ for compact tensile specimen.

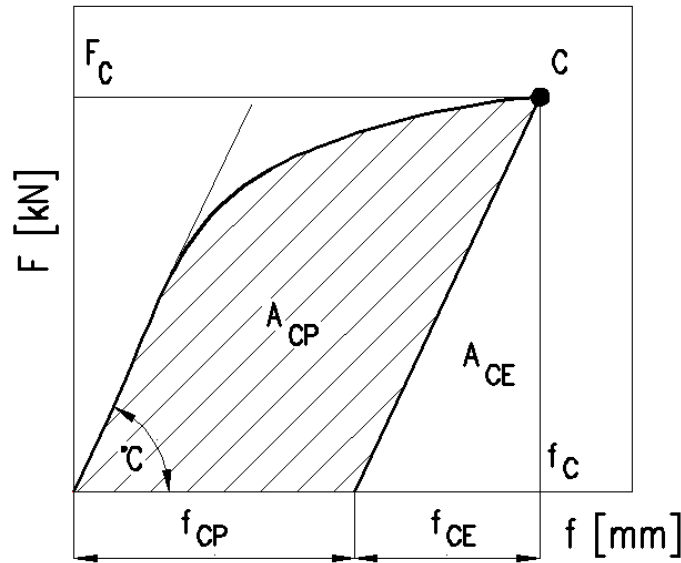


Fig. 4.26 Force F – force displacement f dependence measured during the test to determine J_{IC}

The calculated value of J_C can be considered the fracture toughness J_{IC} , if the condition

$$a, B, (W - a) \geq 50 \cdot \frac{J_C}{R_e + R_m} \quad (4.13)$$

is met.

For comparability of fracture toughness, the critical value of J_C can be expressed as the stress intensity factor K_{IC} using the relationship

$$K_{IC} = \sqrt{\frac{E}{1-\nu^2} \cdot J_C} \quad (4.14)$$

4.3.4 Determination of fracture toughness $\delta_{0,2}$ and $J_{0,2}$ by multi-body testing

The aim of the tests is to determine the dependence $\delta - \Delta a$ and/or $J - \Delta a$ on a series of at least six specimens of the same size and about the same length of the initial fatigue crack. Crack length increment is measured on the fracture surface of the broken specimen and the corresponding values of δ and J are determined by calculation. The individual specimens are subjected to loads of different values of force displacement $f_1, f_2, f_3 \dots f_n$ so that various crack length increments Δa_n arise (see Fig 4.27).

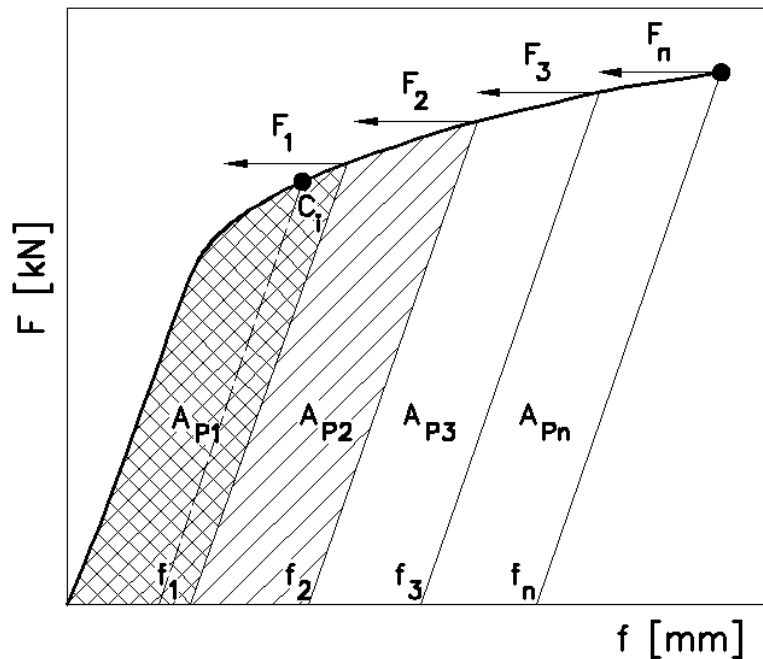


Fig. 4.27 Force F – force displacement f dependence to determine the crack length increments Δa .

After reaching the selected force displacement, the specimen is relieved and the crack increment is visualized by staining the specimen in an oven at temperature about 300°C (see Fig. 4.28). The specimen must be broken apart so as to avoid excessive deformation of the fracture surfaces (e.g. in liquid nitrogen) and crack increments Δa are measured on these fracture surfaces.



Fig. 4.28 Stable crack growth highlighted by staining specimen after its relieving in an oven at 300°C and after being broken apart in liquid nitrogen

Crack increment is measured at 9 evenly-spaced points across the specimen thickness. The measurement accuracy shall be 0.05 mm. The amount of crack length increment Δa is calculated from the relationship

$$a = \frac{1}{8} \left(\frac{\Delta a_1 + \Delta a_9}{2} + \sum_2^8 \Delta a_n \right) \quad (4.15)$$

The value of δ adjusted for the increase in crack length is calculated from equation (4.5) by substituting $(a + \Delta a_i)$ instead of a . The value of J-integral adjusted for the increase in crack length is calculated from the equation

$$J = J_o \left[1 - \frac{(0,75 \cdot X_i - 1) \Delta a}{W - a_o} \right] \quad (4.16)$$

where J_o is value of J for $\Delta a = 0$ and coefficient X_i depends on the type of the body (see Sec. 4.3.3.2).

For $\delta - \Delta a$ dependence, it must apply that $\delta \leq \delta_{\max}$ and $\Delta a \leq \Delta a_{\max}$, where

$$\delta_{\max} \leq \min[B, (W - a)] \cdot \frac{1}{30} \quad (4.17)$$

$$\Delta a_{\max} \leq 0,1 (W - a) \quad (4.18)$$

For J – Δa dependence, it must apply that $J \leq J_{\max}$ and $\Delta a \leq \Delta a_{\max}$, where

$$J_{\max} \leq \min[B, (W - a)] \cdot \frac{R_{p0,2} + R_m}{30} \quad (4.19)$$

$$\Delta a_{\max} = 0,06 (W - a_o) \quad (4.20)$$

Conditions for the validity of δ , J and Δa are schematically shown on Fig 4.29.

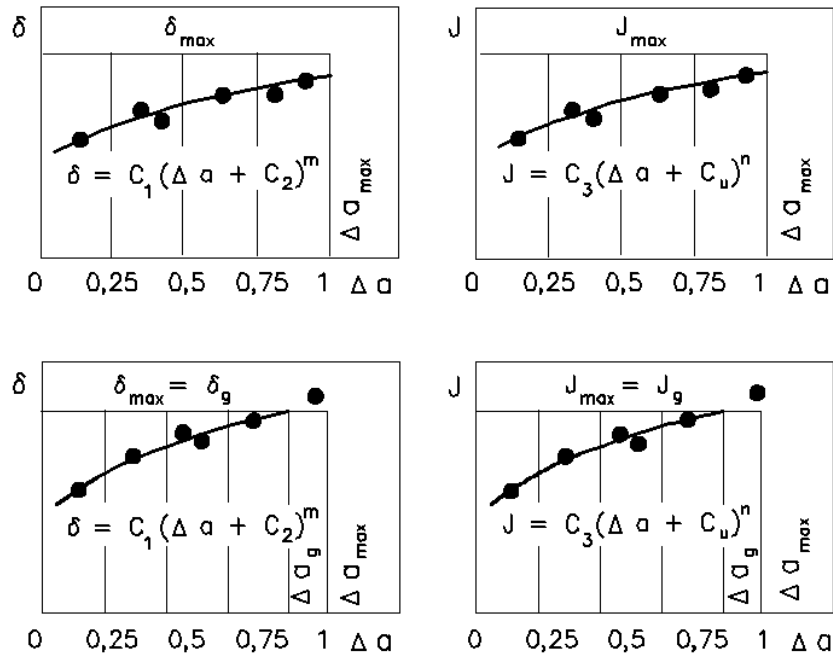


Fig. 4.29 Definition of validity of values for the determination of dependences $\delta - \Delta a$ and $J - \Delta a$

Values of crack length increments for each test specimen are to be evenly distributed between 0 and Δa_{max} . At least one Δa value must lie in the first and last quarter of Δa_{max} . Use the method of least squares to fit the curve with valid values

$$\delta = C_1(a + C_2)^m \quad (4.21)$$

$$J = C_3(a + C_4)^n \quad (4.22)$$

The values of δ and J corresponding to $\Delta a = 0.2$ mm are denoted $\delta_{0,2}$ and $J_{0,2}$. To determine $C_1, C_2, C_3, C_4, m,$ and n constants, it is possible to use following relationships

$$\delta_{0,2} = C_1(0,2 + C_2)^m \quad (4.23)$$

$$J_{0,2} = C_3(0,2 + C_4)^n \quad (4.24)$$

Through characteristics of $J_{0,2}$ the fracture toughness may be expressed at the crack growth $\Delta a = 0.2$ mm by the relationship

$$K_{0,2} = \sqrt{\frac{E \cdot J_{0,2}}{1 - \nu^2}} \quad (4.25)$$

4.3.5 Determination of the reference temperature T_0

The reference temperature T_0 is the temperature, for which the median $K_{JC(\text{med})}$ of the three-parameter Weibull distribution of fracture toughness determined on specimens with thickness of 25.4 mm is equal to the value of $K_{JC(\text{med})} = 100 \text{ MPa}\cdot\text{m}^{1/2}$. The temperature T_0 defines the fracture toughness of carbon and low alloy steels with yield strength range from 275 to 825 MPa and weld metals of these steels. The test procedure for determination of temperature T_0 is described in ASTM Standard E1921 – 10 Standard Test Method for Determination of Reference Temperature, T_0 , for Ferritic Steels in the Transition Range. Estimation of reference temperature T_0 can be done based on the results of impact bend tests by determining the temperature, for which the impact energy determined on specimens Charpy V is equal to $KV = 28 \text{ J}$. The estimate of the temperature T_0 may be performed according to the relationship

$$T_{o(\text{estimate})} = T_{CVN} + C \quad (4.26)$$

where constant C is a function of the shape and size of test specimens used to determine the fracture toughness. For CT specimen with a thickness of 25 mm is $C = -18^\circ\text{C}$; for Charpy specimen with a fatigue crack is $C = -50 \text{ OC}$.

To calculate the median of fracture toughness, it is necessary to get at least six valid K_{JC} values at selected test temperature satisfying the condition

$$K_{JC} \leq (E \cdot R_{p,0.2} \cdot b_o / 30)^{1/2} \quad (4.27)$$

For steels with a body centered cubic (BCC) lattice with yield strength from 275 to 825 MPa, the fracture toughness distribution can be described by the relationship

$$P_f = 1 - \exp \left[- \left(\frac{K_{JC} - K_{\min}}{K_o - K_{\min}} \right)^b \right] \quad (4.28)$$

where $K_{\min} = 20 \text{ MPa}\cdot\text{m}^{1/2}$ and $b = 4$.

It follows that $K_{JC} = K_o$ for $P_f = 1 - e^{-1} = 0.63212$. K_o is therefore approximately 63% quantile of the given distribution. Parameter K_o depends on the temperature

$$K_o = \left[\sum_{i=1}^N (K_{JC(i)} - K_{\min})^4 / N \right]^{1/4} + K_{\min}. \quad (4.29)$$

Median $K_{JC(\text{med})}$ is then calculated from the equation

$$K_{Jc(med)} = [\ln(2)]^{1/4} (K_o - K_{\min}) + K_{\min} \quad (4.30)$$

Reference temperature T_0 is then calculated from the equation

$$T_o = T - \frac{1}{0,019} \ln \left[\frac{K_{Jc(med)} - 30}{70} \right] \quad (4.31)$$

For cases where the test specimens used for the determination of the reference temperature T_0 have a different thickness than 25,4 mm, the above cited standard uses the correction of the specimen size derived on the basis of the theory of the weakest link in the form

$$K_{Jc(X)} = K_{\min} + [K_{Jc(o)} - K_{\min}] \left(\frac{B_o}{B_x} \right)^{1/4} \quad (4.32)$$

where $K_{\min} = 20 \text{ MPa}\cdot\text{m}^{1/2}$

Temperature dependence of fracture toughness constructed on the knowledge of the reference temperature T_0 is called the MASTER curve. For $P_f = 0.50$, it is described by the equation

$$K_{Jc(med)} = 30 + 70 \exp[0.019(T - T_o)] \quad (4.33)$$

It then applies for $P_f = 0.63$ that

$$K_o = 31 + 77 \exp[0.019(T - T_o)] \quad (4.34)$$

It then applies for the general probability P_f that

$$K_{Jc} = 20 + \{11 + 77 \exp[0,019(T - T_o)]\} \left[\ln \left(\frac{1}{1 - P_f} \right) \right]^{1/4} \quad (4.35)$$

For selected probabilities we then get

$$P_f = 0,05 \quad K_{Jc} = 25,23 + 36,64 \exp[0,019 (T - T_o)] \quad (4.36)$$

$$P_f = 0,5 \quad K_{Jc} = 30,04 + 70,25 \exp[0,019 (T - T_o)] \quad (4.37)$$

$$P_f = 0,95 \quad K_{Jc} = 34,47 + 101,3 \exp[0,019 (T - T_o)] \quad (4.38)$$



Summary of terms

After studying the chapter, following terms should be clear to you:

- Unstable fracture, brittle fracture
- Transition temperature
- FATT
- DWT, DWTT
- Compact tensile specimen, Bend test specimen
- Stable crack growth
- Reference temperature T_0
- Life curve $\epsilon_{at} - N_f$
- MASTER curve

Questions

- 12) What is the linear elastic fracture mechanics based on?
- 13) What materials is the elastoplastic fracture mechanics used for?
- 14) Which of the modes of loading is the most important for practice?
- 15) What does the stress intensity factor K express?
- 16) What do we mean by the crack driving force?
- 17) What do we mean by resistance to crack growth R ?
- 18) When the sudden unstable crack growth occurs?
- 19) What determines the size of the plastic zone?
- 20) What determines the fracture toughness K_{IC} of the material?
- 21) What parameters expressing the fracture toughness of the material in the elastoplastic fracture mechanics do you know?

22) What is J - R curve?



Tasks to solve

- Calculate the critical length of crack a_c for an infinitely wide plate under tensile stress $\sigma = 100$ MPa and made of a material having a fracture toughness $K_C = 60$ MPa.m^{1/2}.
- Calculate the critical stress for the formation of a sudden unstable fracture of an infinitely wide plate with a crack length of $2a = 20$ mm made of a material having a fracture toughness $K_C = 80$ MPa.m^{1/2}.
- Calculate the size of a plastic zone in case of plane stress and plane strain for the stress intensity factor $K_I = 60$ MPa.m^{1/2} and material yield strength $R_{p,0.2} = 900$ MPa for the case where there is the redistribution of stress in the area around the crack tip.

5. Procedures for determining the creep characteristics of the metallic materials



Study time: 3 hours



Objective After reading this chapter, you should be able to:

- Define the concept of creep.
- Enumerate the factors that affect the application of creep of materials.
- Explain the concept of limiting temperature T_g .
- Describe the creep curve $\epsilon - t$.
- List the basic characteristics of the creep resistance of material.
- Describe the division of creep tests.
- Describe the methods of extrapolating the results of creep testing.



Presentation

5.1 Definition of the concept of creep

Response of materials to applied external loads in terms of deformation can be divided into three basic types:

- 1) Elastic deformation - reversible, time independent. It depends only on the stress and temperature, because the modulus of elasticity is temperature dependent,
- 2) Anelastic deformation - reversible, time dependent,
- 3) Plastic deformation – irreversible component of deformation, time independent and/or time dependent (creep).

Except for steam boilers (19th century), all energy and chemical facilities operating under static loading at elevated temperatures were developed in the 20th century. All of these devices operate at temperatures at which it must be taken into account the time dependent deformation and related fracture processes.

The term creep means slow plastic deformation of the material taking place at elevated temperature under the action of the external load versus time. Generally, the response of equipment operating at elevated temperatures and the ability to apply creep depends on:

- level of loading,
- temperature,
- chemical composition of the material, and
- structure of the material.

5.2 Limit temperature T_g

In the temperature range, in which creep process is applied, the values of creep rupture strength are always lower than the yield strength of the material (see Fig. 5.1).

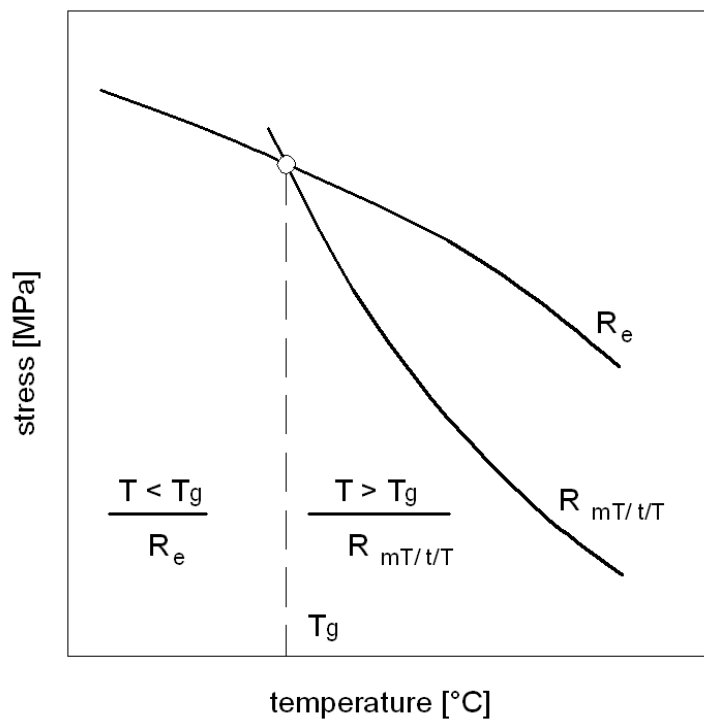


Fig. 5.1 Procedure for determining the limit temperature T_g

“Limit temperature” T_g is the temperature above which the application of creep must be considered in designing the structures as one of the main degradation mechanisms. It is defined as the intersection of the temperature dependence of the yield strength R_e ($R_{p,0.2}$) determined by tensile test and the temperature dependence of creep rupture strength $R_{mT/tT}$. (see Fig. 5.1). $R_{mT/tT}$ is a static tensile stress that leads to failure after time t at temperature T , and is determined by creep rupture tests. At the working temperature $T < T_g$, the creep rupture

strengths are significantly higher than the yield strength and thus it is not necessary to take this degradation mechanism into account when designing the structures. Therefore to determine the allowable stress, use the static yield strength (for low alloy steels $T < \text{about } 450^\circ\text{C}$). At the working temperature $T \geq T_g$, creep processes take place and creep strength $R_{mT/t/T}$ or creep limit $R_{\epsilon/t/T}$ is used for determining the allowable stress. The ratio of the working temperature T and the melting temperature T_t in K is known as homologous temperature.

5.3 Creep curve $\epsilon - t$

Creep curve indicates the time dependence of deformation at constant temperature and level of tension. The high temperature creep curve ($T \approx 0.4 T_t$ and above for steels and $T \approx 0.8 T_t$ for nickel-based alloys) distinguishes three time stages (see Fig. 5.2)

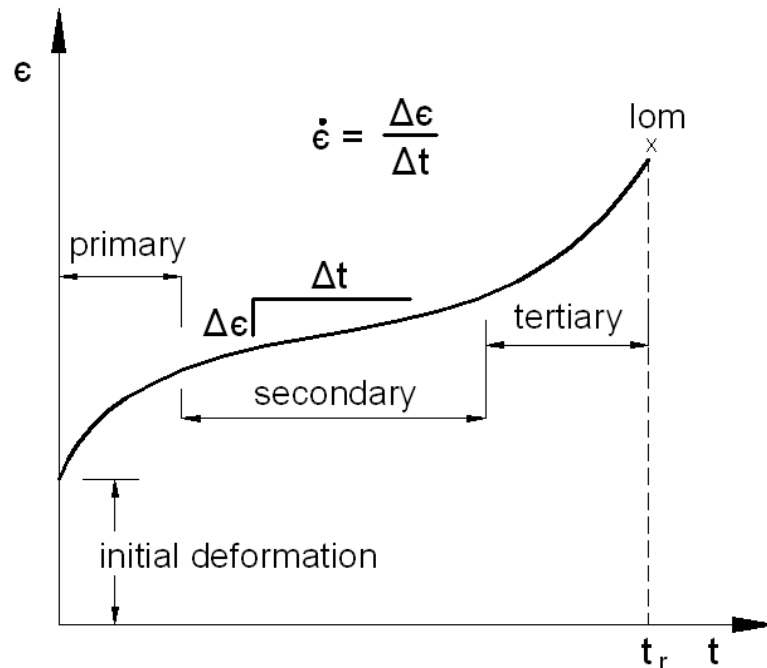


Fig. 5.2 Schematic representation of three time stages at the high temperature creep curve

In the first phase, known as a primary (transient) creep, creep velocity decreases with time because the deformation hardening is stronger than dehardening. At temperatures $T \leq 0.3 T_t$, where T_t denotes the melting point, the primary creep is the only strain response of the material. It is sometimes referred to as logarithmic creep and takes place even in the absence of thermal activation.

The second stage is characterized by a linear relationship between strain and time, and is called secondary creep. This type of creep occurs only at sufficiently high temperatures ($T \geq 0.4 T_f$) at which the recovery process is able to compensate the effects of deformation hardening. This type of creep is the most important from a practical standpoint. At stresses substantially lower than the yield strength, it represents a significant part of the overall life of components working at elevated temperatures. Conversely, if the applied stress is high, the secondary creep is reduced until the inflection point between the primary and tertiary creep.

The third stage, known as tertiary creep is characterized by the sharp increase in strain rate until fracture. Fractures are initiated as cavities at grain boundaries resulting in the intercrystalline character of fracture (see Fig. 5.3)

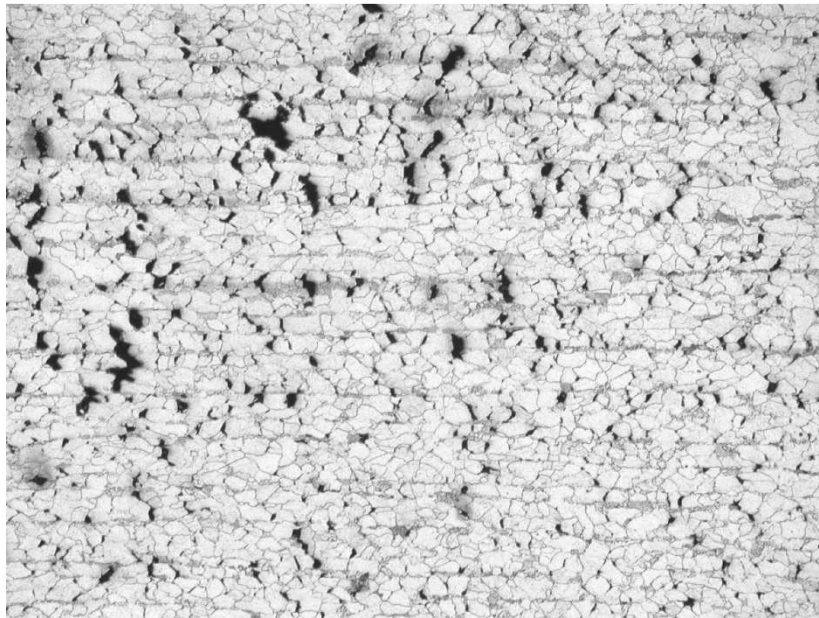


Fig. 5.3 Example of creep cavitation damage

5.4 Basic characteristics of the creep resistance of materials

The basic characteristics of the creep resistance of a material are:

- 1) Rate of secondary creep $\dot{\epsilon}_s = \frac{\Delta \epsilon}{\Delta t}$ - rate of creep in the secondary stage (stage of steady creep).
- 2) Creep rupture strength $R_{mT/tT}$ - tensile stress that causes a fracture at a selected temperature after a certain predetermined period of time.

- 3) Creep limit $R_{\varepsilon/t/T}$ – stress that causes deformation of a certain size at a selected temperature after a certain predetermined period of time. Typically, the creep limit for $\varepsilon = 0.2\%$ (construction of turbines), or $\varepsilon = 1.0\%$ (construction of boilers) is given. Calculation period typical for high pressure boilers and turbines is $2.25 \cdot 10^5$ hours and for aircraft engines up to $2 \cdot 10^4$ hours.

As auxiliary characteristics that govern the long-term plasticity of the material, the creep tests also determine the fracture elongation A_r [%] or fracture contraction Z [%].

5.5 Uniaxial creep testing of metallic materials in tension

For conducting creep tests, there is a generally defined schedule which indicates that it is necessary to perform the tests at 2 to 4 temperature levels in increments of 25 to 50°C, and at several stress values for each selected temperature, while it is desirable that the selected test stress is evenly divided into areas of low and high values. The shortest time to rupture should not be less than about 200 hours, and vice versa, the longest time to failure of the specimen must be at least 1/3 of the planned life of the material (this condition is often referred to as extrapolation ratio = 3). Also the highest value of test temperature is defined, which should not be higher against the anticipated working temperature by more than 50°C.

Creep tests of metallic materials are performed according to ČSN EN ISO 204 Metallic materials - Uniaxial creep testing – Method of test. The test consists in heating the specimen to a nominal temperature and its deformation by a constant tensile load or constant tensile stress applied in the direction of a longitudinal axis for a certain period of time or until fracture. Creep tests can be divided into:

- 1) Tests with measured deformation that allow to quantify the rate of secondary creep and creep limits $R_{\varepsilon/t/T}$ depending on the stress and temperature from creep curves $\varepsilon - t$ set using
 - continuous measurement of deformation over time, which allows to construct the entire creep curve, and
 - intermittent tests in which specimens are periodically relieved and deformation caused by creep is usually measured using a punch on specific part of the specimen.

Figures 5.4 to 5.6 show creep curves of steel grade P22 (10CrMo9-10) determined at temperatures of 575°C, 600°C and 625°C through a continuous measurement of deformation in time on specimens with an edge (see Sec. 5.5.1) with specific length of 100 mm.

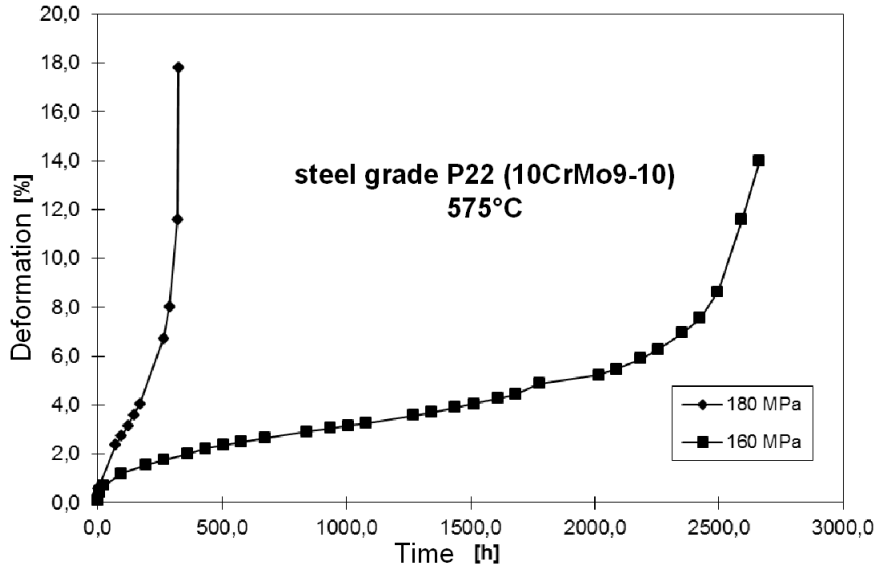


Fig. 5.4 Creep curves of P22 grade steel determined at 575°C at stresses of 160 and 180 MPa

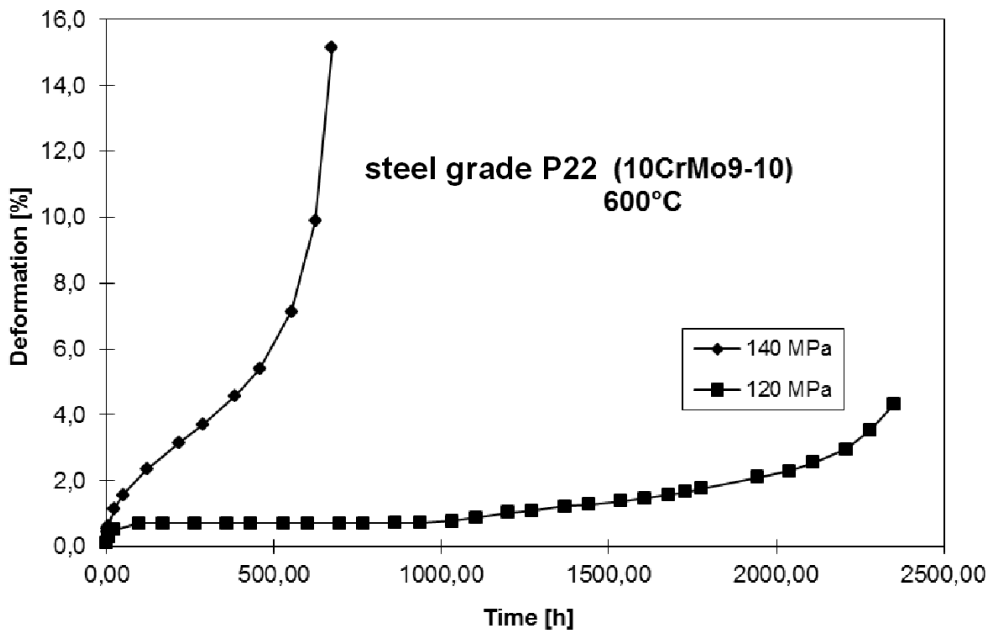


Fig. 5.5 Creep curves of P22 grade steel determined at 600°C at stresses of 120 and 140 MPa

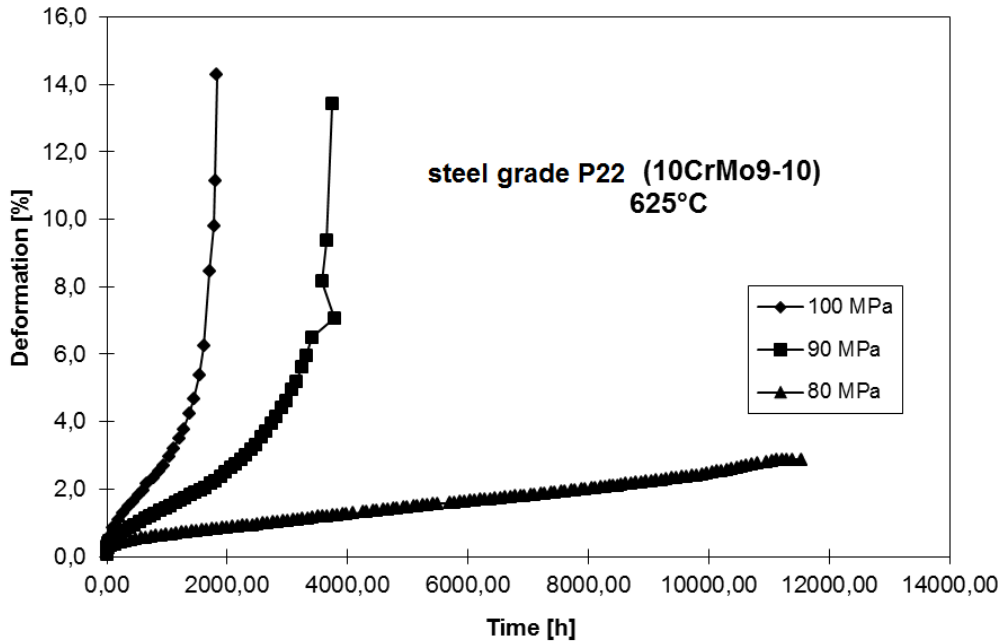


Fig. 5.6 Creep curves of P22 grade steel determined at 625°C at $\sigma = 80, 90$ and 100 MPa

Figure 5.7 then illustrates dependences of the rate of secondary creep on the stress for the above temperatures in log - log coordinates, which were determined from the measured creep curves.

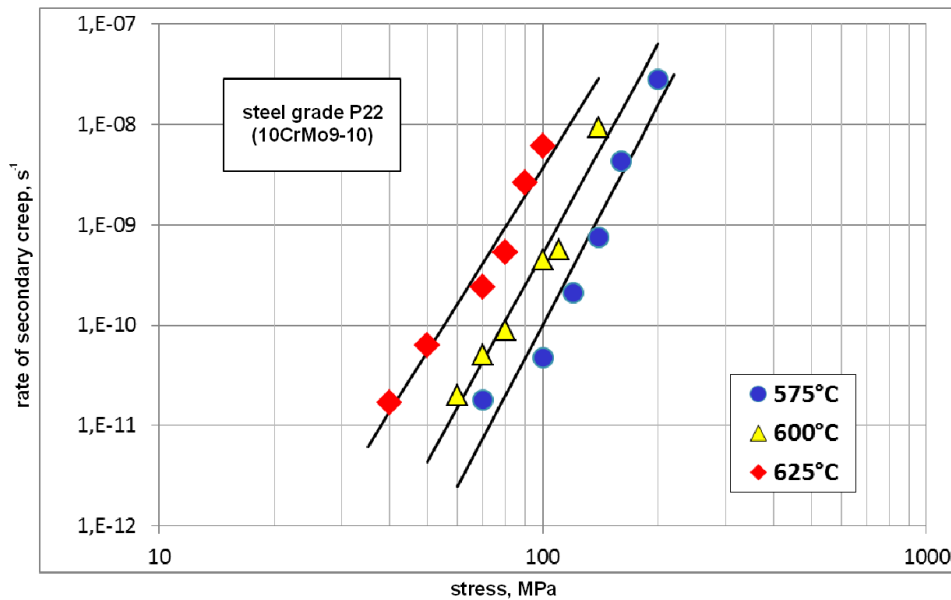


Fig. 5.7 Dependences of the rate of secondary creep on the stress for P22 grade steel at temperatures of 575°C, 600°C and 625°C.

- 2) Tests to failure under constant load for determining the creep rupture strength $R_{mT/tT}$. Creep strength values are generally determined on the basis of short-term creep tests (see Fig 5.8) and subsequent interpolation or extrapolation of the results for the calculation periods. Extending the testing period guarantees greater security and accuracy of extrapolation of the results of creep testing and allows for the verification of methods used for the transmission of results from short-term tests. Mandatory requirement for a credible extrapolation of the results of creep tests specified in ISO 6303 (and also in material standards of creep-resistant steels) is to achieve at least 30% of the time to fracture for which the results are extrapolated (i.e. just 30,000 hours for extrapolation to 100,000 hours).

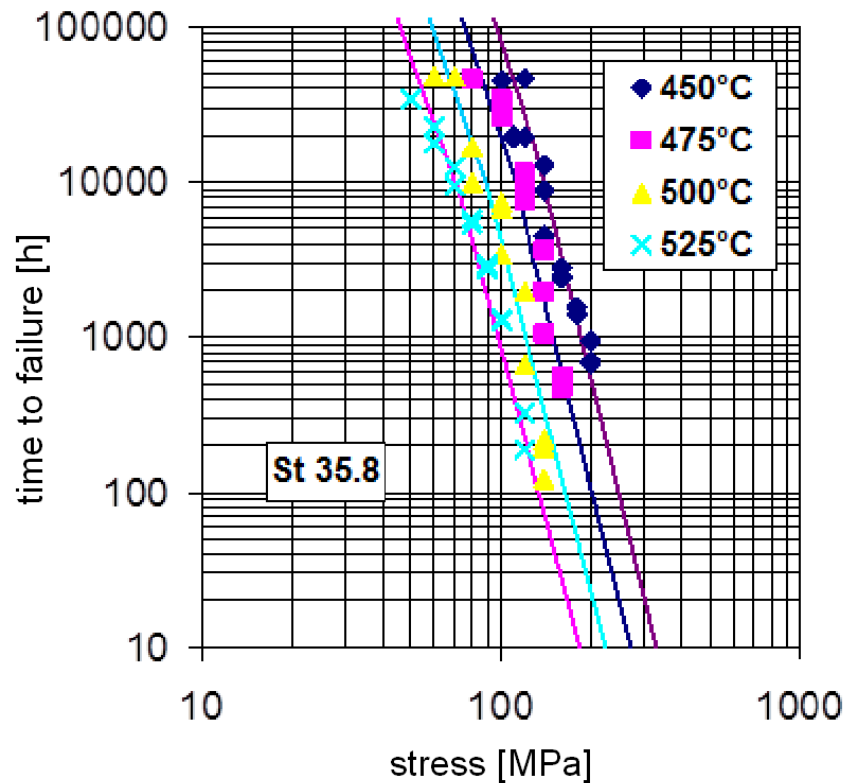


Fig. 5.8 Time to failure – stress dependences specified for St 35.8 grade steel for four temperatures

5.5.1 The shape and dimensions of test specimens

Most commonly used for creep tests are following specimens

- 1) smooth cylindrical test specimens with a recess (see Fig. 5.9, 5.10), and

2) smooth cylindrical test specimens with sharp edges (see Fig. 5.11) with a nominal diameter of $3 < D \leq 30$ mm. It generally applies for the initial specific length L_0 (length between the measured length marks on the specimen measured at ambient temperature before test) that $L_0 > 5D$. L_c is the test length (the length of the parallel portion of the tapered cross-section of the specimen). In special cases the cross-section of the specimen can be square, rectangular or have other shape.

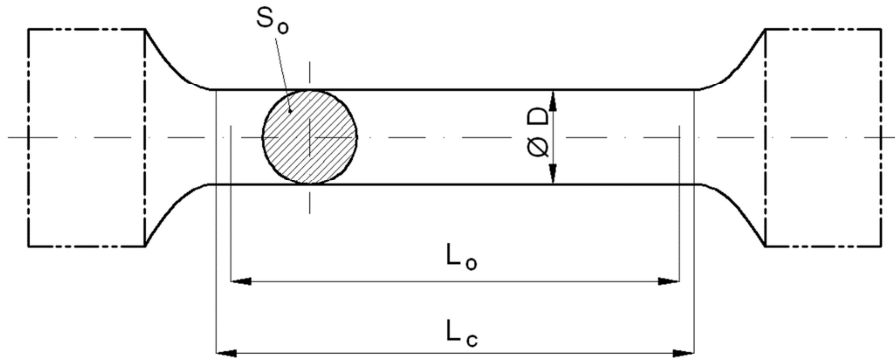


Fig. 5.9 Specimen with a recess and measured length inside the test length

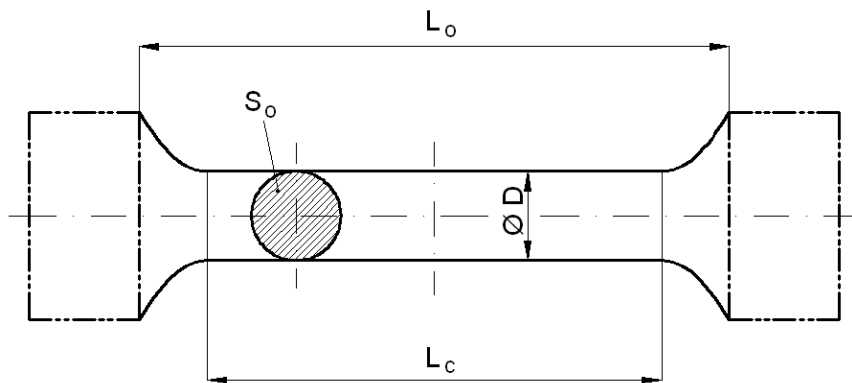


Fig. 5.10 Specimen with a recess and measured length outside the test length

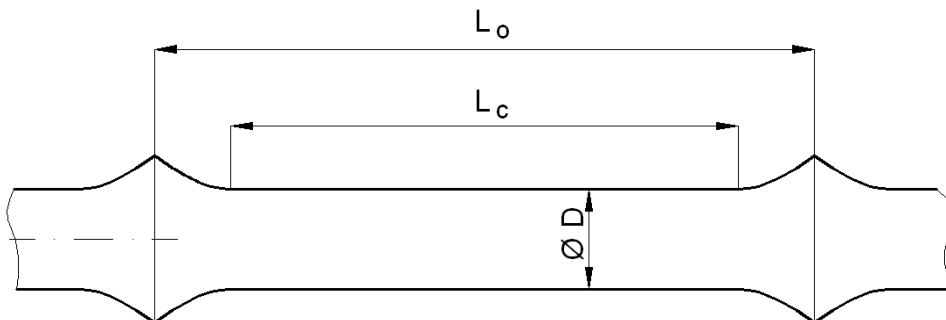


Fig. 5.11 Specimen with small sharp edges

5.6 Methods of extrapolating the results of creep testing

When designing energy and chemical facilities or structures whose components are subjected to both high temperatures and load during operation and therefore creep must be considered as one of the dominant degradation mechanisms, it is necessary to know the long-term creep characteristics. In the case of equipment components with a life expectancy of around 200,000 working hours (typical design life of fossil fuel fired boilers), it is necessary for obtaining the creep characteristics to use the results of shortened creep tests, since long-term testing is very time consuming and therefore costly. But it is still necessary to respect that for reliable determination of the creep rupture strength for 200,000 hours the longest time to rupture in the completed test at a given temperature must reach at least 70,000 hours (about 8 years). This condition is inevitable in development of new materials and determination of their creep resistance. In practice, the materials already established in the relevant material standards are most commonly subjected to creep test in the range from 1,000 to 30,000 hours, with a subsequent use of various extrapolation methods to obtain long-term creep characteristic for 10^5 hours. By comparing the obtained values of creep rupture strength with material data, it is possible to assess the extent to which the tested material meets or does not meet its specification. The most widely used methods of extrapolating the results of creep tests are divided into two basic groups:

- graphical methods, and
- parametric methods.

5.6.1 Graphical method of extrapolating the results of creep testing

Graphical methods are generally considered easier than parametric methods. They can also be used, for example, in the assessment of residual service life of material after its exploitation. The basic principle of graphical methods of results extrapolation can be summarized in three main points:

- making a scatter chart, most often in the bi-logarithmic (**log σ - log t**) or semi-logarithmic (**σ - log t**) system,
- fitting isotherms **$R_{mT/t/T} = f(T)$** or **$R_{\epsilon/t/T} = f(T)$** , or **$t_r = f(T)$** between the obtained results, where t_r is the time to rupture,

- extension of the isotherms by extrapolation for the required operation time (e.g. $2 \cdot 10^5$ hours), and deduction of extrapolated properties, or for the selected working temperature, which is a procedure that is most frequently used in determining the residual life.

The biggest problem associated with the use of graphical extrapolation methods seems to be shortcomings arising from the coordinate system used, and the related width of testing period. If tests to fracture are performed in a wide range of stress, it happens that the slope of the line interleaved with experimental points of $\sigma - t_r$ dependence in semilogarithmic or bilogarithmic coordinates need not be constant, and the whole line is then divided into several sections with a different slope. Any change in the slope then corresponds to the transition from one creep deformation mechanism to another. The dependence of stress - time to rupture t_r is then determined in general expression by a curve that bends toward lower stress (longer times to rupture) and the results of creep testing then can be dangerously overstated (see Fig 5.12). This figure shows how the real creep rupture strength will be overestimated based on short-term creep test results (here limited to 30,000 hours, extrapolation is indicated by dotted lines) if the material exhibits a change in the creep deformation mechanism in the given temperature-time interval.

The opposite problem will manifest itself in the evaluation of tests to rupture in semilogarithmic coordinates $\sigma - \log t$, where the line equation has the form:

$$\log t = \log B - \beta \cdot \sigma \log e. \quad (5.1)$$

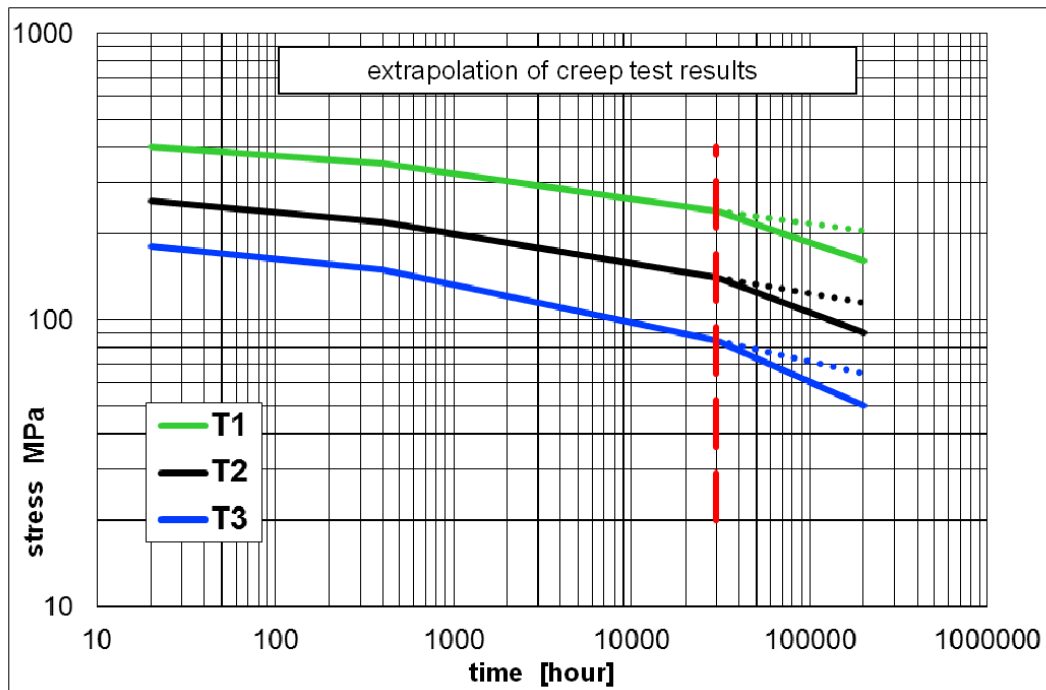


Fig. 5.12 Overstatement of creep strength in the extrapolation of results

This dependence is then determined by a curve that tends to higher stress values and so the extrapolation results can be greatly undervalued. Generally, unless the tests are long enough, we cannot accurately determine which of the systems is more suitable for extrapolation, however, at lower temperature it is preferable to use a representation in bilogarithmic system $\log \sigma - \log t$, while at higher temperatures (in the recovery region) it is preferable to use the system in semilogarithmic coordinates.

5.6.2 Parametric methods of extrapolating the results of creep testing

The principle of extrapolation using parametric methods is to use data from relatively short-term creep tests, which are typically performed at higher than operating temperatures. In such case, it is much more likely that the same physical mechanism of creep will apply both in test and under operating conditions. Two basic creep testing variables - temperature and time – we thus convert to only one parameter, which is a function of the applied stress. Among the existing equations and correlation parameters, the best known and most widely used are as follows:

- Methods based on Arrhenius equation:

- Larson–Miller (L-M) method,
 - Sherby–Dorn (S-D) method,
 - Manson–Haferd (M-H) method, and
 - Seifert method.
- Methods base on empirical equations:
 - SVÚM.

5.6.2.1 Larson–Miller (L-M) parametric method

The basis for deriving the parametric relationship proposed by Larson-Miller is the Arrhenius equation, which expresses the creep rate as a function of stress and determines it as a time change of thermally activated processes in the following shape:

$$f(\sigma) = \dot{\epsilon} = \frac{d\epsilon}{dt} = A.e^{\left(\frac{-Q}{RT}\right)} \quad (5.2)$$

where: A is the constant,

Q is the activation energy,

R is the universal gas constant (8.314 Jmol⁻¹K⁻¹),

T is the temperature in K.

Assuming for simplicity that the actual creep rate throughout the test will be always constant, then:

$$\dot{\epsilon} = \frac{d\epsilon}{dt} = \frac{\epsilon}{t} \quad (5.3)$$

where: ϵ is the amount of permanent deformation at the end of the test,

t is the time to rupture.

The original Arrhenius equation (5.2) then transfers to the form:

$$\frac{1}{t} = \frac{A}{\epsilon} .e^{\left(\frac{-Q}{RT}\right)} \quad (5.4)$$

If we denote $\frac{A}{\varepsilon} = C$, then after logarithming and modification the equation (5.4) reads as follows:

$$\frac{Q}{2,3R} = T(C + \log t_r) = P_{LM}, \quad (5.5)$$

where: P_{LM} – Larson–Miller parameter of correlation,

C – material constant without physical significance.

The accuracy of the results achieved is strongly dependent on the value of the constant C , in which the model assumes that it is independent of stress, temperature, and possibly even the material. In practice, however, it was observed that in the area of higher stresses the constant C becomes higher and conversely, in the area of lower stresses the constant C is also lower. By incorrect choice of the size of the constant C , errors from ± 10 to $\pm 40\%$ can be achieved. The value of the constant C can be interpreted as an extrapolated intersection in dependence of $\log t_r - 1/T$ (see Fig. 5.13). With L-M parametric method isostress lines intersect at values of $1/T=0$ and $\log t_r = -C$.

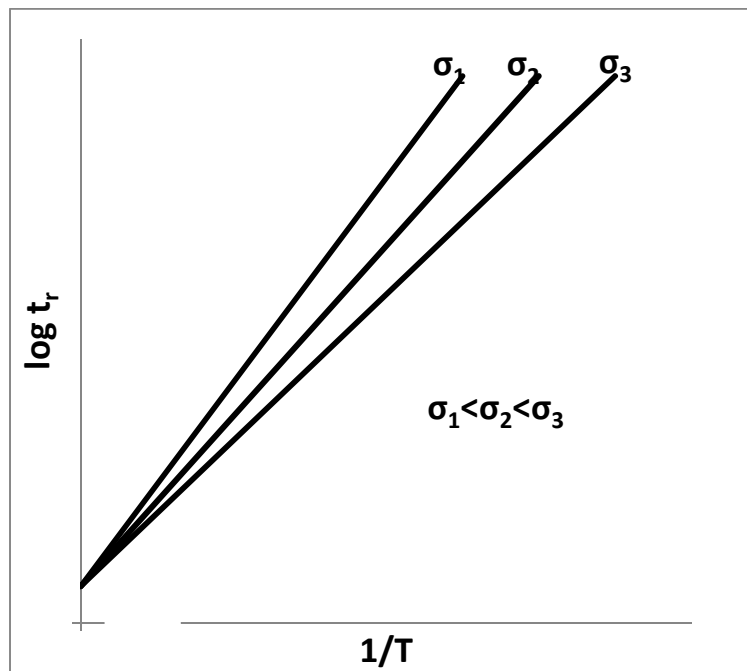


Fig. 5.13 Relationship between temperature, stress, and time to rupture in the Larson-Miller model

The parametric relationship proposed by Larson-Miller is generally expressed as a linear function of $\log \sigma$ at which equation (5) passes into the form:

$$T(C + \log t) = a_0 + a_1 \cdot \log \sigma \quad (5.6)$$

This linear regression equation, however, was abandoned due to the fact that the linear relationship of $\log t$ to $\log \sigma$ does not exist in a wide range of stress and it means that neither the dependence of L-M parameter on $\log \sigma$ is linear. At present, the most widely used is therefore, the polynomial L-M equation of the 2nd or 3rd order, where the dependence of L-M parameter on $\log \sigma$ is expressed as a polynomial equation, and e.g. for the 3rd order L-M equation it takes the following shape:

$$T(C + \log t) = a_0 + a_1 \cdot \log \sigma + a_2 \cdot \log^2 \sigma + a_3 \cdot \log^3 \sigma \quad (5.7)$$

5.6.2.2 Sherby-Dorn (S-D) parametric method

In this approach, creep is considered a thermally activated process, which is based, as with L-M parameter, on the Arrhenius relationship. If the creep is a thermally activated phenomenon, then the change in temperature under otherwise identical conditions must affect the rate of creep. S-D criterion is based on the parameter

$$t \cdot e^{\frac{-Q}{RT}} \quad (5.8)$$

whereby it can be said that the value of deformation ε under constant stress is uniquely determined by function of a quantity, which can be described as:

$$\theta = t \cdot e^{\frac{-Q}{RT}} \quad (5.9)$$

and is a function of temperature and time. Two different temperatures and times then correspond with a certain amount of creep strain at a given stress expressed using function θ_i , if following relation applies between these pairs:

$$\theta_i = t_1 \cdot e^{\frac{-Q}{RT_1}} = \dots = t_n \cdot e^{\frac{-Q}{RT_n}} \quad (5.10)$$

By subsequent logarithming of equation (5.10), while considering the condition of fracture $\theta=\theta_r$ and time $t=t_r$, we get parametric S-D equation in the form:

$$P_{S-D} = \log \theta_r = \log t_r - Q/RT \quad (5.11)$$

where: P_{S-D} – Sherby-Dorn parameter,

D – constant.

While the Sherby-Dorn parameter does have the same theoretical basis as the Larson-Miller parameter, it is based on different assumptions through which different equations are achieved. The main difference with these two parameters is mainly the dependence of activation energy on stress. For L-M parameter we assume the dependence of activation energy on stress, while for S-D parameter we don't. The activation energy is thus the slope of dependence of $\log t_r$ on $1/T$ (see Fig. 5.14).

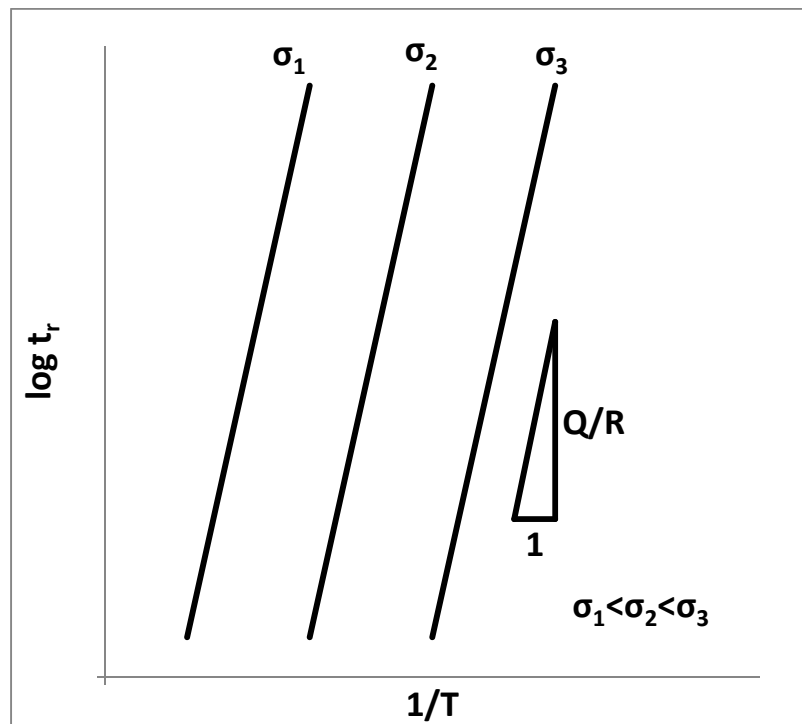


Fig. 5.14 Relationship between temperature, stress, and time to rupture in the Sherby-Dorn model

5.6.2.3 Manson–Haferd (M-H) parametric method

Parametric relationship designed by Manson and Haferd is based on purely empirical evidence, when the creep tests were carried out at constant load and variable temperature. In

their observations they revealed deviations arising from the use of L-M parametric equation, which they believed are due to the nonlinear dependence of $\log t_r$ on $1/T$. M-H parameter is therefore based on an empirical observation that the dependence of $\log t_r$ on $1/T$ may be substituted by the dependence of $\log t_r$ on T for a number of cases and it forms a straight line for a constant stress. Straight lines corresponding to different stresses converge around a point which has the coordinates $[T_a, \log t_a]$ (see Fig. 5.15). M-H parameter for a given stress value is determined as the reciprocal value of the slope of a given straight line in the form:

$$P_{M-H} = \frac{\log t_r - \log t_a}{T - T_a} \quad (5.12)$$

where: P_{M-H} - Manson-Haferd parameter,
 $\log t_a, T_a$ – material characteristics.

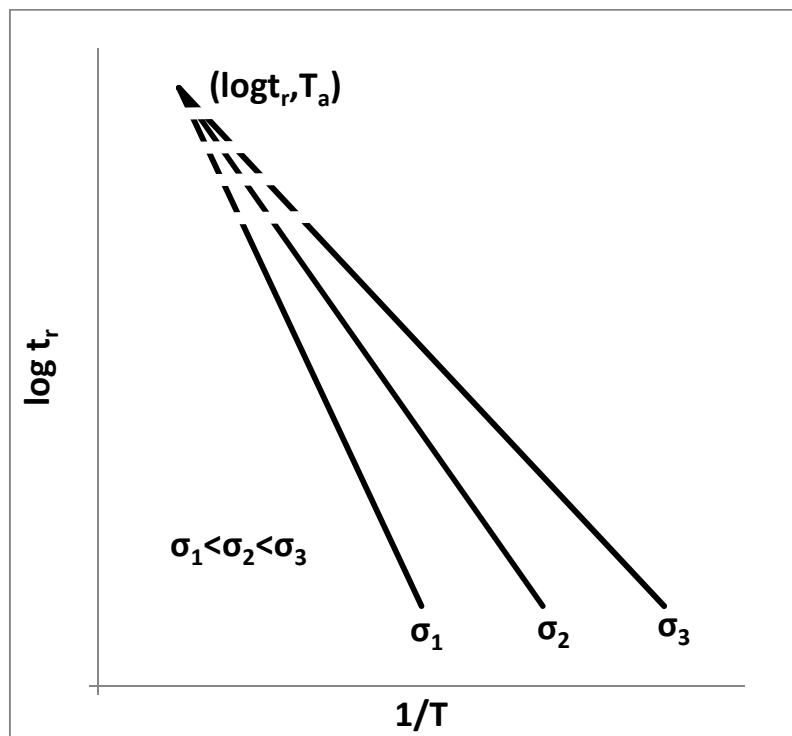


Fig. 5.15 Relationship between temperature, stress, and time to rupture in the Manson-Haferd model

5.6.2.4 Seifert method

Another frequently used parametric method is the Seifert equation. It expresses the applied stress (creep rupture strength) as a quadratic function of temperature-time parameter P in the form:

$$\log \sigma = A_0 + A_1 P + A_2 P^2 \quad (5.13)$$

where: σ – applied stress (creep rupture strength),

$A_{0,1,2}$ – constants,

P – temperature-time parameter, which is defined for this equation by following relationship:

$$PT(C + \log t_r) \cdot 10^{-4} \quad (5.14)$$

5.6.2.5 SVÚM equation

Another equation, very frequently used to extrapolate the results of creep testing in the conditions of the Czech Republic, is the equation developed in the earlier National Research Institute for Materials (Státní výzkumný ústav materiálu - SVÚM), whose constants for some of the most commonly used Czech creep resistant steels were also directly referred to in the material standards in the past. This parametric equation, unlike the previous ones, is not based on physical models, i.e. the Arrhenius equation, but purely on empirical equations that express the dependence of the time to rupture on the applied stress and temperature through functions in the form:

$$\log(t) = A_1 + A_2 \cdot f(T) + A_3 f(T) \cdot g(\sigma) + A_4 \cdot g(\sigma), \quad (5.15)$$

$$f(T) = \log \left| \frac{1}{T} - \frac{1}{A_s} \right| \quad (5.16)$$

$$q(\sigma) = \log [\sinh (\sigma \cdot T \cdot A_6)] \quad (5.17)$$

where: T is temperature,

A_{1-6} are constants.

It is understandable that for the calculation of such complex systems of equations with multiple variables, which, moreover, are not linearly dependent, it is necessary to use computers.

5.7 Practical examples of the evaluation of creep test results using the parametric equations

Figures 5.16 to 5.19 as an example of one heat concerning steel P 91 (X10CrMoVNbN 9-1) show the results of processing the creep tests using individual parametric equations. This heat was tested at temperatures of 575, 600 and 625°C and the total testing time exceeded 315,000 hours. The data file also included tests having the time to rupture even longer than 40,000 hours. For such large files the results of creep rupture strength estimate are only very little dependent on the process of their extrapolation itself, as is evident from the figures.

Most creep testing programs are mainly targeted at verifying the current creep resistance of a given steel of a given manufacturer, as long-term creep resistance is not and cannot be the subject of acceptance tests at the supplier of metallurgical products. But the European Standard for the production of boilers includes a condition for components operating in creep that “... the supplier of material must provide the boiler manufacturer with a written declaration stating that the delivered product meets all specified properties and that the manufacturing processes are the same as those used for steels, for which test results have been obtained.”

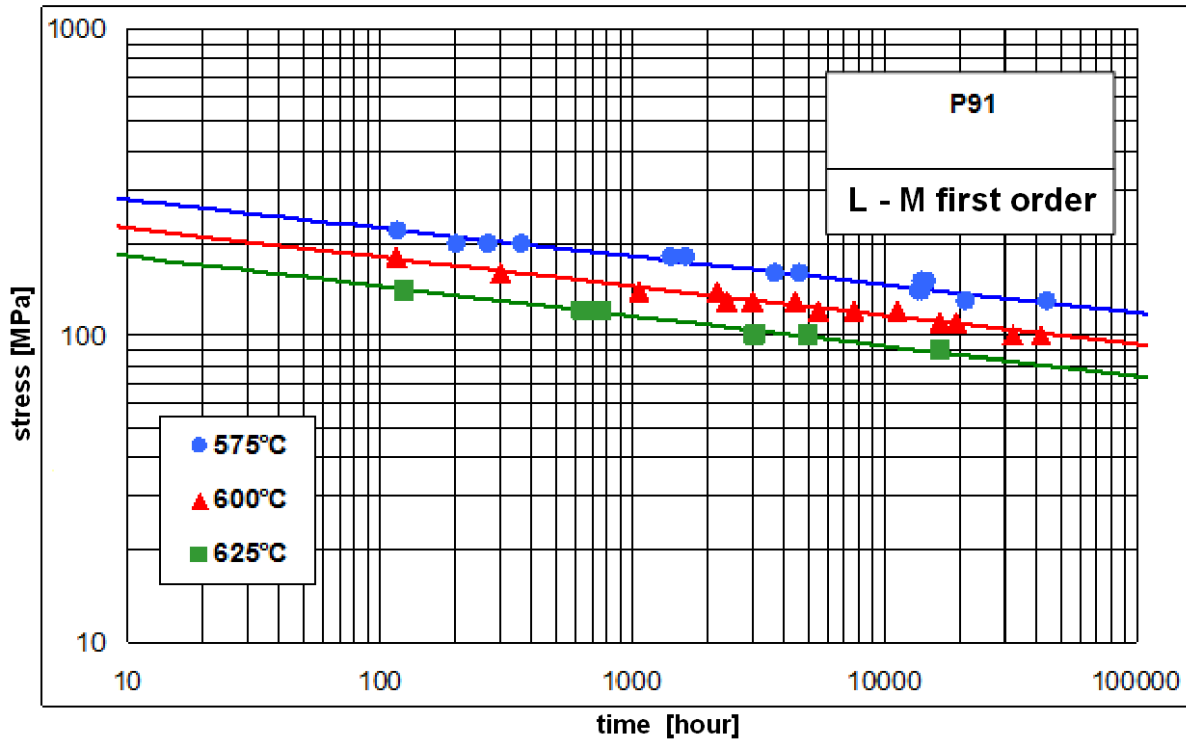


Fig. 5.16 Results of creep testing of P91 steel processed by L-M equation of the 1st order

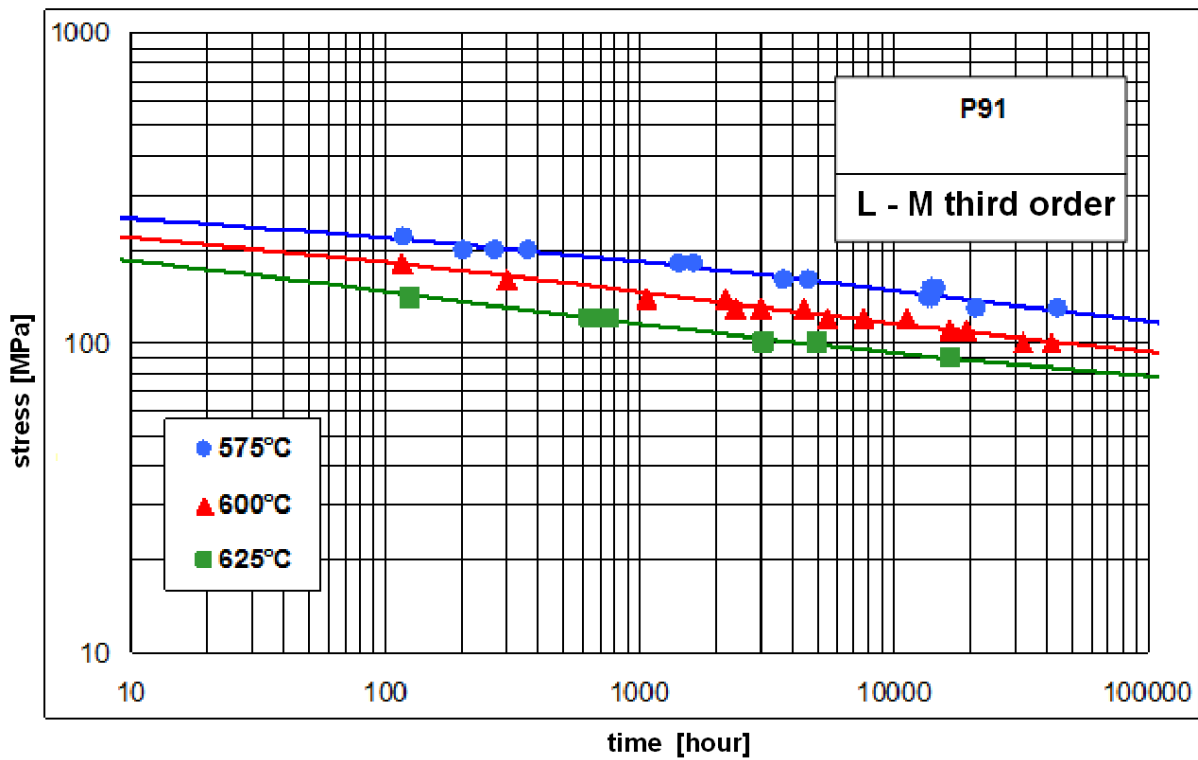


Fig. 5.17 Results of creep testing of P91 steel processed by L-M equation of the 3rd order

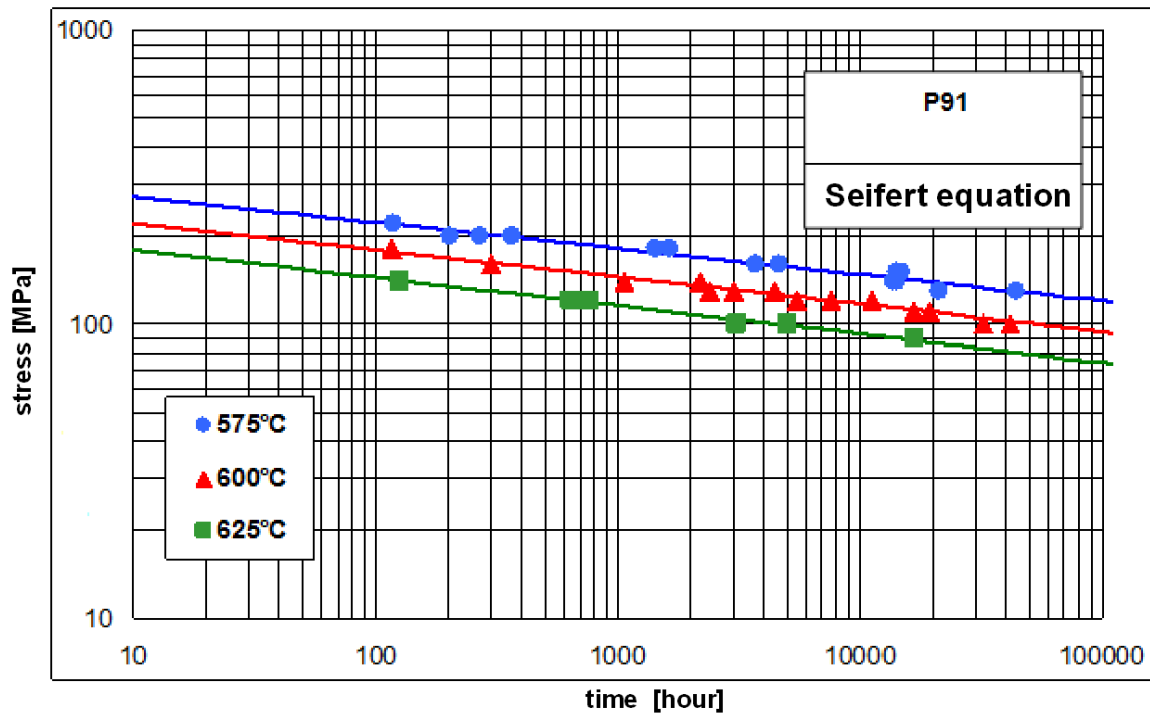


Fig. 5.18 Results of creep testing of P91 steel processed by Seifert equation

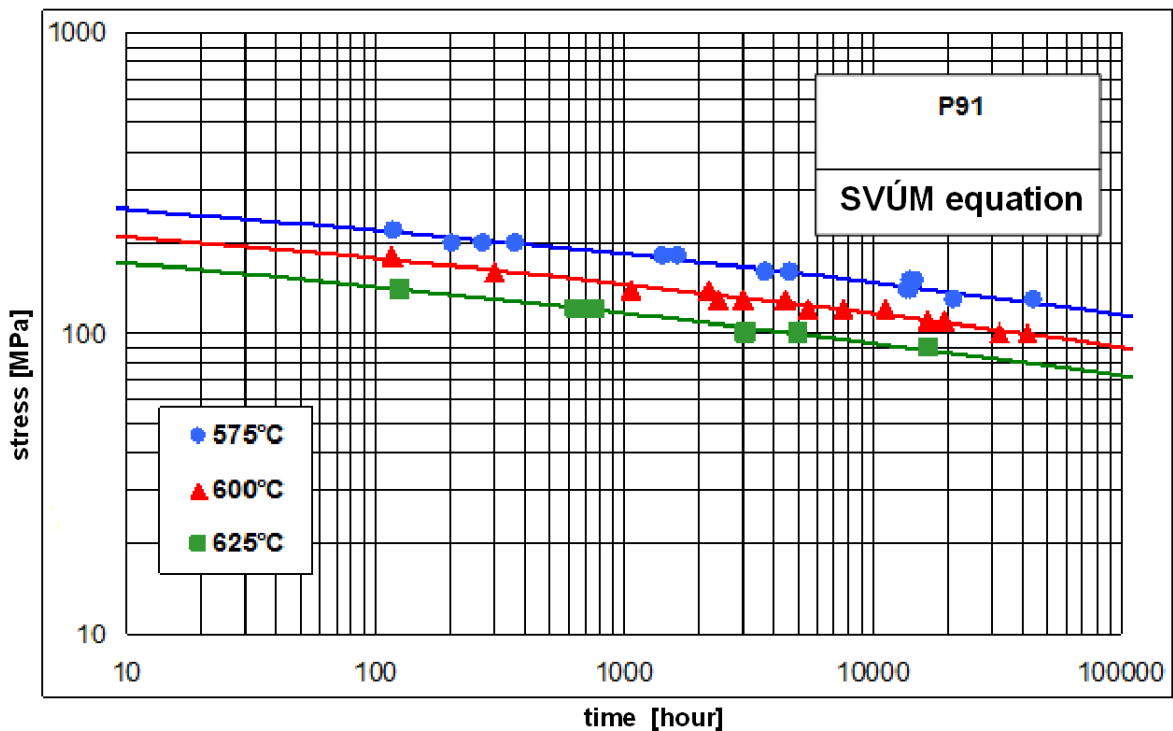


Fig. 5.19 Results of creep testing of P91 steel processed by SVÚM equation

The creep characteristics of various steels are listed in the material standards in a tabular form of temperature-time dependence of the mean values of creep limit and creep rupture strength. For design purposes, we then work with minimal values which represent 80% of the

mean values. This approach is induced by the fact that the creep resistance of a given steel grade may vary up to 20% as a result of:

- permitted variance in the chemical composition within the same brand of steel,
- different content of accompanying and trace elements and different steel microcleaness,
- chemical heterogeneity of the material,
- different way of producing both steel and metallurgical final product,
- differing thermal processing, and thus different microstructure, which has a very significant effect on creep resistance,
- errors made in determining the creep resistance in the creep laboratories,
- different operating and test conditions of a given material, and
- technological and structural influences.

After harmonization of Czech material standards with EU standards, creep characteristics of each brand of creep-resistant steels and alloys are set out in the material, as well as product standards, such as:

ČSN EN 10302: Creep resisting steels, nickel and cobalt alloys

ČSN EN 10028-2 Flat products made of steels for pressure purposes - Part 2: Non-alloy and alloy steels with specified elevated temperature properties

ČSN EN 10216-2: Seamless steel tubes for pressure purposes - Technical delivery conditions - Part 2: Non-alloy and alloy steel tubes with specified elevated temperature properties

ČSN EN 10222-2: Steel forgings for pressure purposes - Part 2: Ferritic and martensitic steels

Table 6.1 shows the values of creep rupture strength for P235GH and P265GH grade steels listed in Annex A of ČSN EN 10216-2.

Tab. 6.1 Values of creep rupture strength for steels P235GH a P265GH

Steel designation		Temperature °C	Values of creep rupture strength in MPa ^{a)b)c)d)}			
Grade	Number		10,000 hours	100,000 hours	200,000 hours	250,000 hours
P235GH	1.0345	400	182	141	128	122
P265GH	1.0425	410	166	128	115	109
		420	151	114	102	97
		430	138	100	89	86
		440	125	88	77	74
		450	112	77	66	64
		460	100	66	56	54
		470	88	56	46	44
		480	77	47	33	30
		490	67	39	26	-
		500	58	32	24	-



Summary of terms

After studying the chapter, following terms should be clear to you:

- **Anelastic deformation**
- **Creep of material**
- **Limit temperature T_g**
- **Creep curve**
- **Rate of secondary creep**
- **Creep rupture strength**
- **Creep limit**
- **Homologous temperature**
- **Larson–Miller parameter**
- **Sherby–Dorn parameter**



Questions about the curriculum learnt

- 1) What do we mean by creep?
- 2) What determines the limit temperature T_g ?
- 3) How the creep rupture strength is defined?
- 4) What is the homologous temperature?
- 5) What methods of extrapolating the results of creep testing do you know?
- 6) What parametric methods of extrapolating the results of creep testing do you know?
- 7) How the Larson–Miller parameter is expressed?



Tasks to solve

The table shows the results of creep tests of P22 steel at temperatures 525°C, 550°C, 575°C and 600°C. Plot of dependence of stress on the Larson-Miller parameter in the form $P_{L-M} = (T + 273) \cdot [C_{L-M} + \log(t)]$, $C_{L-M} = 20$.

Test No.	Temperature T (°C)	Stress σ (MPa)	Time t (hour)	Ductility (%)	Contraction (%)
1	525	280	14	43.6	83.2
2	525	255	57	32.8	85.5
3	525	235	173	38.4	85.2
4	525	210	359	48.8	87.7
5	525	190	726	62.6	88.3
6	525	165	2602	45.6	85.9
7	525	145	5772	41.6	83.3
8	525	125	16072	35.6	78.3
9	525	115	30734	38.6	79.3
10	550	240	160	32.0	87.0
11	550	215	327	60.0	89.3
12	550	190	399	46.8	86.7
13	550	165	422	58.8	88.2
14	550	145	962	48.4	84.2
15	550	125	2834	42.8	87.7
16	550	105	11309	46.3	83.0
17	575	180	49	57.6	85.3
18	575	150	211	56.0	86.8
19	575	130	798	54.0	86.9
20	575	110	2065	48.8	83.6
21	575	90	6407	51.9	87.2
22	575	80	16491	41.8	78.0
23	575	75	19699	28.0	70.0
24	600	155	51	55.2	87.3
25	600	140	124	44.6	81.9
26	600	110	466	60.8	91.1
27	600	95	849	56.4	91.7
28	600	85	1398	56.4	91.7
29	600	65	4891	52.0	83.5
30	600	50	15633	56.3	92.5
31	600	40	21040	40.6	93.7



References

- [1] HERNAS, A. – JONŠTA, Z. – TVRDÝ, M. – ČÍŽEK, L. – PURMENSKÝ, J.: Žárupevné oceli a slitiny. Vydavatel'stvo ZUSI – Žilina, ISBN 80-968605-6-9.
- [2] ČSN EN 12952-2 Vodotrubné kotle a pomocná zařízení – Část 2: Materiály pro části kotlů a příslušenství namáhaných tlakem.
- [3] ASM Handbook, Volume 8, Mechanical Testing and Evaluation.
- [4] ČSN EN ISO 204 Kovové materiály – Zkoušení tečení jednoosým tahem – Zkušební metoda. Úřad pro technickou normalizaci, metrologii a státní zkušebnictví, říjen 2009.
- [5] STRNADEL, B.: Řešené příklady a technické úlohy z materiálového inženýrství. Ostravské tiskárny, a.s., 1998.

6. Evaluation of resistance of structural steels to stress corrosion cracking in aqueous environments at temperatures from 23 to 300°C



Study time: 2 hours



Objective: After reading this chapter, you should be able to

- Define the concept of stress corrosion cracking.
- Define factors that influence the process of stress corrosion cracking.
- Describe the dependence of the stress corrosion crack growth rate on the stress intensity factor K .
- Define a threshold for the occurrence of stress corrosion cracking.
- Define the factors influencing the process of stress corrosion cracking in aqueous environments.
- Describe the mechanisms of stable crack growth in aqueous environments.
- Describe the process for evaluating the resistance to stress corrosion cracking.



Presentation

6.1. Introduction

For many nuclear and conventional power generating facilities and structures made of high-strength steels exposed to the effects of the aqueous environment during long-term operation, the stress corrosion cracking was identified as a cause of cracks of size exceeding allowable defects.

By the term stress corrosion cracking we understand the initiation and stable crack growth due to the simultaneous action of tensile stress (from a static external loading or own tension) and corrosive environment. The initiation and stable growth of a crack as a result of this process, however, occurs only if the characteristics of the environment, the state of stress

and properties of the material reach a certain critical level at the same time. Otherwise, the initiation and growth of crack may not occur at all.

The process of stress corrosion cracking in aqueous environments is influenced by a large number of factors (see Figure 6.1), which can be divided into three main groups:

1. factors including the effect of the method of stress, especially the state of stress in the critical points of the structure,
2. exploitation conditions (characteristics of the aqueous environment, temperature regime), and
3. metallurgical factors.

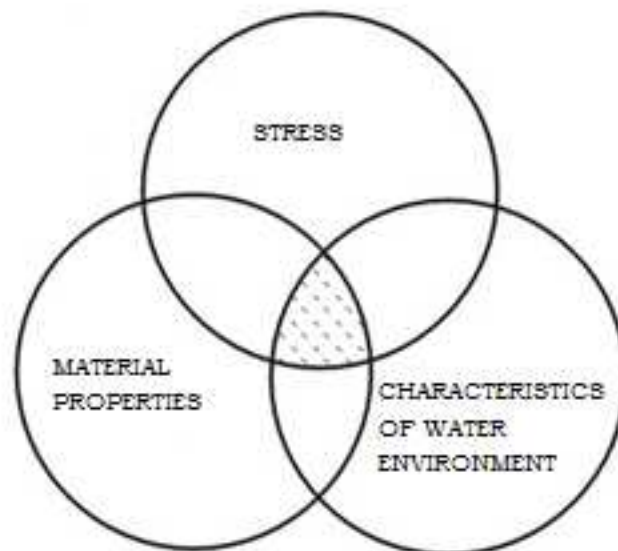


Fig. 6.1 Factors whose simultaneous action is the cause of initiation and stable crack growth in aqueous environments

Increasing demands on operating parameters, durability and reliability of the above mentioned structures and equipment lead to changes in the work of designers and engineers, as well as expanding requirements on construction materials. Subcritical defects of allowable size may also arise by another mechanism, usually during production, and in some types of structures they are present at the already at commissioning. The stage of crack initiation may be suppressed in such cases, or disappearing altogether. The presence of defects such as cracks in the operating structure thus leads to a requirement that newly developed

construction materials have the best properties not only in the phase of initiation, but also in the phase of stable crack growth.

The study of stable crack growth patterns is the focus of much attention since the early 70s of the last century, when a new concept of structural design, the concept of damage tolerance, was introduced, which allows the initiation and stable growth of defects even during the operation of the structure. Stable growth of defects such as cracks can be described using either a basic parameter of linear elastic fracture mechanics - stress intensity factor K [$\text{MPa}\cdot\text{m}^{1/2}$] and/or using parameters of elastoplastic fracture mechanics – crack tip opening displacement δ [mm] and J-integral [N/mm].

Figure 6.2 shows schematically the dependence of stress corrosion crack growth rate on the stress intensity factor K as a result of stress corrosion cracking. Stable crack growth by stress corrosion cracking is characterized by the existence of a threshold value K_{ISCC} . All the dependence of da/dt vs. K can be divided into three significantly different stages. In the first stage, there is a very strong dependence of the stress corrosion crack growth rate on K . In the second stage, after the value K_p and corresponding crack growth rate $(da/dt)_p$ are reached, the rate of growth is independent of or very weakly dependent on the level of K . Independence of the crack growth rate on K suggests that the rate of growth in this area is controlled by the rate of electrochemical reactions, kinetics of transport of anions or cations to the crack face or other non-mechanical factors.

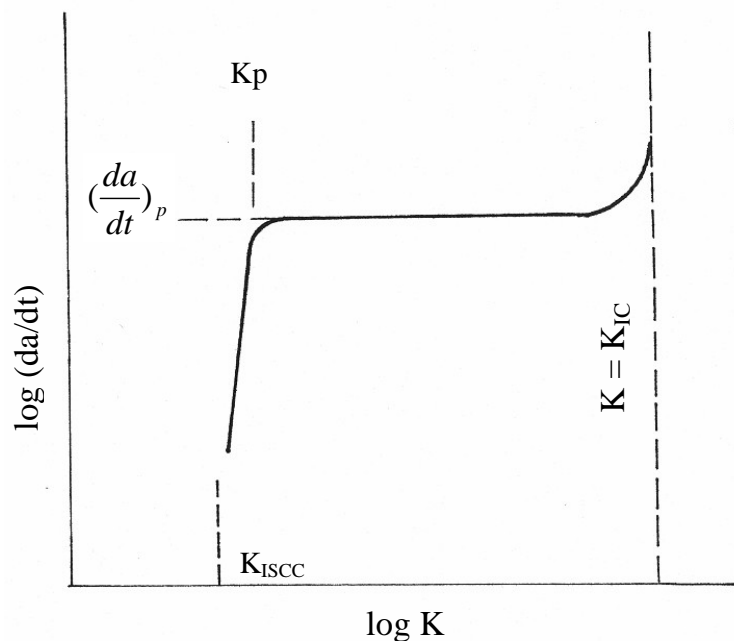


Fig. 6.2 Schematic representation of the crack growth kinetics under the simultaneous application of static stress and corrosive environment

Level of the rate $(da/dt)_p$ depends on the properties of the steel/aqueous environment. In the third stage, the rate of stress corrosion crack once again increases with K until a fracture toughness K_{IC} is reached.

6.2 Mechanisms of stable crack growth in aqueous environments

For the system of aqueous environment/steel, the literature mentions two basic reasons:

1. hydrogen embrittlement of a microvolume of material before the face of a growing crack, and
2. anodic dissolution on the face of a growing crack.

Both mechanisms may act simultaneously as atomic hydrogen is liberated by hydrolysis of iron ions, i.e. as a result of anodic dissolution on the face of the crack. Which of the mechanisms shall play a dominant role is determined by:

1. properties of the material, and especially its chemical composition, microstructure and yield strength, and
2. parameters determining the properties of the aqueous environment, especially temperature, corrosion potential, water pH, conductivity, and concentration of anions.

6.2.1 Mechanism of hydrogen embrittlement

The term hydrogen embrittlement means decrease in plastic properties of the material caused by the presence of hydrogen. The hydrogen embrittlement can be viewed from two angles:

1. Internal hydrogen embrittlement without the presence of a corrosive environment that is caused by hydrogen absorbed by the material during production, heat treatment or various technological operations.
2. External hydrogen embrittlement caused by the atomic hydrogen which is in contact with the metal surface, or is released on the free surface of the metal from the surrounding environment containing hydrogen ions (e.g. H_2O , H_2S).

Stable growth of cracks caused by the simultaneous action of static stress and aqueous environments is controlled by a sequence of consecutive processes, which are schematically shown in Figure 6.3.

These sub-processes are:

- ❖ Transport of a corrosive environment to the face of the crack.
- ❖ Electrochemical reactions of a corrosive environment with the newly formed surfaces, which lead to the hydrogen liberation.
- ❖ The absorption of hydrogen on the crack face.
- ❖ Transport of hydrogen into areas in which it causes embrittlement.
- ❖ Interaction of hydrogen with metals leading to embrittlement (decrease in the cohesive strength of the grain boundaries, affection of the mobility by dislocation, etc.).

The resulting crack growth rate is then controlled by the slowest of the aforementioned processes.

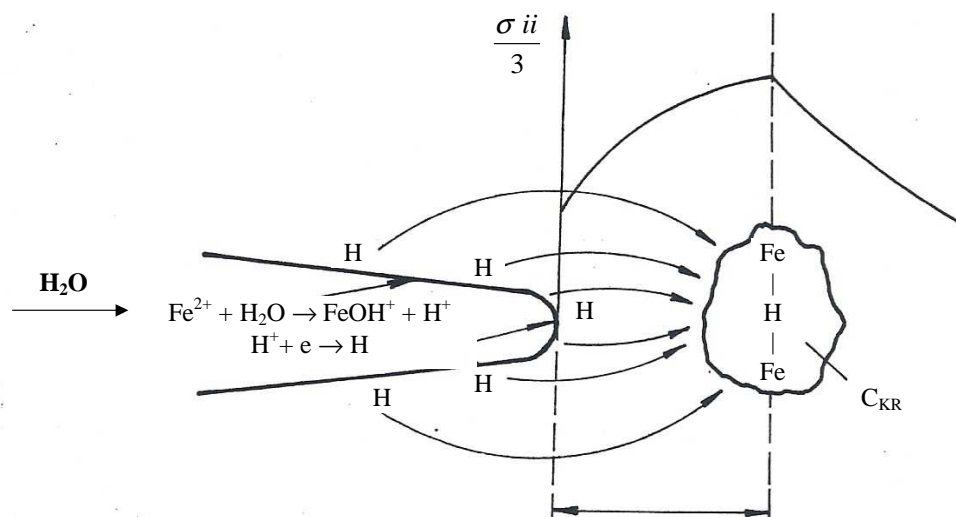


Fig. 6.3 Schematic representation of the processes leading to hydrogen embrittlement during stable crack growth in the aqueous environments

Figure 6.4 summarizes the results of measuring the rate of stress corrosion crack growth in the regime $P = \text{constant}$ (stress corrosion cracking) to stress intensity factor K in aerated distilled water at 30°C, 50°C, 70°C, and 90°C for high-strength steel 38MnSiCr2Ni2Mo. The obtained dependence is characterized by:

1. The occurrence of a threshold value K_{ISCC} , which is independent of the water temperature.

2. The occurrence of two stages that differ in the strength of relationship of the crack growth rate on K.

In the first stage, after the threshold K_{ISCC} is reached, the crack growth rate strongly depends on K and is independent of the distilled water temperature. Value of K_{ISCC} , calculated from the results obtained for $da/dt = 1 \cdot 10^{-7}$ mm/s, is equal to $K_{ISCC} = 13,5 \text{ MPa}\cdot\text{m}^{1/2}$.

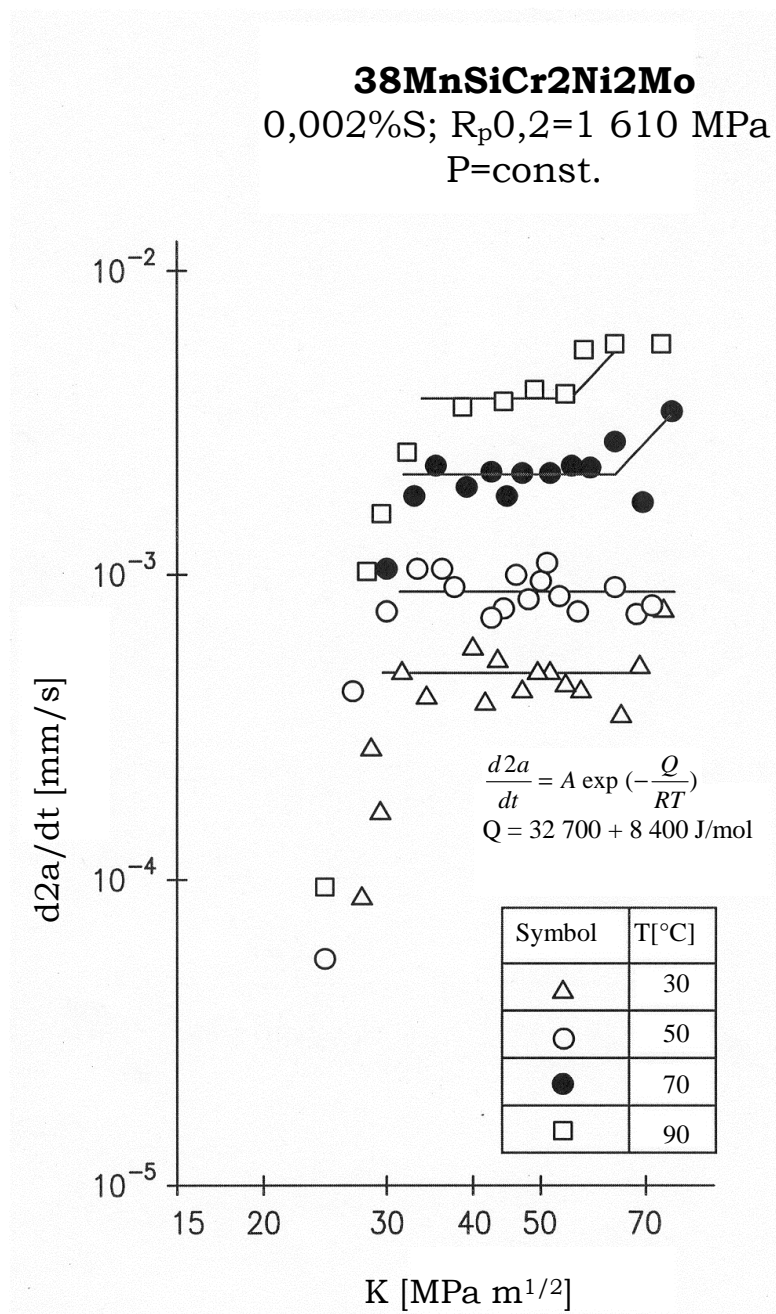


Fig. 6.4 Effect of water temperature in the range of 30 – 90°C on the kinetics of growth of corrosion cracks due to stress corrosion cracking with high strength steel 38MnSiCr2Ni2Mo with low content of sulphur (0.002%) and phosphorus (0.006%).

In the second stage, the crack growth rate is only dependent on the water temperature. The activation energy of the controlling process calculated from the measurement results in the second stage is equal to $Q = 32\,700 \pm 8400$ J/mol. Based on the comparison of activation energies for the growth of fatigue cracks and growth of cracks due to stress corrosion cracking it can be concluded that stable crack growth is controlled, for both types of loading, by a single process. The calculated activation energies are in close agreement with the activation energy of the solubility of hydrogen in iron grid α ($Q = 28600$ J/mol).

Fractographic analysis of the fracture surfaces produced by the stable crack growth due to stress corrosion cracking showed that the stable crack growth exclusively occurred through an intercrystalline decohesion of original austenitic grains (see Fig. 6.5).



Fig. 6.5 Morphology of the fracture surface produced by the stable crack growth in high strength steel 38MnSiCr2Ni2Mo due to stress corrosion cracking in 70°C hot water

6.2.2 Mechanism of anodic dissolution

There are a number of literary evidence that stable crack growth due to stress corrosion cracking in the aqueous environment with a temperature higher than 250 ° C is primarily the result of application of the mechanism of anodic dissolution in both low-alloy bainitic steels and austenitic stainless steels.

Stable crack growth induced by the presence of the aqueous environment and the tensile stress is in this case the result of periodical repetition of the process of breaking the oxide film on the crack face, the anodic dissolution on the crack face and the subsequent

passivation of the exposed surfaces. The increase in deformation at the crack face required for breaking the oxide film can be produced by a monotonically increasing load or creep (creep process) at constant load.

After the oxide film is broken, the exposed crack face is subject to the effects of aqueous environment, whose aggressiveness depends on the concentration of anions at the crack tip. Aggressive environment at the crack tip is maintained and enhanced by the dissolution of MnS inclusions and/or the gradient of the potential between the crack mouth and its face, which depends on the concentration of oxygen dissolved in water. The crack face progresses due to anodic dissolution. Simultaneously, the crack face is being gradually covered with an increasing passivation layer and the crack progress slows down. The phased nature of the failure, which is the result of a periodic repetition of processes of breaking the oxide film, anodic dissolution and subsequent passivation of the exposed surfaces at the crack tip is evidenced by the characteristic fractographic features observed on the fracture surfaces produced by stable crack growth due to stress corrosion cracking, whose characteristic layout resembles the grooves (striation) (see Fig. 6.6).

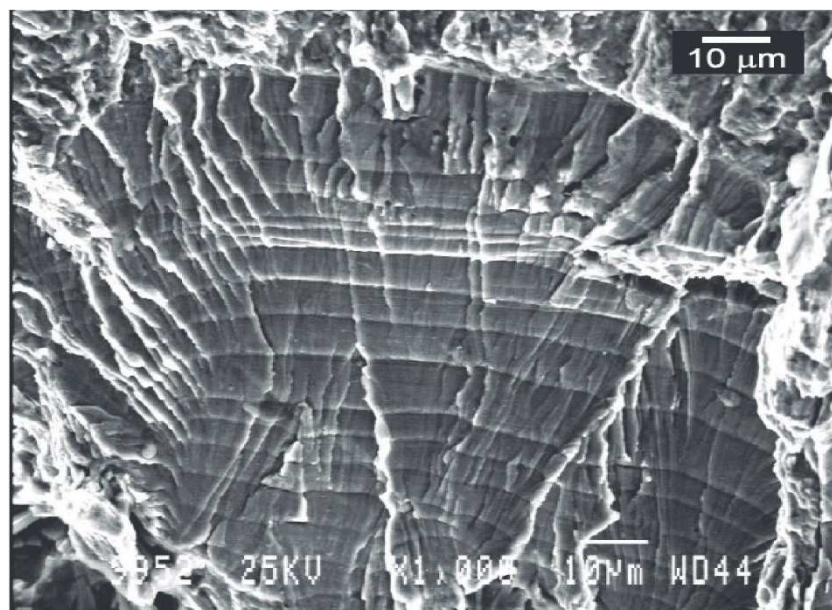


Fig. 6.6 Micromorphology of the fracture surface produced upon slow loading of CT specimen made of 08CH18N10T grade steel in the deaerated demineralised water at a temperature of 275°C with the addition of 100 ppm Cl⁻ ($u = 0,0005$ mm/min.)

Kinetics of stable crack growth due to anodic dissolution depends on how the type of loading, environmental characteristics and properties of the material affect the rate of

recovery of the aqueous environment on the crack face, rate of breaking the oxide film and the rate of passivation of exposed surfaces at the crack tip.

Rate of crack growth produced by the mechanism of anodic dissolution can be advantageously applied to the amount of metal dissolved at the crack tip using Faraday's law.

$$v = \frac{da}{dt} = \frac{M}{z \cdot \rho^* \cdot F} i(t) \quad (6.1)$$

where M and ρ^* are the atomic weight and specific weight of the metal from the crack tip,

F is the Faraday's constant ($F=96500 \text{ C}\cdot\text{mol}^{-1}$),

z is the average number of electrons involved in the process of oxidation of a single atom of metal,

$i(t)$ is the time dependence of the current density, which is caused by corrosion processes at the crack tip.

6.3 The procedure for evaluating the resistance of steels to stress corrosion cracking

The most commonly used method for evaluating the resistance of steels to stress corrosion cracking in the aqueous environments is a method of testing at low strain rate according to ČSN ISO 7539-7. Smooth cylindrical bodies and/or test specimens with an initial fatigue crack are loaded by the cross-arm of test machine moving at a low speed of $10^{-3} \div 10^{-7}$ mm/min. Test results are compared with the results of tests conducted in air at a selected temperature. With smooth cylindrical bodies, the sensitivity to stress corrosion cracking is expressed as the ratio of contraction Z determined in corrosive environments and contraction of the material determined in air. For specimens with an initial fatigue crack the R curves (dependence of $J - \Delta a$ or $\delta - \Delta a$) measured in air and in corrosive environments are compared (see Fig. 6.7). This figure illustrates R curves determined for 10GN2MFA grade steel in aerated and deaerated demineralised water at temperatures of 250°C and 290°C at cross-arm movement speed $u=1,7 \cdot 10^{-5}$ mm/s. At water temperatures of 250°C and 290°C the resistance of 10GN2MFA grade steel to stress corrosion cracking is significantly dependent on the concentration of oxygen dissolved in water. Reducing the concentration of oxygen dissolved

in water below 10 ppb resulted in suppression of stress corrosion cracking in the monitored heat of 0GN2MFA grade steel (S=0.008%).

10GN2MFA
C(T), B = 11 mm
water 250°C, 290°C
crosshead speed 0.001 mm/minute

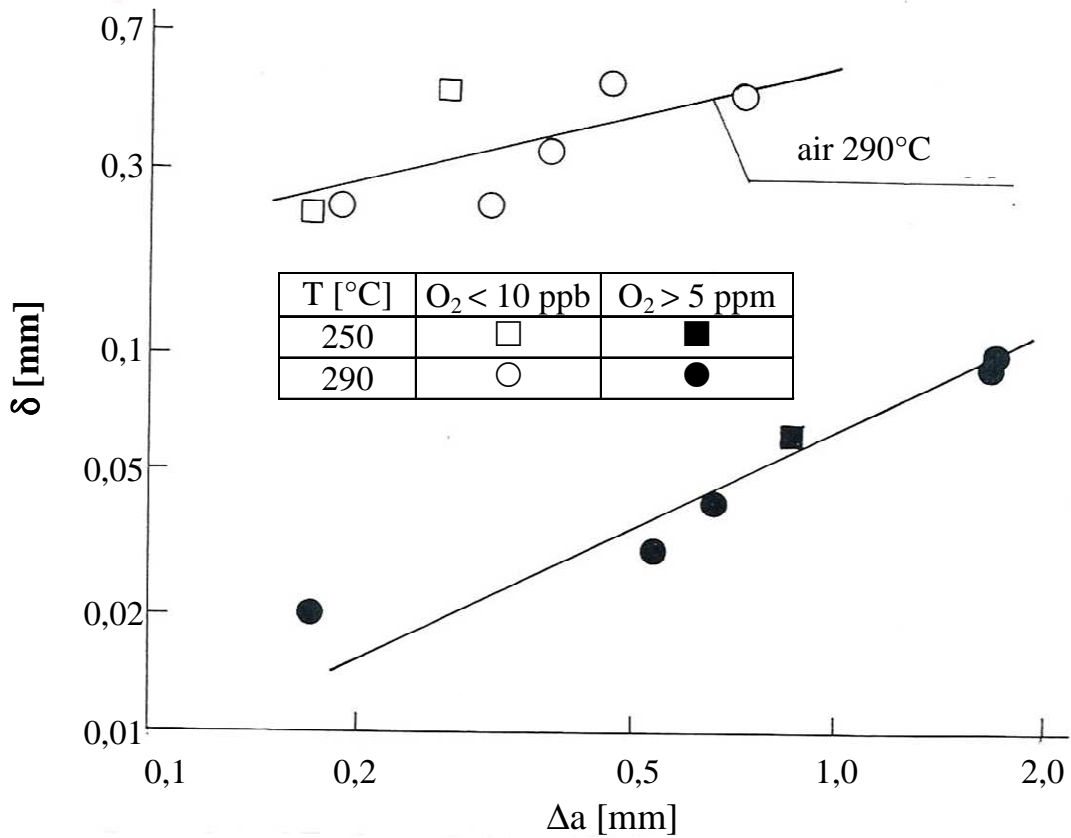


Fig. 6.7 Dependence of $\delta - \Delta a$ determined at the cross-arm movement speed of $1.7 \cdot 10^{-5}$ mm/s at two significantly different concentrations of oxygen at temperatures of 250°C and 290°C



Summary of terms

After studying the chapter, following terms should be clear to you:

- **Stress corrosion cracking**
- **Threshold K_{ISCC} for stress corrosion cracking occurrence.**
- **Mechanism of hydrogen embrittlement.**
- **Mechanism of anodic dissolution.**
- **Hydrogen absorption on the crack face.**



Questions about the curriculum learnt

- 8) What do we mean by stress corrosion cracking?
- 9) What determines the threshold value K_{ISCC} ?
- 10) What do we mean by hydrogen embrittlement?
- 11) What sub-processes lead to hydrogen embrittlement at the stable crack growth in the aqueous environments?
- 12) What sub-processes control the mechanism of anodic dissolution?
- 13) What procedure for evaluating the resistance of steels to stress corrosion cracking you know?



References

- [1] MATOCHA, Karel: Korozní únava a korozní praskání konstrukčních ocelí ve vodních prostředích o teplotě 20 – 300°C. Habilitační práce. VŠB – TU Ostrava, 2006.
- [2] ČSN EN ISO 7539-7 Koroze kovů a slitin – Zkoušky koroze za napětí – Část 7: Zkoušení při malé rychlosti deformace.
- [3] Corrosion issues in light water reactors. Stress corrosion cracking. European Federation of Corrosion Publication Number 51. Edited by D. Féron and J.-M. Olive, Woodhead publishing limited, Cambridge England. ISSN 1354-5116.

7. Evaluation of resistance of steels to hydrogen embrittlement in environments containing hydrogen sulphide (H₂S)



Study time: 2.5 hours



Objective: After reading this chapter, you should be able to

- Define basic types of degradation mechanisms in hydrogen sulphide environments.
- List the standards for the evaluation of resistance of steels to HIC and SSC.
- Describe the procedure for the evaluation of resistance of steels to HIC.
- Describe what CLR, CTR, CSR and CAR parameters express.
- Name the standard for evaluation of resistance of steels to simultaneous action of a tensile stress and hydrogen sulphide environments.
- List the four basic test method described in NACE TM 0177-2005 Standard.
- Explain the difference between the evaluation of resistance to sulphide stress cracking (SSC) and stress corrosion cracking according to NACE TM 0177-2005 Standard.



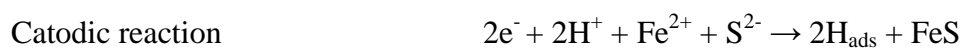
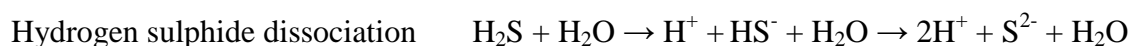
Presentation

7.1 Introduction

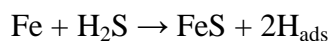
Seamless pipes and steel sheets used in the manufacture of welded pipes for the extraction and transportation of oil and natural gas, manufacturing of oil storage tanks and pressure tanks in oil refineries, are exposed to moist acidic environments that contains a certain proportion of hydrogen sulphide H₂S. Hydrogen sulphide is a colourless gas smelling of rotten eggs.

- 1) It is extremely poisonous (can cause fatal poisoning in doses of 1000 to 2000 ppm),
- 2) is heavier than air,
- 3) easily liquefies, and
- 4) it is soluble in water (0.4 g/100 ml at 20°C).

From liquid and gaseous environments containing a certain proportion of hydrogen sulphide, hydrogen can penetrate into the material and cause its degradation. Dissolving in water produces the hydrosulphuric acid H₂S. Generally, it is assumed that atomic hydrogen occurs in hydrogen sulphide environments due to the dissociation of hydrogen sulphide in the presence of water in accordance with the following reactions:



The overall reaction is sometimes simply written as follows:



These reactions can take place both in gas and liquid media, in the case of gases, however, the presence of a specific proportion of moisture is necessary. In a completely dry gas, degradation effects of hydrogen sulphide have no effect since it will not be dissociated. It is always an acidic environment and the effect of hydrogen sulphide is accentuated at lower pH values.

7.2 Basic types of degradation mechanisms in hydrogen sulphide environments

In the case of carbon and low alloy steels three main types of degradation mechanisms in an environment containing hydrogen sulphide are distinguished. It is a hydrogen-induced cracking (HIC), followed by sulphide stress cracking (SSC) and finally the stress-oriented hydrogen-induced cracking (SOHIC). As the name implies, all of these types of damage manifest through the formation of cracks in the steel. Features of cracks for each type of hydrogen embrittlement are schematically represented in Figure 7.1.

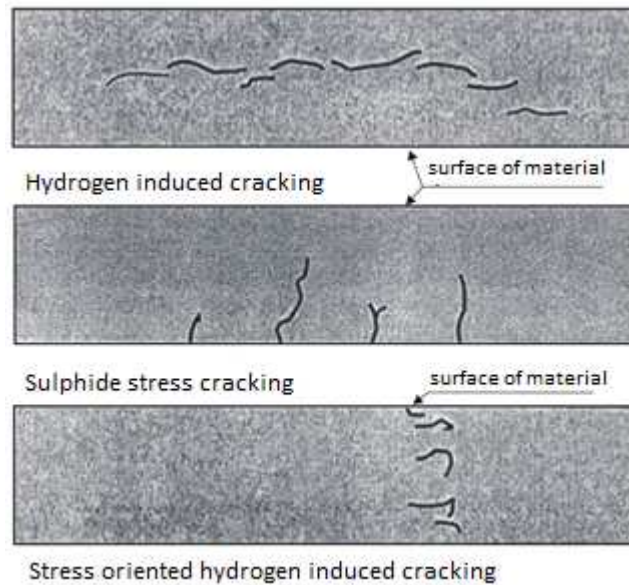


Fig. 7.1 Schematic representation of the character of cracks for the basic types of hydrogen embrittlement in hydrogen sulphide environments

7.2.1 Hydrogen-induced cracking (HIC)

This type of damage you may encounter mainly in pipes and plates made of carbon-manganese steels of lower strength level (ultimate tensile strength of less than about 550 MPa) used for oil pipelines, gas pipelines, gas and oil storage tanks, or pressure vessels in oil refineries. This is a form of internal damage by hydrogen without the interaction of external loading. Sometimes, this type of damage becomes known as stepwise cracking (SWC) due to the nature of cracks, which can form characteristic steps on the scratch patterns. Should there be cracks near the surface, it may produce blisters on the surface. Examples of damage caused by the mechanism of hydrogen induced cracking are documented in Fig. 7.2.

Theory, which in this case quite satisfactorily explains the formation of cracks, is the oldest theory of hydrogen embrittlement, i.e. the theory of aerostatic stress. Hydrogen, which gets into the steel as a result of electrochemical reactions, recombines in favourable locations of the metallic matrix, creating here a locally high tension, which may result in cracking. (see Fig. 7.2). Potential site for hydrogen recombination is probably the interface of non-metallic inclusions and metal matrix, and the segregation strips in steel.

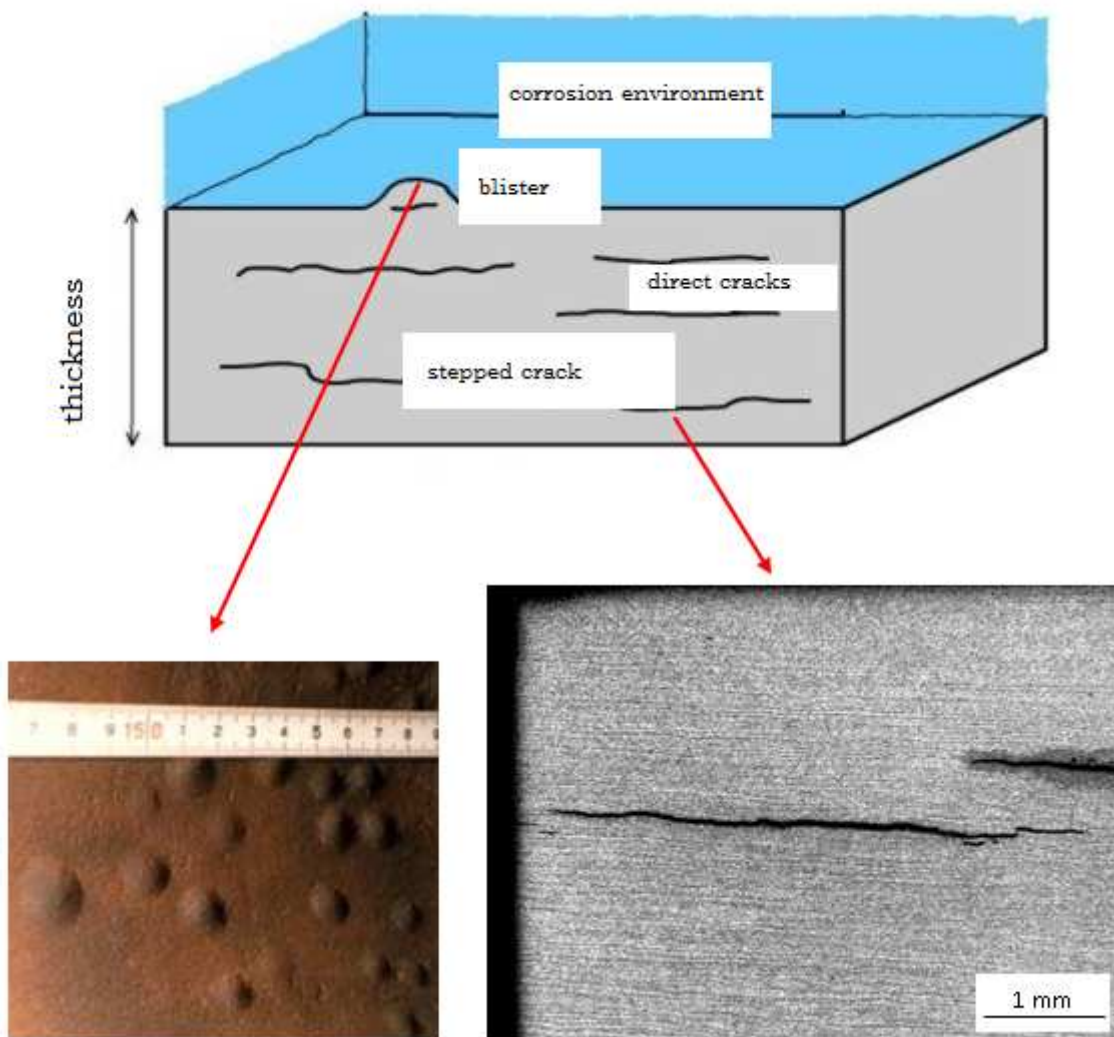


Fig. 7.2 Examples of damage to steel caused by hydrogen-induced cracking

7.2.2 Sulphide stress cracking

This type of damage is most often a problem of materials with medium, sometimes higher strength levels, which are stressed by external loads. The damage occurs under the simultaneous application of tensile stress and the environment containing hydrogen sulphide. The most important parameters that influence the aggressiveness of the environment are the environment pH and partial pressure of hydrogen sulphide. It is assumed that this damage is mainly attributable to atomic hydrogen which causes hydrogen embrittlement of steel in accordance with generally accepted mechanisms (decohesion theory, theory of the critical hydrogen concentration, eventually the theory of hydrogen - plastic deformation interaction),

which by interaction of tensile stresses leads to the initiation and growth of cracks. Based on the analysis of results of laboratory tests and operational experience, it can be concluded that the susceptibility to sulphide stress cracking increases with the increase of hardness (strength) of the material, or with the presence of local harder areas in the steel structure. A characteristic manifestation of degradation of metallic materials at simultaneous interaction of hydrogen and the external load is the formation of so-called “fish eyes”. They are circular quasi-cleavage areas in the centre of which nonmetallic inclusion is situated, or was, that initiated the damage of material (see Fig. 7.3).

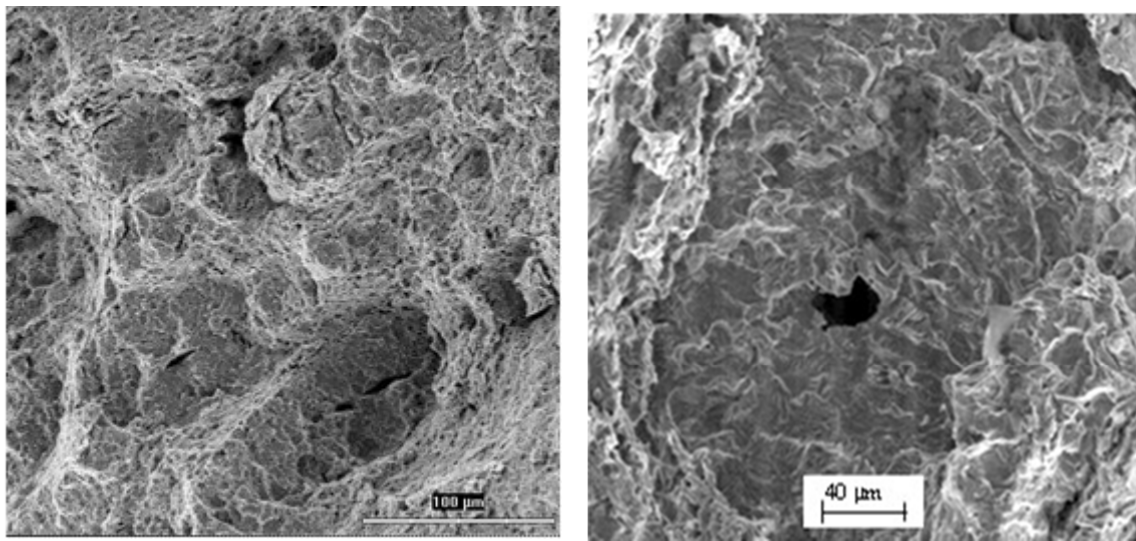


Fig. 7.3 The occurrence of fish eyes on the fracture surface of X60 grade steel

7.2.3 Stress-oriented hydrogen-induced cracking

This special type of hydrogen embrittlement occurs primarily in the heat affected areas of welded joints. A typical feature is the presence of cracks parallel to the surface which are in a row one above the other and are sometimes partially interconnected with sections perpendicular to the surface of the material. The assumption prevails that damage is related to the existence of softened zones in the heat-affected area that were annealed in the intercritical interval of temperatures, i.e. between A_{C1} and A_{C3} . When externally loaded or at higher internal stresses these areas may be subjected to the load above the yield strength, which may lead to formation of cracks, since it can cause significant hydrogen-plastic deformation interaction. This type of hydrogen embrittlement may occur even in high-quality steels, which are as basic materials resistant to hydrogen induced cracking.

7.3 Procedures for evaluating the resistance of steels to HIC and against the concurrent action of tensile stress and hydrogen sulphide environment

Since 1984, NACE (National Association of Corrosion Engineers) Standard has been used for evaluating the resistance of steels to HIC (**NACE TM 0284-2011 Standard Test Method – Evaluation of Pipeline and Pressure Vessel Steels for Resistance to Hydrogen-Induced Cracking**). In 2000, the Czech standard ČSN EN 10229 “Evaluation of resistance of steel products to hydrogen induced cracking (HIC)” came into effect. Evaluation according to this standard is essentially identical to the NACE Standard.

For the evaluation of resistance of steels to the concurrent action of tensile stress and hydrogen sulphide environments, **NACE Standard TM 0177 – 2005: Laboratory Testing of Metals for Resistance to Sulfide Stress Cracking and Stress Corrosion Cracking in H₂S Environments** is used. By the term sulphide stress corrosion cracking we call the failure that occurs at ambient temperature, while stress corrosion cracking is a failure that occurs at elevated temperatures. The test procedure to evaluate the resistance of carbon and low-alloy steels to SSC for acidic environments is referred to in ČSN EN ISO 15 156-2 standard and for corrosion-resistant and other crack-resistant alloys in ČSN EN ISO 15156-3 standard.

7.3.1 Evaluation of the resistance of steels to hydrogen-induced cracking (HIC)

The test consists in a metallographic evaluation of the occurrence of cracks on the scratch patterns of three specimens of dimensions 100 mm x 20 mm x thickness, which were previously exposed to acidic test solution saturated with hydrogen sulphide at the temperature of $25 \pm 3^\circ\text{C}$. Collection of test samples for exposure depends on the thickness of the evaluated component and for metal plates it is illustrated in Figure 7.3. All samples are prepared in advance with dimensions by 0.25 mm larger than is the final thickness or height. This addition is then removed on both sides by wet grinding on a rotating disc or in any other comparable manner. Main surfaces of test specimens are then ground by standard metallographic method with 320 grit sandpaper.

Exposure of samples must be carried out in communicating airtight vessels that are large enough to accommodate samples (see Fig. 7.4). According to NACE Standard TM 0284, the ratio of the solution volume and the surface of sample must be at least 3 ml/cm^2 .

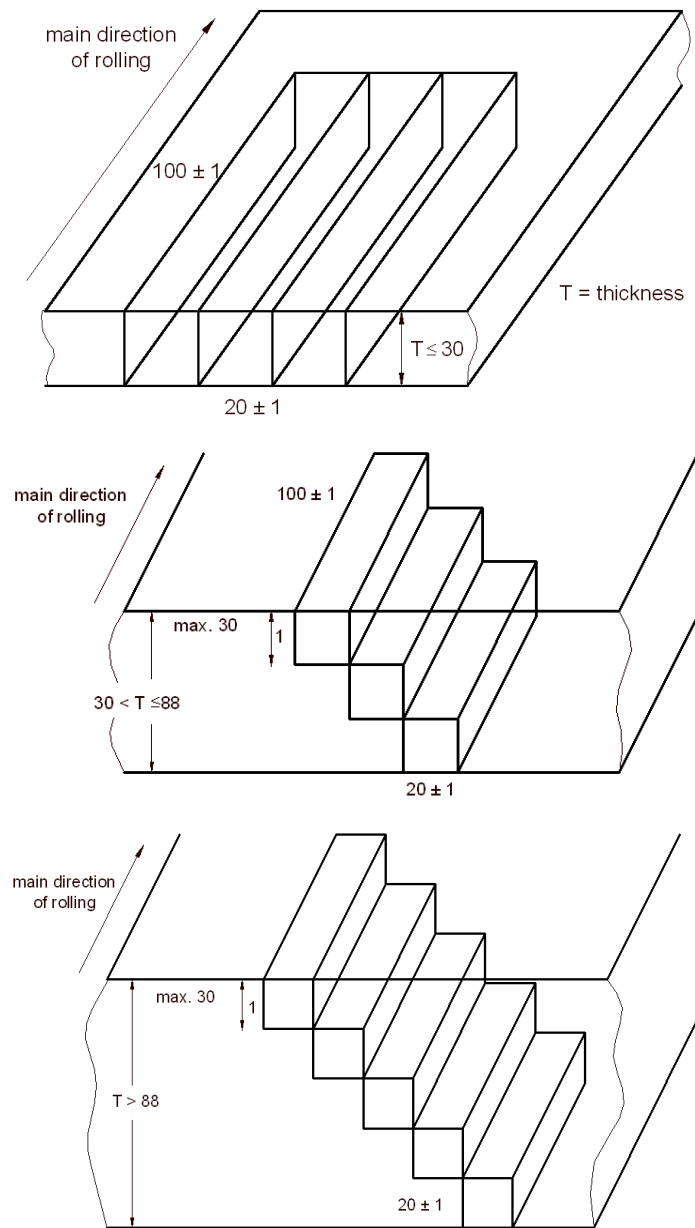


Fig. 7.3 Collection of samples for exposure by the sheet metal thickness



Fig. 7.4 Airtight vessels used for exposure of samples in the company MATERIÁLOVÝ A METALURGICKÝ VÝZKUM, s.r.o.

Samples are placed in vessels in a manner illustrated in Figure 7.5.

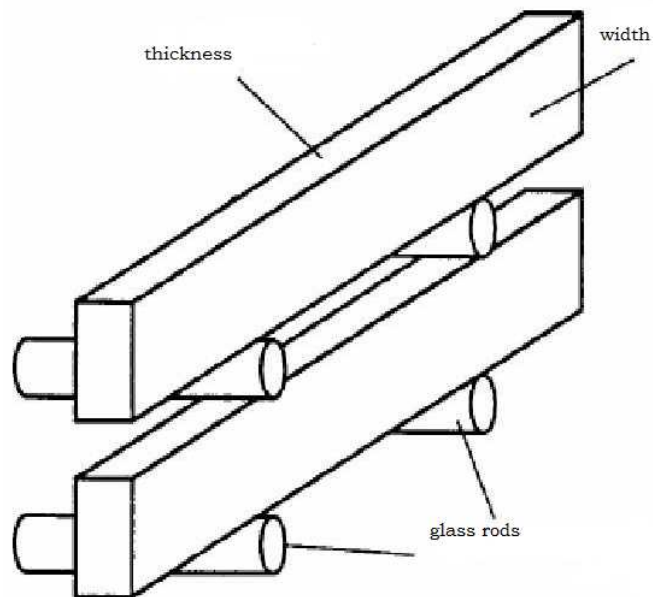


Fig. 7.5 Method of placing samples in glass vessels.

The standard allows the use of two kinds of test solutions. Solution A is made up of sodium chloride (5 wt. %), acetic acid (0.5 wt. %), hydrogen sulphide and distilled water. Its initial pH should be 2.7 ± 0.1 and pH after the test shall not be greater than 4.0. Test solution B consists of hydrogen sulphide and synthetic seawater. The initial pH must be in the range 8.1 - 8.3, final must be between 4.8 and 5.4. If pH values are not met, the test results are not valid. At first, nitrogen is bubbled through the solution, followed by hydrogen sulphide to the concentration of min 2.3 ppm. Exposure time is normally 96 hours, but in some cases it can be extended up to 720 hours based on customer requirements.

After exposure to the test solution, three metallographic samples are prepared from each test specimen oriented perpendicular to a length of 100 mm. The method of collecting samples for preparation of three metallographic sections is illustrated schematically in Figure 7.6.

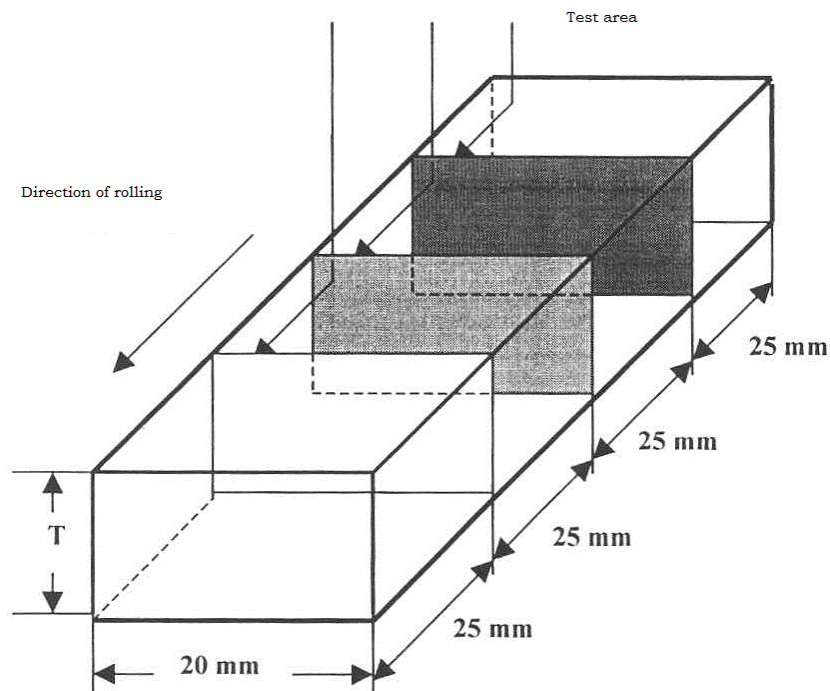


Fig. 7.6 The method of collecting samples for preparation of metallographic sections

Crack parameters are then measured on the metallographic sections at 100x magnification - the length (a) and thickness (b) (see Fig. 7.7). Cracks being less than 1 mm away from the surfaces of the sample are not included in the evaluation. Following parameters are then determined from the measured values:

Crack Length Ratio - CLR,

Crack Thickness Ratio - CTR,

Crack Sensitivity Ratio - CSR

according to the following relationships:

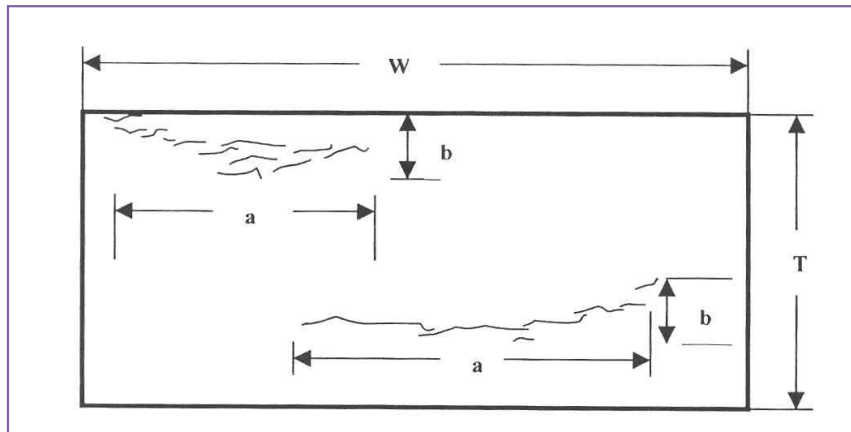


Fig. 7.7 The process of measuring lengths and widths of cracks on the metallographic section

$$CLR = \frac{\sum a}{W} 100 \quad [\%] \quad (6.1)$$

$$CTR = \frac{\sum b}{T} 100 \quad [\%] \quad (6.2)$$

$$CSR = \frac{\sum(a \cdot b)}{W \cdot T} 100 \quad [\%] \quad (6.3)$$

where a is the crack length [mm],
 b is the crack thickness [mm],
 W is the sample width [mm],
 T is the sample thickness [mm].

The above crack parameters are determined for every metallographic section, and also as averages of three values of the initial test specimen. The test results apply to three test specimens, a total of nine metallographic sections.

NACE Standard TM 0284 does not address the criteria by which materials can be rated as satisfactory or unsatisfactory. This is always subject to negotiation between the supplier and the customer. Metallurgical companies usually offer their customers products (steel sheets) with guaranteed maximum values for the crack parameters in the appropriate test solutions. These steel sheets are further divided into several quality classes (see Tab. 7.1). In principle, it can be stated that acceptable is CLR value of 5-15% (solution A) and CLR value of ca 0% (solution B).

Tab 7.1 Guaranteed values of crack parameters of selected carbon steel sheets (solution A)

Steel manufacturer	Product (steel sheet) name	CLR [%]	CTR [%]	CSR [%]
Dillinger Hütte GROUP	DICREST 5	≤ 5	≤ 1.5	≤ 0.5
	DICREST 10	≤ 10	≤ 3	≤ 1
	DICREST 15	≤ 15	≤ 5	≤ 2
	DICREST 15*	≤ 0.5	≤ 0.1	≤ 0.05
Masteel UK, Ltd	MASTERHIC 5	≤ 5	≤ 1.5	≤ 0.5
	MASTERHIC 10	≤ 10	≤ 3	≤ 1
	MASTERHIC 15	≤ 15	≤ 5	≤ 2
ArcelorMittal GROUP	CarElso ®HIC Premium	≤ 5	≤ 1.5	≤ 0.5

* Valid for testing in the test solution B

Besides standard HIC tests according to NACE Standard TM 0284, in practice, sometimes also modified single-sided tests are used, in which only one side of the specimen is in contact with a corrosive solution and hydrogen may diffuse away through the outer surface of the material. In this case, on the one hand, the hydrogen content in hydrogen traps changes

and on the other, there is a change in the hydrogen content in the inter-nodal positions of the crystal lattice. Single-sided tests (see Fig 7.8) are justified, because in practice only the inner wall of the pipe or pressure vessel is in contact with aggressive medium.

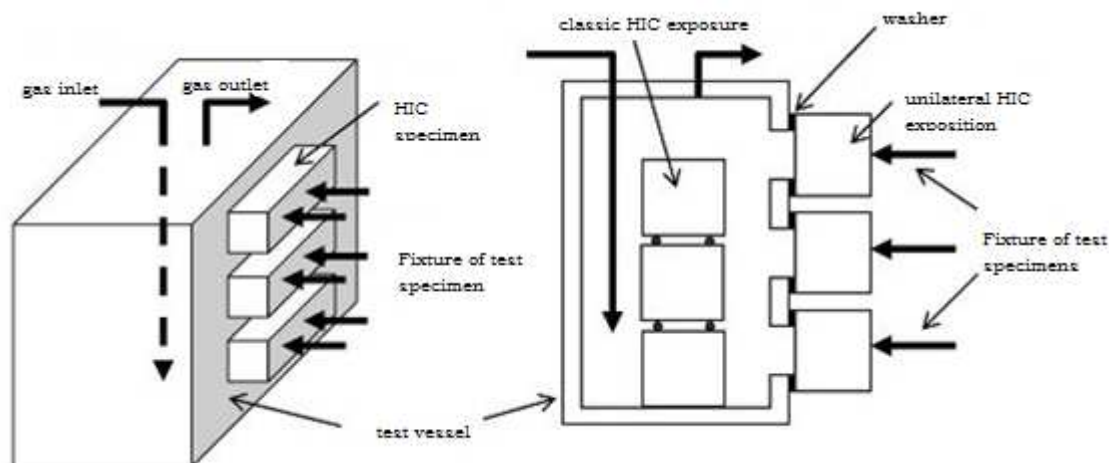


Fig. 7.8 Schematic representation of a single-sided HIC test

From a practical point of view it should be noted that while the methodology of evaluation of HIC cracks seems very simple, to get the right results is often a big problem. In many cases, the exposure in the test solution leads to formation of very thin cracks that are not identifiable on metallographic sections in the polished state, even after normal etching. For these cracks to be visible, it is necessary to polish and etch the samples repeatedly, and the final etching must be very shallow so that the cracks do not merge with the surrounding microstructure. In terms of device integrity, these cracks are of course as dangerous as cracks wide open.

New customer requirement for high-strength metal sheets for acidic environments is the CAR (Crack Area Ratio) parameter - proportional area of cracks defined as the ratio of crack area in the evaluated sample. This parameter is not included in NACE Standard TM 0284, because it cannot be determined metallographically. It is evaluated using ultrasonic test equipment in the immersion bath with X-Y manipulator. The only place in the Czech Republic where it is possible to measure this parameter is the company TRINECKÉ ŽELEZÁRNY, a.s. by means of UPR4 SCRI Ultrasonic Testing Machine from Krautkrämer (see Fig. 6.9). In addition to CAR parameter, this device also enables to provide CLR, CTR and CSR parameters and thereby make a complete assessment of the material resistance to HIC.

Evaluation of samples is performed on a 4-axis scanner on which a probe is mounted that performs the scan (control) using the pulse reflection method at room temperature. Always 80% of the volume of the specimen is scanned, i.e. without the surface layers.

All testing parameters (position of the probe, the dimensions of the specimen, ultrasonic and scanning parameters) are stored and so the test is 100% repeatable. The device also enables a time-saving control by testing several specimens at once, but with a separate evaluation of the required parameters for each such specimen.



Fig. 7.9 General view of the ultrasonic equipment by Krautkrämer

The result of each test is given in the report, which lists all evaluated parameters (see Fig 7.10). The great advantage of this method is the speed at which the evaluation of resistance to HIC is determined. While the evaluation of a sample on UPR4 SCRI Ultrasonic Testing Machine takes approximately 10 minutes, the metallographic evaluation of three sections takes about 15 hours.

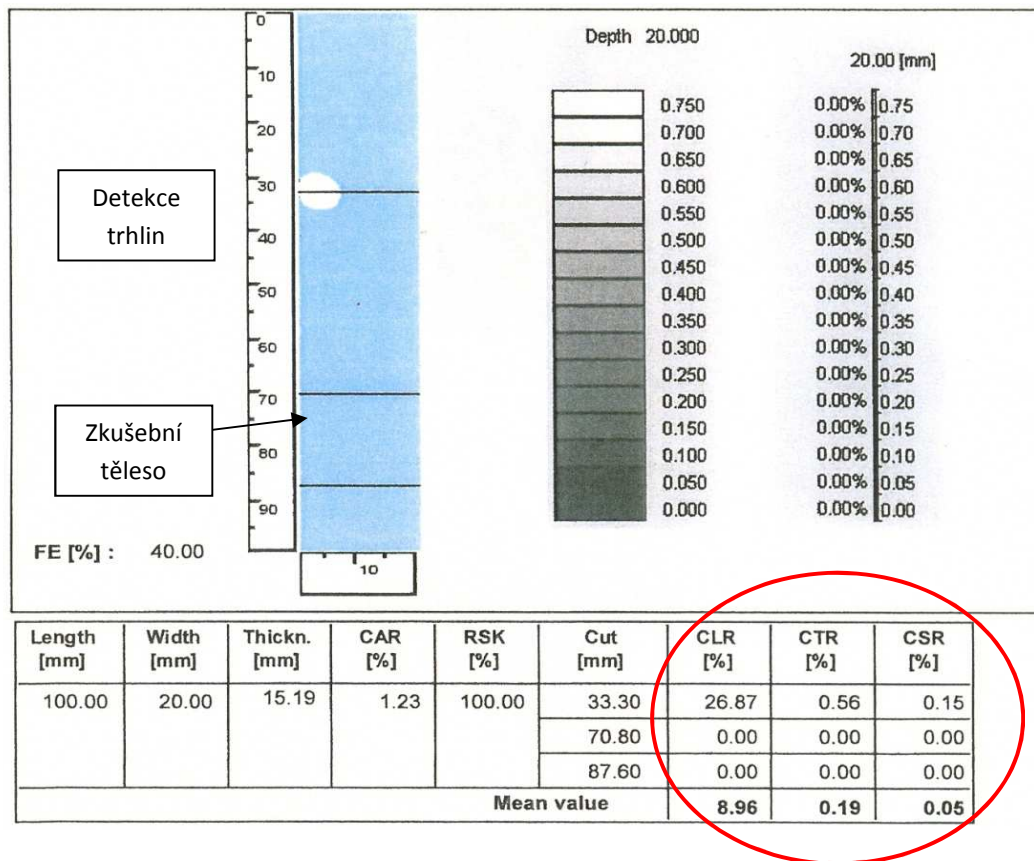


Fig. 7.10 Protocol on the result of test on the ultrasonic equipment by Krautkrämer

7.3.2 Evaluation of the resistance of steels against concurrent action of tensile stress and hydrogen sulphide environment

Evaluation of the resistance of steels against concurrent action of tensile stress and hydrogen sulphide environment is performed according to **NACE Standard TM 0177-2005 Laboratory Testing of Metals for Resistance to Sulfide Stress Cracking and Stress Corrosion Cracking in H₂S Environments**. According to this standard, the resistance of metals, especially steels, to sulphide stress cracking (room temperature, atmospheric pressure) and to stress corrosion cracking (elevated temperatures and pressures) is evaluated.

Evaluation of the resistance of steels to sulphide stress cracking consists in loading the test specimen in the test solution saturated by hydrogen sulphide at room temperature under static load below the yield strength. The threshold stress is determined that after a certain test duration (normally 720 hours) does not lead to a body failure or initiation of defects on the

surface of the samples that are visible under tenfold magnification. Example of longitudinal cracks on the specific part of the test bar after SSC test is shown in Fig. 7.11.



Fig. 7.11 Longitudinal cracks on the specific part of the test bar after SSC test – X70 grade steel

Test solutions are essentially the same as in NACE Standard TM 0284, but it is also possible to adjust the test solution so as to obtain a specific pH value. Again, NACE Standard does not specify any criterion that would allow deciding whether the material is resistant to SSC or not. Most evaluations, however, are based on the fact that the material must withstand the load that is at least equal to 0.8 times the yield strength.

The Standard describes four test methods:

- Method A – Tensile test (NACE Standard Tensile Test)
- Method B – Bending test (NACE Standard Bent-Beam Test)
- Method C – Test using “C” rings (NACE Standard C-Ring Test)
- Method D – Test for determining the crack growth resistance (NACE Standard Double-Cantilever Beam Test)

7.3.2.1 Method A – NACE Standard Tensile Test

This method is the most widely used method of evaluating the resistance of steels to SSC. During the test, the specimen can be loaded with a constant load (Constant Load Dead Weight Device). In this case we are talking about a soft loading mode. Specimen loading may be also

deduced in special jigs on the basis of the body being loading to a constant level of strain corresponding to the desired level of loading (hard loading mode). Figure 7.12 shows test devices of “Dead Weight” type used in the company Arcelor Mittal Ostrava to evaluate the resistance of steels to SSC.



Fig. 7.12 Dead Weight Device in Arcelor Mittal Ostrava

The most widely used type of specimen is shown in Figure 7.13.

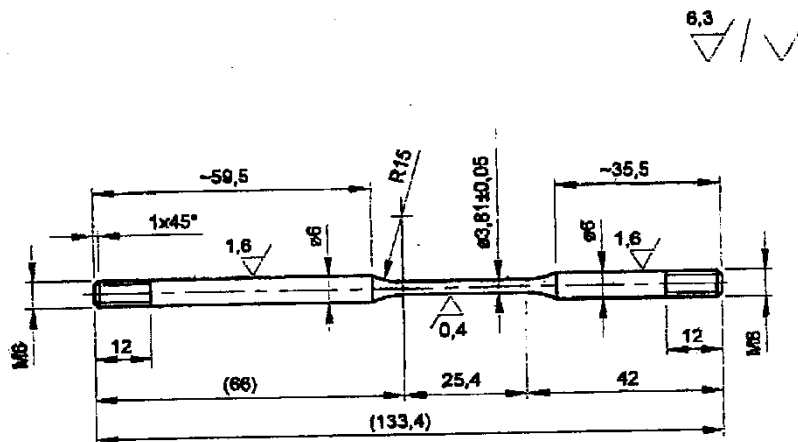


Fig. 7.13 Dimensions of the specimen used for evaluation of resistance to SSC

Schematic representation of the test chamber for testing in the "Dead Weight" device is shown in Figure 6.14

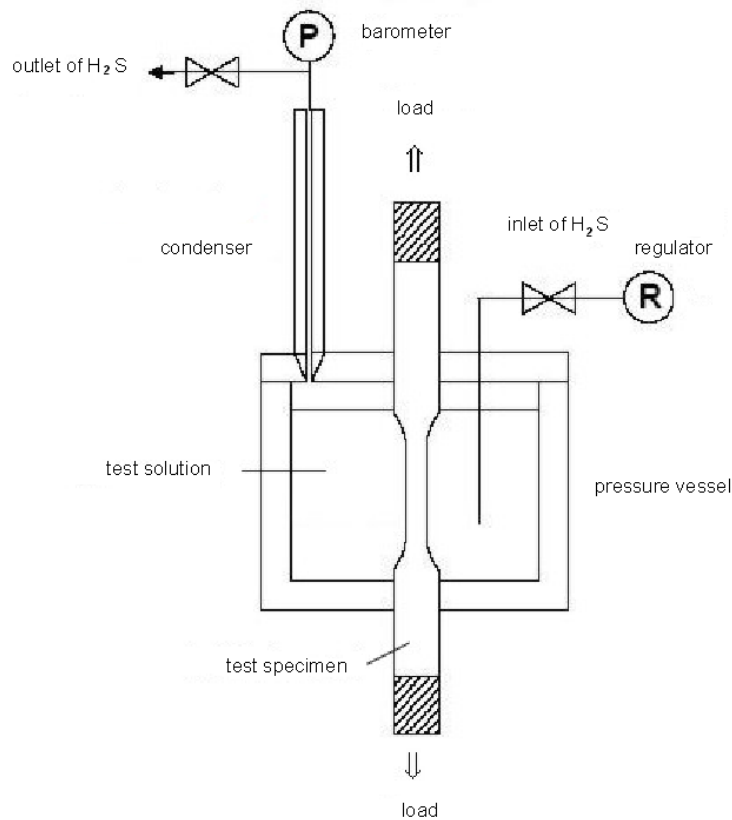


Fig. 7.14 Schematic representation of the test chamber for SSC tests

Figure 7.15 shows the test jig which allows deduction of the loading force using a screw resting on disc springs.

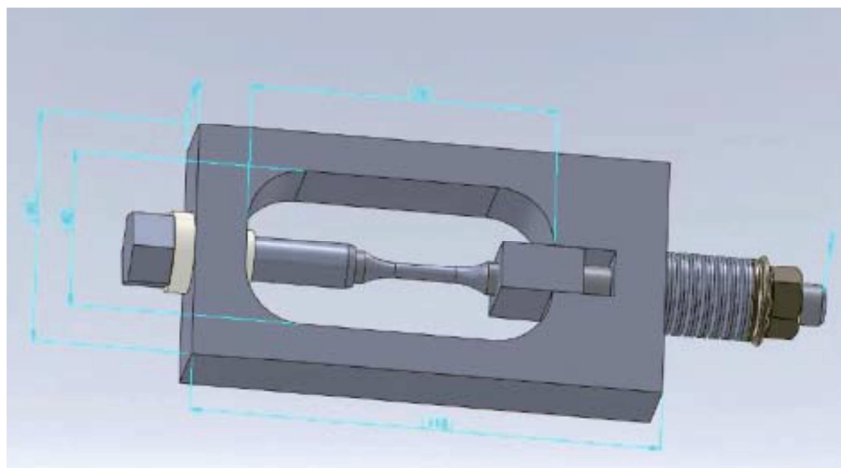


Fig. 7.15 Loading of a specimen in a jig with disc springs

The test specimen is insulated from a sample with a Teflon liner, which is located on the opposite side of the jig than the springs. The specimen is loaded in the jig using the longitudinal strain sensor and then it is exposed to the test solution.

The cylindrical test specimens with a specific part diameter of 3 mm, loaded in test frames according to ASTM Standard G49-85, can also be used to evaluate the resistance to SSC (see Fig. 7.16).

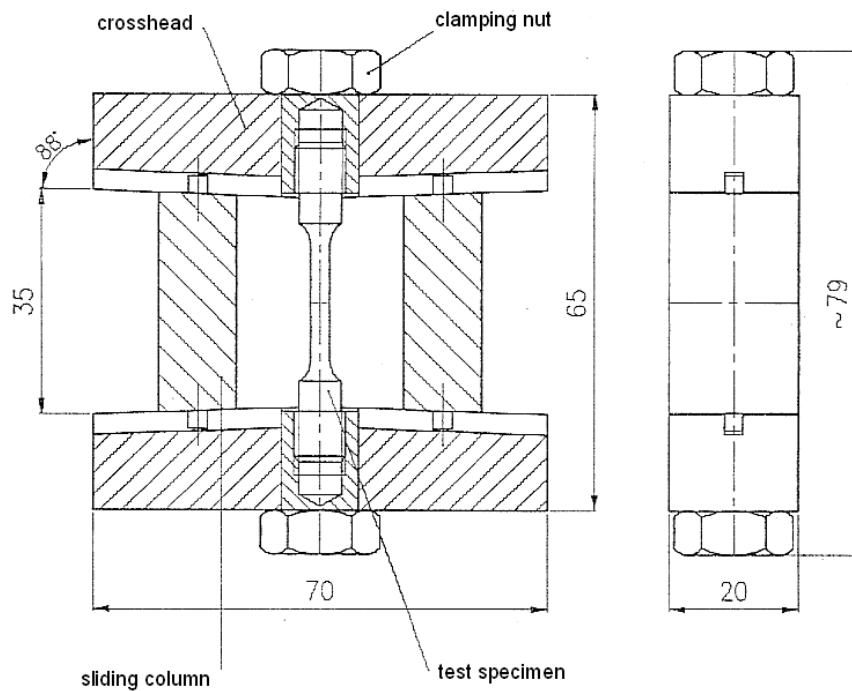


Fig. 7.16 Dimensions of the load frame according to ASTM Standard G 49-85 used for loading smooth cylindrical bodies with a specific part diameter of 3 mm

Loading of specimens in the test frame is due to movement of the posts in a specially manufactured jig. A longitudinal strain sensor with a 10 mm base is attached to the test specimen under load that allows loading the test specimen to a preselected value of the total strain (see Fig. 7.16). From σ - ϵ dependence determined by a tensile test on the same specimens at a selected test temperature, the stress to which the specimen is pre-loaded can be subtracted. Test specimens thus prepared are then placed in a test solution and subjected to the required exposure time (see Fig. 7.17).



Fig. 7.16 The procedure of loading specimens in a test frame



Fig. 7.17 Exposure of specimens loaded in test frames according to ASTM Standard G 49-85



Summary of terms

After studying the chapter, following terms should be clear to you:

- Degradation mechanisms in an environment containing hydrogen sulphide
- Hydrogen induced cracking
- Sulphide stress cracking
- Stress-oriented hydrogen induced cracking
- NACE Standard TM 0284.
- CLR, CTR, CSR, and CAR parameters
- NACE Standard TM 0177 – 2005
- Fish eyes
- Method A – NACE Standard Tensile Test.



Questions about the curriculum learnt:

1. What degradation mechanisms apply in hydrogen sulphide environments?
2. What we mean by HIC?
3. What we mean by SSC?
4. What standards are used for the evaluation of resistance of steels to HIC and/or SSC?
5. By what criteria specimens are taken from metal sheets for the evaluation of HIC?
6. What parameters are measured in HIC tests?
7. What test methods for evaluating the resistance to SSC do you know?
8. What are the fish eyes?



References

- [1] http://www.corrosionclinic.com/different_types_of_corrosion.htm [cit. 2012-07-10].
- [2] Research Report on Characterization and Monitoring of Cracking in Wet H₂S Service, API Publication, Washington, D. C., 1994.
- [3] /ANSI/NACE MR 0175/ ISO 15156. *Petroleum and Natural Gas Industries - Materials for Use in H₂S Containing Environments in Oil and Gas Production – Parts 1, 2 and 3*, Second edition 2009-10-15.
- [4] NACE Standard TM 0284-2011. *Evaluation of Pipeline and Pressure Vessel Steels for Resistance to Hydrogen Induced Cracking*. NACE Int., Houston, Texas, USA, 2011, 24 s. ISBN 1575901633.
- [5] ČSN EN 10229. *Hodnocení odolnosti ocelových výrobků vzniku trhlin indukovaných vodíkem (HIC)*. Praha: Český normalizační institut, 2000.
- [6] NACE Standard TM 0177-2005. *Laboratory Testing of Metals for Resistance to Sulfide Stress Cracking and Stress Corrosion Cracking in H₂S Environments*. NACE Int., Houston, Texas, USA, 2005.
- [9] CARNEIRO, A., R., RATNAPULI, C., R., LINS, C., F., V. The Influence of Chemical Composition and Fracture of API Linepipe Steels on Hydrogen Induced Cracking and Sulfide Stress Cracking, *Mat. Sci. Eng. A* 357, 2003, s. 104 – 110.
- [10] Dillinger Hütte GTS. *Products* [online]. [cit. 2012-04-08]. Dostupné z: <http://www.dillinger.de/dh/produkte/sparte/index.shtml.en>
- [11] KITTEL, J. et al. Hydrogen Induced Cracking (HIC) Assessment of Low Alloy Steel Linepipe for Sour Service Application – Laboratory Testing. In: *Eurocorr 2007*. Freiburg, Německo. 2007. CD-ROM.
- [12] SOJKA, J. *Odolnost ocelí vůči vodíkové křehkosti*. Vyd. 1. Ostrava: Vysoká škola báňská - Technická univerzita Ostrava, Fakulta metalurgie a materiálového inženýrství,

Katedra materiálového inženýrství, 2007, 108 s.
ISBN 978-80-248-1648-7.

- [13] ASTM G49 - 85. *Standard Practice for Preparation and Use of Direct Tension Stress-Corrosion Test Specimens*. ASTM Int., West Conshohocken, PA, USA, 2011.
- [14] ASTM G39 - 99. *Standard Practice for Preparation and Use of Bent-Beam Stress-Corrosion Test Specimens*. ASTM Int., West Conshohocken, PA, USA, 2011.

8. Evaluation of mechanical properties of structural steels using penetration tests



Study time: 2.5 hours



Objective: After reading this chapter, you should be able to:

- Define the concept of actual and initial mechanical properties.
- Describe the principle of penetration test.
- Describe types of penetration tests.
- Describe the areas of the force-displacement dependence measured during the “Bulge” test
- Describe the quantities measured for determining the strength properties and fracture behaviour of materials from the results of penetration tests.
- Describe methods to determine the yield strength and ultimate strength from the results of penetration tests.
- Describe the method to determine the transition behaviour from the results of penetration tests.
- Describe methods to determine the fracture toughness from the results of penetration tests.



Presentation

8.1 Introduction

Qualified assessment of the integrity and/or remaining life of long-term operating facilities, or the pursuit of a reasonable extension of their design life, which brings substantial financial savings, requires the knowledge of the actual level of a wide range of mechanical characteristics of the materials used. Their knowledge is also essential for:

- optimizing the operating modes,
- optimizing the intervals of operational checks, and
- optimizing the long-term plan of maintenance and repairs.

The use of standardized procedures for determining the required actual mechanical characteristics of operated facilities may, in addition to unavoidable shutdowns and operational constraints, cause significant damage to them during the collection of the test material, as well as during subsequent repairs carried out mostly by welding.

Even more complicated is the situation in the evaluation of mechanical properties using standardized procedures in localized areas, such as coatings, surface layers formed by thermochemical treatment, weld deposits or welding joints (including properties of heat-affected zones - HAZ). Evaluation of mechanical properties of coatings and surface layers formed by thermochemical treatment is restricted mainly to the hardness measurement. Evaluation of mechanical properties of individual areas of HAZ of welded joints can be performed by indirect methods based on laboratory simulations of these localized areas.

Besides the actual mechanical properties, the assessment of the degree of degradation of material properties due to long-term operation requires knowledge of the initial (zero) state of the material. In most cases, however, the initial properties of the materials of evaluated components are not known and the actual mechanical properties are compared with the properties mentioned in the material standards or test certificates of base semi-finished products.

As a result of technological operations during manufacture, the mechanical properties of materials at the beginning of the operation of an equipment or structure may significantly differ from those of the base semi-finished products. Traditional methods of obtaining test material for control of technological processes in the manufacture of components are based on additions or reference samples of materials that go through the whole technological cycle with the manufactured component.

To determine the actual properties of the materials of long-term operating facilities or initial properties of the materials of structures and equipment placed into service, which take into account all technological operations during their manufacture, it is necessary to minimize the amount of required test material, best taken from the most critical points of components, without violating their integrity, if possible, and therefore the need for subsequent repairs, while maintaining its representativeness. This requirement led to:

- 1) the development of technological processes and devices that allow taking the test material from the outer and/or inner surface of an assessed component, while maintaining its integrity and without the need for subsequent repairs,
- 2) the development and implementation of methods that use for determination of strength, brittle fracture and creep characteristics of materials penetration tests carried out on disc-shaped specimens with a diameter up to 8 mm and/or test bodies of a square shape with a side of 10 mm and thickness up to 0.5 mm.

With the high precision of current tensile testing machines, computer control of the testing process and outputs in the form of digital recording, on the one hand, and knowledge of the impact of structural factors and test conditions, on the other hand, the current penetration tests provide a high level of precision and reproducibility of results comparable to conventional tests of mechanical properties carried out on standardized test specimens.

8.2 Principle of a penetration test

The principle of a penetration test consists in penetration of a shaped punch through the flat disc-shaped or square specimen, with a thickness of $0.2 \div 0.6$ mm until its failure. Schematic layout of the penetration test is shown in Figure 8.1.

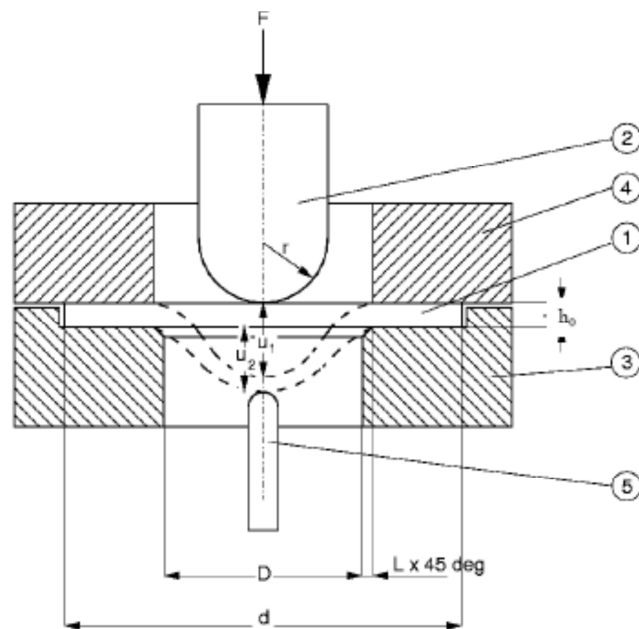


Fig. 8.1 1 – disk-shaped specimen, 2 - punch, 3 – receiving die 4 – clamping die, 5 – deflection measurement

During the test, the load – punch displacement dependence (u_1) or load – sample deflection dependence (u_2) in the load axis is measured.

According to the shape of the penetrating part of the punch and method of specimen attachment, we divide the penetration tests to the ball penetration test (ball punch test), shear penetration test (shear punch test), and bending penetration test (disc bend test). In the ball penetration test, the steel or ceramic ball or punch with a hemispherical head is forced through. By the method of clamping the sample, we divide the ball tests to “Bulge Punch Test” and “Punch Drawing Test”. If the specimen is clamped between the lower supporting matrix and the upper pressure matrix, it is the so called “Bulge Punch Test”. If the specimen is laid loosely on the lower supporting matrix, it is the so called “Punch Drawing Test”.



Fig. 8.2 Shape of punch used for ball and shear tests

In the shear test, a sharp-edged circular punch is used (see Fig. 8.2) and the specimen is clamped between the lower supporting matrix and the upper pressure matrix. And in the bending penetration test is a cone-shaped punch is forced through the sample lying loosely on the supporting matrix.

8.3 Ball penetration test (Bulge Punch Test)

During this test, a specimen clamped between the lower supporting matrix and the upper pressure matrix is forced through by a punch with a hemispherical head and/or steel/ceramic ball until failure. CEN Workshop Agreement recommends a disc-shaped specimen for this test, with 8 mm in diameter and 0.5 mm thick, yet also square bodies are acceptable. The thickness of the test specimen should be in the range $0.2 \div 0.6$ mm. Figure 8.3 shows an example of a jig for carrying out the ball “Bulge” test at room temperature. After the sample

is placed in the lower supporting matrix, the matrix is inserted into a bushing and the test sample is clamped through the guide bushing by the pressure matrix.

Then the punch is inserted into the guide bushing through the opening in the pressure matrix and the jig is placed in the frame of the testing device (see Fig. 8.4) and loaded in a constant rate mode of the punch movement by the rate in the range $0.2 \div 2$ mm/min.



Fig. 8.3 Test jig for ball “Bulge” test at room temperature



Fig. 8.4 Laying of test jig in the frame of the testing device

In the course of loading, the force – punch displacement dependence and/or the force – sample deflection dependence in the load axis is measured. Characteristic recording of the course of the force – punch displacement dependence during the ball “Bulge” test is shown in Figure 8.5. This dependence can be generally divided into five regions (I, II, III, IV, and V):

Region I

This region is characterized by a micro-plastic deformation of the specimen under the punch due to a high initial contact stress. But the predominant deformation of the sample in the region far away from this contact is elastic and unloading of the test specimen from any point in this region produces no permanent macroscopic deformation.

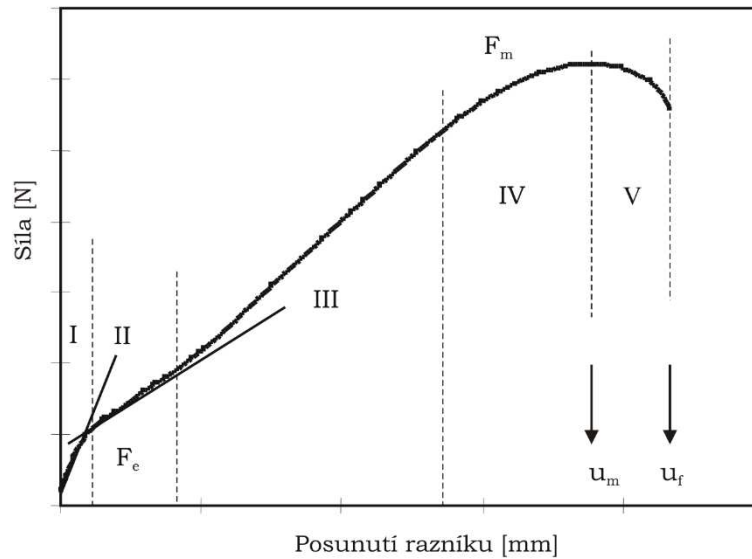


Fig. 8.5 Typical force-punch displacement dependence during the ball test at room temperature

Region II

This region is characterized by a departure from linearity associated with the spread of the plasticized area across the thickness of the specimen and subsequently in the radial direction. In connection with this, there is a decrease in the rate of loading, which is explained by the so called membrane effect at a continuous change in the angle of contact of the penetrating ball with the deformed sample. This region is referred to as plastic bending.

Region III

At the beginning of this stage determined by the inflection point of the force - punch displacement dependence, the transition from the plastic bending to membrane stretching takes place. This region depends on the characteristics of the material hardening.

Region IV

At this stage, a neck is being formed with a rising force in the area of contact between the punch and specimen, which has the effect of reducing the inclination of the force – punch displacement dependence.

Region V

A crack is initiated at the beginning of this stage. During the steep decline of force the biaxial state of stress leads to the growth of a crack along the perimeter of the specimen (see Fig. 8.6) and/or at the top of the “cap”.

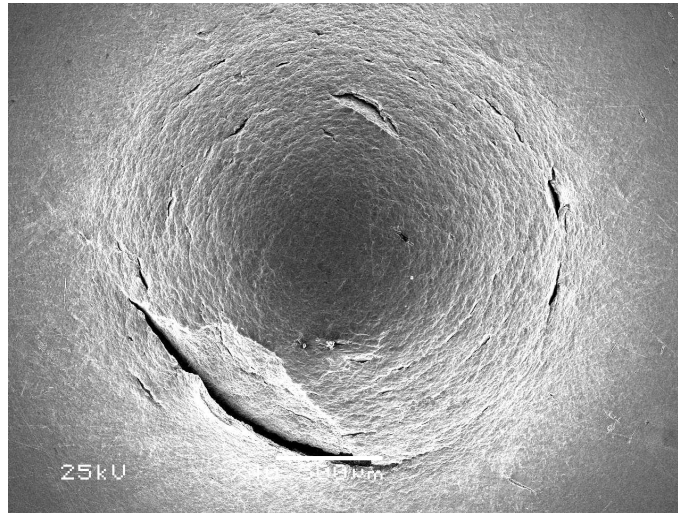


Fig. 8.6 Typical failure of a disc-shaped specimen during the ball “bulge” test at room temperature (S355J2G3 grade steel)

From the above dependence and shape of a damaged specimen, following quantities are determined that are used to measure the strength properties and fracture behaviour of materials:

- F_e [N] the force characterizing the transition from linearity to the stage associated with the development of plastic deformation across the thickness of the sample,
- F_m [N] the maximum force recorded during the penetration test,
- u_m [mm] the punch displacement corresponding to F_m ,
- u_f [mm] the punch displacement corresponding to the specimen failure that by convention corresponds to 20% decrease in the maximum force during the penetration test ($F_f = 0.8 \cdot F_m$),
- E^{SP} [J] fracture energy calculated from the area under the force – punch displacement dependence until the moment of the specimen failure.
- ε_f [1] $\varepsilon_f = \ln(h_0/h_f)$ – effective fracture deformation (h_0 is the initial thickness of the sample, h_f is the minimum thickness of the damaged sample).

Figure 8.7 illustrates the force – punch displacement dependences determined for 15128 grade steel thermally treated to three significantly different levels of strength properties.

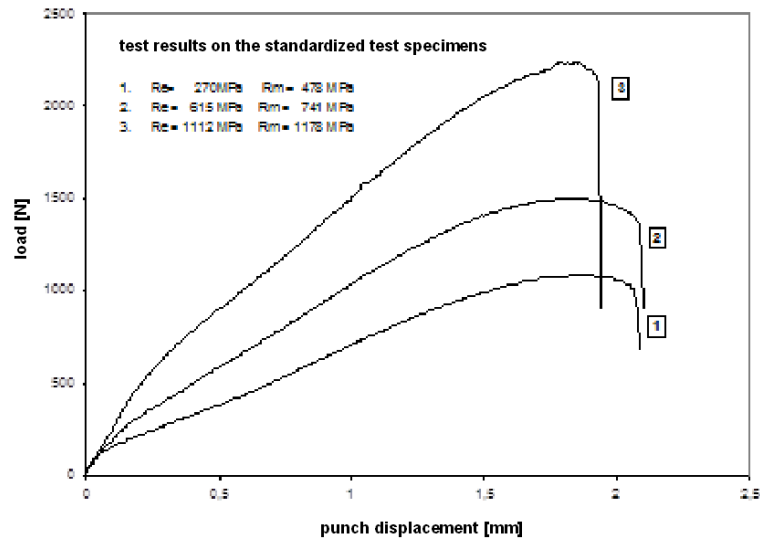


Fig.8.7 The force – punch displacement dependences determined for three strength levels of 15128 grade steel

Figure 8.7 clearly shows that with an increasing yield strength and ultimate strength of the material, also the force F_e characterizing the transition from stage I to stage II (see Fig 8.5) increases during the penetration test, as well as the maximum force F_m . It is therefore evident that the force – punch displacement dependence determined during the penetration test contains information about the elastoplastic behaviour and strength characteristics of the material under biaxial state of stress.

Character of the force - punch displacement dependence is further influenced by the radius of ball/punch, diameter of the hole in the lower matrix D (see Fig 8.1) and the initial thickness of a specimen h_0 .

The force characterizing the transition from linearity to the stage associated with the development of plastic deformation across the thickness of sample F_e size is not significantly affected by the punch radius r or diameter D of the hole in the lower matrix, but depends significantly on the sample thickness h_0 (see Fig 8.8).

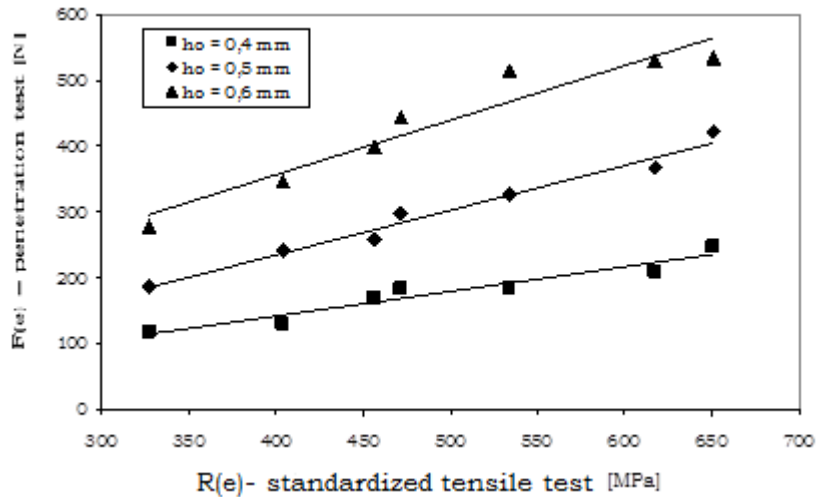


Fig. 8.8 Effect of the test disc thickness on the level of force F_e during the penetration “Bulge” test of 15128 grade steel at room temperature ($r = 1$ mm, $D = 4$ mm)

The maximum load during the penetration test increases with an increasing strength of the material, with an increasing radius r of the punch and with the test disc thickness h_0 (see Fig. 8.9).

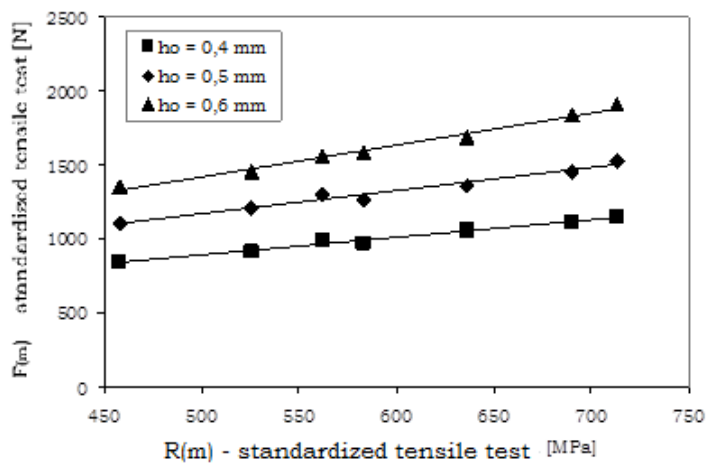


Fig. 8.9 Effect of the test disc thickness and ultimate strength of 15128 grade steel on the level of force F_m during the penetration “Bulge” test at room temperature ($r = 1$ mm, $D = 4$ mm).

8.4 CWA 15627 Small Punch Test Method for Metallic Materials

Practical use of this method was discouraged by absence of any standardized procedure. In September 2004, the European Committee for Standardization (Comité Européen de Normalisation – CEN) organised the CEN Workshop Agreement 21 “Small Punch Test

Methods for Metallic Materials”. In December 2007, CEN published CWA 15 627 “Small Punch Test Method for Metallic Materials“. CEN Workshop Agreement is a technical convention within CEN, owned by CEN as a publication, which reflects the consensus of particular experts and organisations responsible for its contents (participation of 32 organisations from 13 countries). CWA therefore represents a lower level of consensus than is represented by a European standard. CWA 15627 is divided into two separate parts:

❖ Part A: A Code of Practice for Small Punch Creep Testing.

This part describes the procedure for performing time-dependent penetration tests at elevated temperatures, which cause the application of creep. Furthermore, this part contains ANNEX A1: “Relationship to uniaxial creep test properties”, in which the equation proposed by various authors are specified, describing the relationship between the uniaxial tensile stress in the standardized creep test and the force loading the specimen during the creep penetration test for the same time to failure.

❖ Part B: A Code of Practice for Small Punch Testing for Tensile and Fracture Behaviour.

This part describes the procedure for performing time-independent penetration tests at room temperature, increased temperature (up to 400°C) and low temperature and determining the characteristics obtained from the force – punch displacement dependence and from the damaged specimen. Furthermore, this part contains ANNEX B1: “Derivation of tensile and fracture material properties“, in which the procedures for determining the yield strength, ultimate strength, ductility and brittle fracture properties are specified (FATT, J_{IC} , K_{IC} at room temperature) from the results of penetration tests.

8.5 Procedure for performing time-independent penetration tests

This procedure gives you instructions for performing time-independent penetration tests at room temperature, increased temperature (up to 400°C) and/or decreased temperature. Their goal is to determine the characteristics subsequently used to estimate the strength and brittle fracture characteristics of materials (R_e , $R_{p, 0.2}$, R_m , A , FATT and J_{IC} or K_{IC}). It was designed especially for the evaluation of the mechanical properties of metallic materials, but can also be used for the evaluation of other types of materials. It includes requirements for:

1. test devices, loading system and measurement of the deflection of sample,
2. preparation of a test specimen (recommended is a disc-shaped test specimen with a diameter of 8 mm and thickness of 0.5 mm),
3. data collection, and

4. rate of loading. The rate of punch displacement should be in the range $0.2 \div 2$ mm/min.

During the penetration test, the dependence of force - punch displacement or force – sample deflection to the failure is measured (see Fig. 8.10).

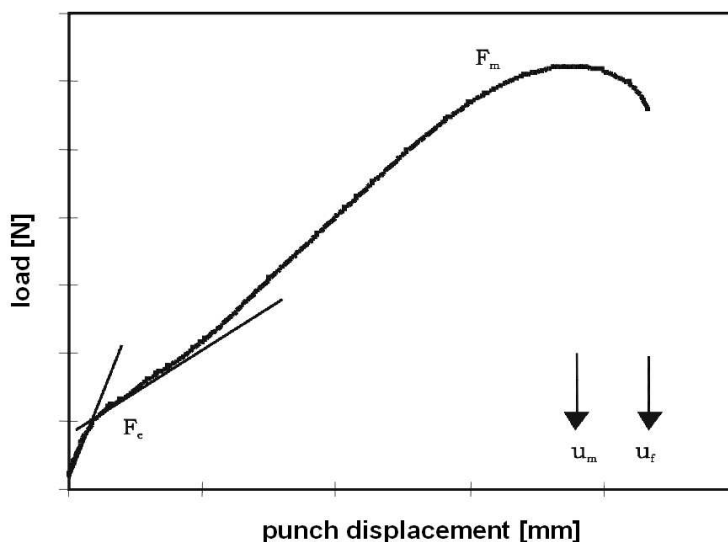


Fig. 8.10 The force – punch displacement dependence measured during the penetration test

From the above dependence and damaged test specimen following quantities are determined that are used for specification of strength characteristics and fracture behaviour of materials:

- F_e [N] the force characterizing the transition from linearity to the stage associated with the development of plastic deformation across the thickness of the sample,
- F_m [N] the maximum force recorded during the penetration test,
- U_m [mm] the punch displacement corresponding to F_m ,
- u_f [mm] the punch displacement corresponding to the specimen failure that by convention corresponds to 20% decrease in the maximum force during the penetration test ($F_f = 0.8 \cdot F_m$),
- E^{SP} [J] fracture energy calculated from the area under the force – punch displacement dependence until the moment of the specimen failure,
- ε_f [1] $\varepsilon_f = \ln(h_0/h_f)$ – effective fracture deformation (h_0 is the initial thickness of the sample, h_f is the minimum thickness of the damaged sample).

Figure 8.11 illustrates the procedure for determining the force F_e from the force – punch displacement dependence. To determine the fracture strain ε_f , it is necessary to measure the

minimum thickness of the damaged sample. Procedure for determining the minimum thickness of the sample is shown schematically in Figure 8.12. To provide sufficient accuracy, the value h_f is measured using a scanning electron microscope (SEM) (see Fig. 8.13).

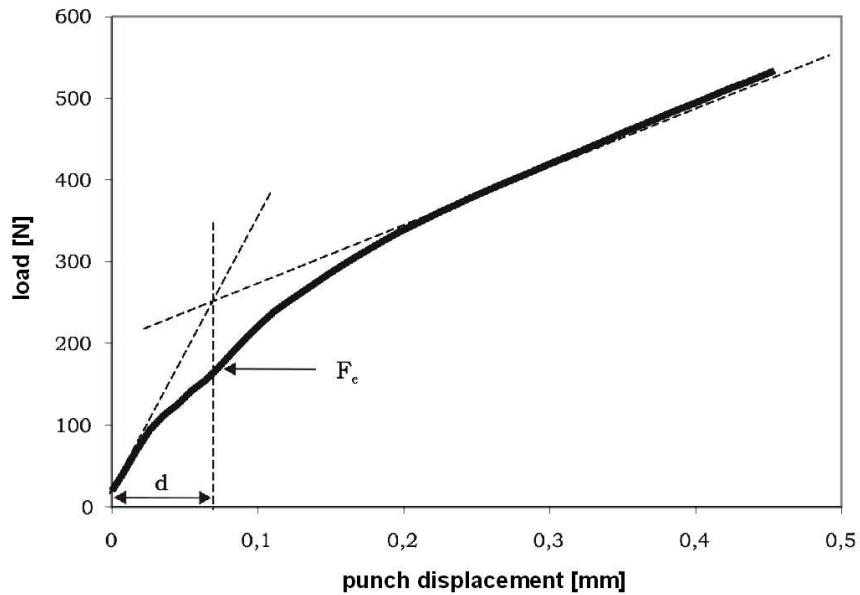


Fig. 8.11 Procedure for determining the force F_e from the force – punch displacement record

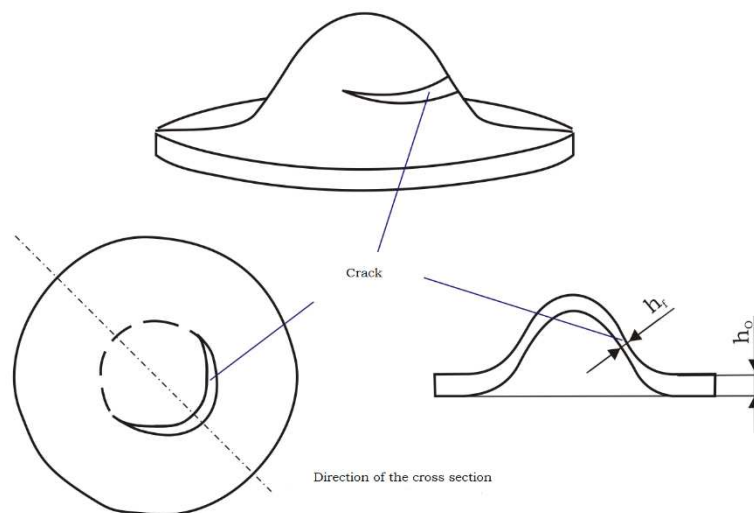


Fig. 8.12 Procedure for determining the minimum thickness of damaged sample h_f

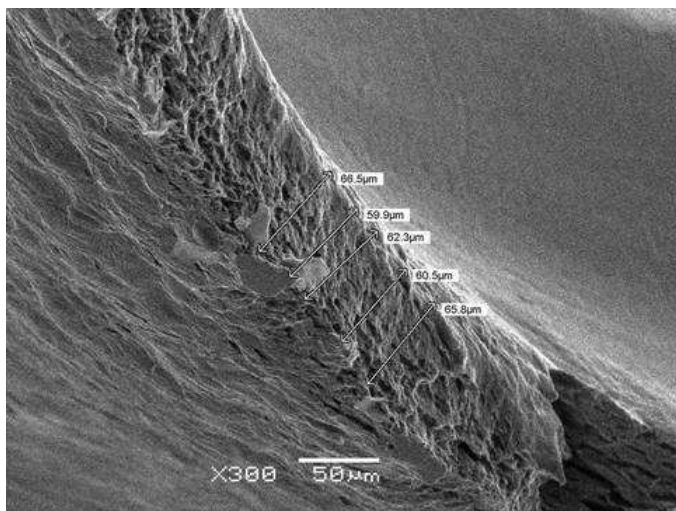


Fig. 8.13 Procedure for determining the minimum thickness of damaged penetration disc

The dependence of the force – punch displacement is significantly affected by temperature (see Fig. 8.14). For this reason, the penetration test must be performed at constant temperature. For heating or cooling the sample during penetration tests at elevated or low temperatures any method may be used that reliably ensures that the above requirement is met and allows measurement of sample temperature with a sufficient accuracy.

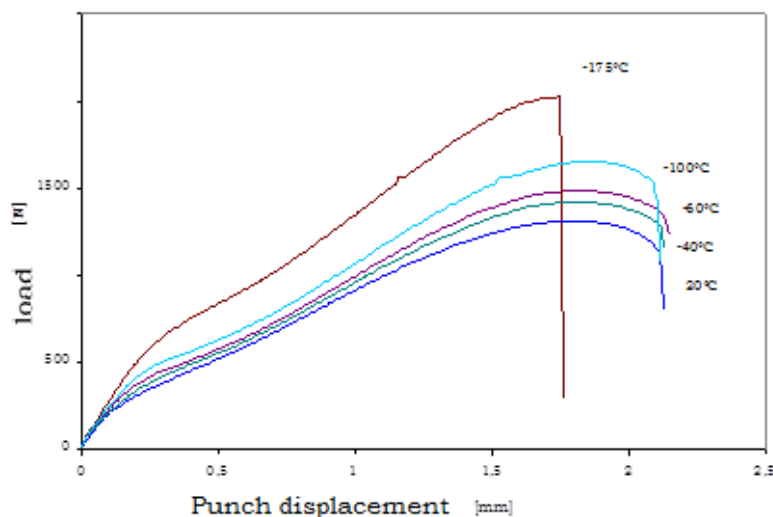


Fig. 8.14 Influence of temperature on the shape of the force – punch displacement dependence

Figure 8.15 shows the test equipment for penetration tests at elevated temperatures (400°C) and its placing within the frame of the electromechanical test equipment INOVA TSM 10.



Fig. 8.15 Test equipment for penetration tests at elevated temperatures (up to 400°C)

Diagram of equipment used for testing at negative temperatures up to about -193°C is shown in Figure 8.16. Figure 8.17 then shows its placing within the frame of the electromechanical test equipment INOVA TSM 10.

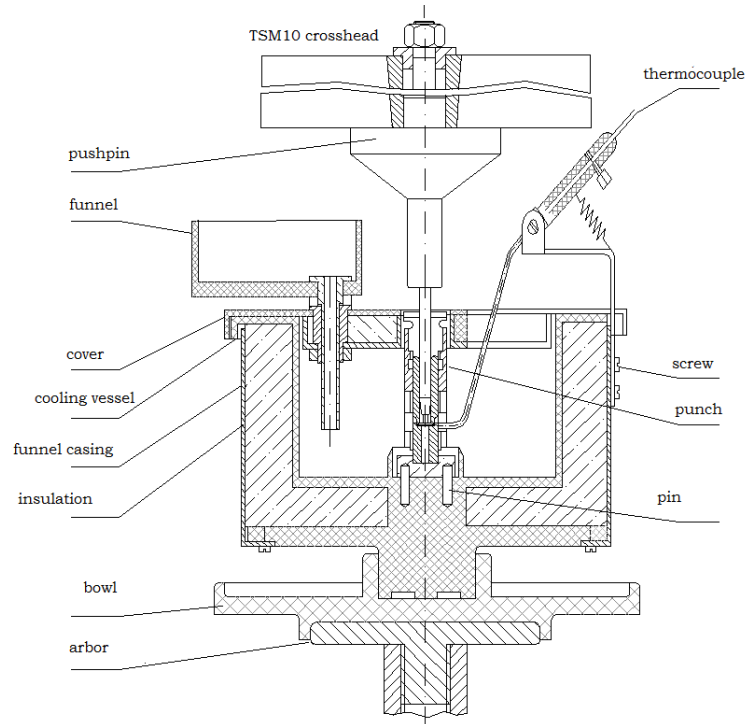


Fig. 8.16 Diagram of equipment used for penetration tests at low temperatures

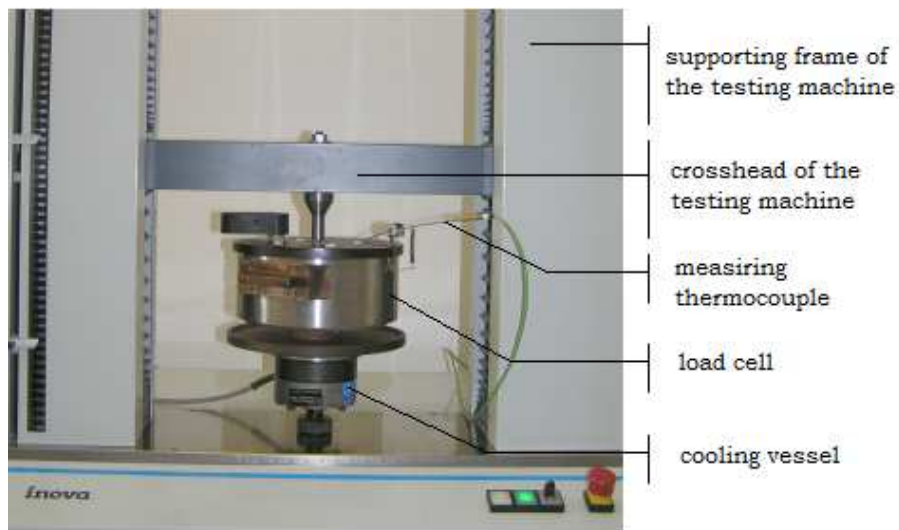


Fig. 8.17 Test equipment for penetration tests at low temperatures

8.6 Determination of mechanical characteristics from the results of penetration tests

The result of a penetration test is the dependence of the force – punch displacement. All quantities obtained from this dependence (F_e , F_m , u_m , u_f , E_{SP}) are more or less dependent on the punch radius r , the diameter of the lower supporting matrix D and the initial thickness of the test sample h_0 . The methods used to determine the strength and brittle fracture characteristics from the results of these tests must therefore respect this fact.

8.6.1 Determination of the yield strength R_e ($R_{p,0,2}$) and the ultimate strength R_m of steel from the results of penetration tests

There are two significantly different approaches to the determination of the yield strength and the ultimate strength of the material from the force – punch displacement dependence:

1. Determination of the yield strength and the ultimate strength of the material from the empirically established correlations between the results of standard tensile tests and parameters of penetration tests.
2. Methods making use of mathematical modelling using the finite element method and neural networks.

Figures 8.18 and 8.19 show correlation dependences for the yield strength and ultimate strength determined in the company MATERIÁLOVÝ A METALURGICKÝ VÝZKUM s.r.o., for 15 128 grade steel.

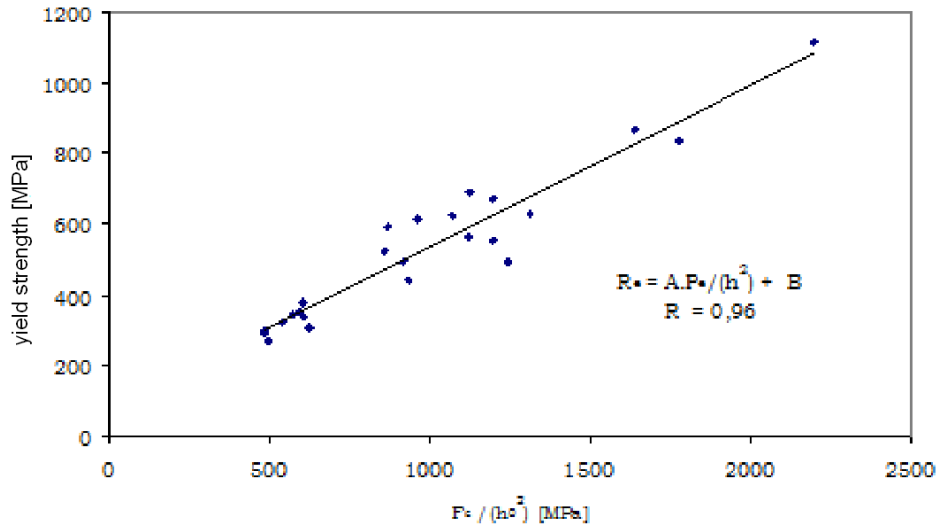


Fig. 8.18 Correlation dependence between the yield strength and size of force F_c determined for 15 128 grade steel

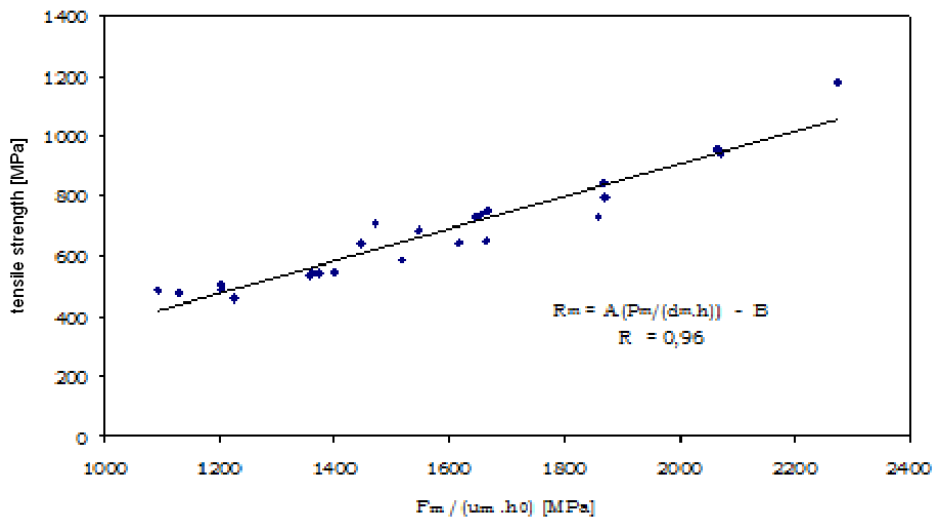


Fig. 8.19 Correlation dependence between the ultimate strength and parameters of penetration test determined for 15 128 grade steel

Given that the quantities F_c , F_m and u_m are significantly affected by both the equipment used for penetration testing and thickness of the penetration sample, the published correlation dependences are not generally applicable and must be determined for a given test equipment and used shape of the test sample.

8.6.2 Determination of the transition behaviour of steel from the results of penetration tests

Based on the results of impact bending tests and the results of penetration tests in the temperature interval from -196°C to $+60^{\circ}\text{C}$, it has been clearly demonstrated that in steels, in which the temperature dependence of notch toughness determined on Charpy V-notch specimens exhibits a transition behaviour, the transition behaviour can also be observed in the temperature dependence of the fracture energy of the penetration test (see Fig. 8.20). This fact is utilized for determining the transition temperature DBTT (Ductile Brittle Transition Temperature) of the brittle–ductile fracture transition from the results of penetration tests. Transition temperature may be determined either by temperature FATT (Fracture Appearance Transition Temperature) or T_{41J} , i.e. the temperature corresponding to impact energy 41J. Figure 8.21 shows temperature dependences of the fracture energy determined by penetration tests in the material of turbine casing (422740.6) and turbine rotor made from CrMoV steel. The fracture energy gradually increases with the decreasing temperature until it reaches a maximum value, and in further reducing the temperature it begins to decline significantly. Transition temperature T_{SP} is defined as the temperature corresponding to half the sum of the highest and lowest fracture energy in the transition area determined from experimentally measured data using the method of least squares.

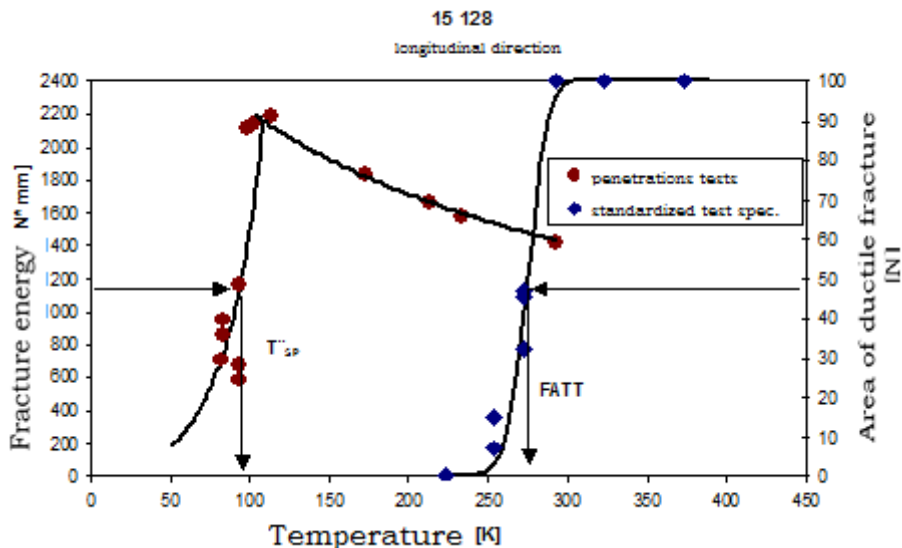


Fig. 8.20 Comparison of the temperature dependence of fracture energy during the ball “Bulge” test and the temperature dependence of the proportion of ductile fracture

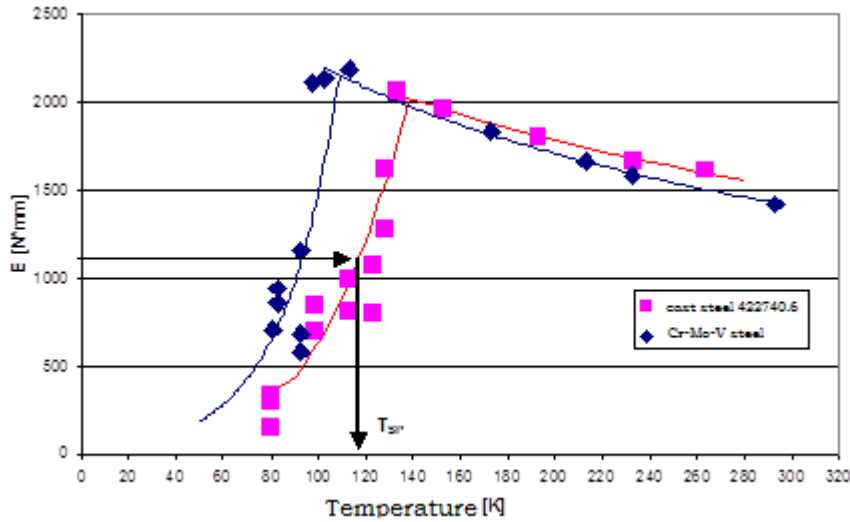


Fig. 8.21 Temperature dependence of the fracture energy of the penetration test for turbine casing and turbine rotor made of CrMoV steel

Many works prove the existence of a simple relationship between the transition temperature T_{SP} (Small Punch Ductile Brittle Transition Temperature) determined on the basis of the results of penetration tests, and FATT, determined on the basis of impact bending tests on Charpy V-notch specimens in the form:

$$FATT = \alpha \cdot T_{SP} \quad (8.1)$$

or

$$FATT = \alpha \cdot T_{SP} + \beta \quad (8.2)$$

Figure 8.22 illustrates the correlation dependence between FATT and T_{SP} determined in the company MATERIÁLOVÝ A METALURGICKÝ VÝZKUM s.r.o. for carbon and low-alloy steels.

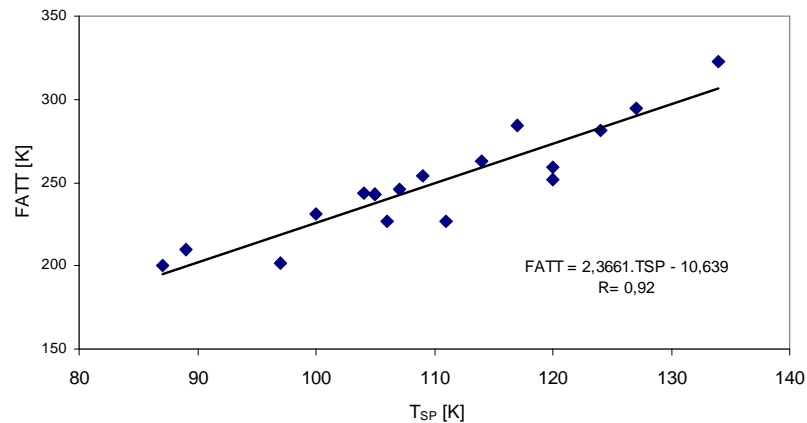


Fig.8.22 Correlation dependence between FATT and T_{SP} determined for carbon and low-alloy steels. T_{SP} was determined in the ball “Bulge” penetration test

8.6.3 Estimation of the fracture toughness from the results of penetration tests

There are three approaches to estimate the fracture toughness (K_{IC} and J_{IC}) of the material from the results of penetration tests. Two of them are based on empirical correlations, the third, designed by EPRI, is based on an analysis of the results of a penetration test and determination of the strain energy density corresponding to the crack initiation in the penetration test.

8.6.3.1 The two-stage method to determine K_{IC}

Estimate of fracture toughness in this case is made on the basis of:

1. determination of the empirical interdependence between the transit temperature T_{SP} determined from the results of the penetration tests in the temperature range $-185^{\circ}\text{C} \div +20^{\circ}\text{C}$ and FATT determined from the results of impact tests on Charpy V-notch specimens,
2. knowledge of empirical interdependence between FATT and K_{IC} .

8.6.3.2 Direct estimation of the fracture toughness from the results of penetration tests

For cases, where the fracture behaviour of structural steels is described by parameters of elastoplastic fracture mechanics, the relationship between J_{IC} and equivalent fracture strain ϵ_f

was derived. The value of J_{IC} is correlated with the fracture strain ε_f of the sample using the relation:

$$J_{IC} = K \cdot \varepsilon_f - J_0 \quad (8.3)$$

where K and J_0 are constants. Effective fracture strain ε_f is expressed by relation

$$\varepsilon_f = \ln \left(\frac{h_0}{h_f} \right) \quad (8.4)$$

Figure 8.23 shows the empiric correlation for determining the fracture toughness expressed by parameter $J_{0,2BL}$ for 15 128 grade steel.

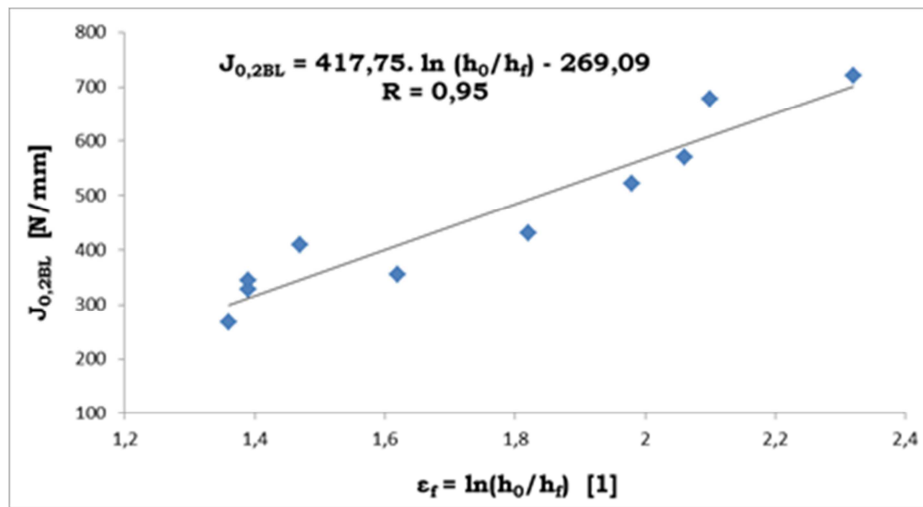


Fig. 8.23 Empiric correlation for determining the fracture toughness from the results of penetration tests for 15 128 grade steel.

8.6.3.3 EPRI-FAA innovative approach to the estimate of the fracture toughness J_{IC}

This approach, designed for EPRI by FAA (Failure Analysis Associates, Inc.), evaluates the fracture behaviour based on the density of the strain energy required to initiate cracks in the penetration test. The procedure used to determine the fracture toughness of the material from the result of a single penetration test is as follows:

- ❖ recording the dependence of load – punch displacement during the penetration test, while monitoring the surface of the specimen to identify the moment of crack initiation,
- ❖ determining the dependence $\sigma - \varepsilon$ for tensile test from the dependence of load – punch displacement obtained during the penetration test (see Sec. 4.1.2),

- ❖ determining the density of strain energy corresponding to the crack initiation during the penetration test,
- ❖ determining the fracture toughness J_{IC} from the estimate of the force, at which the critical density of the strain energy is reached at the crack face with a standard test specimen for determining the fracture toughness.



Summary of terms

After studying the chapter, following terms should be clear to you:

- Penetration test
- Punch with a hemispherical head
- Bulge test, shear test, bending test
- CEN Workshop Agreement
- Transition temperature of the penetration test
- FATT
- Stages of the ball penetration test
- Fracture energy E^{SP}
- Fracture strain ε_f .



Questions about the curriculum learnt

- 1) What are the actual mechanical properties?
- 2) What is the principle of the penetration test?
- 3) What is the difference between “Bulge” test and shear test?
- 4) What mechanical characteristics are determined by penetration tests?
- 5) What methods of determining the yield strength and the ultimate strength from the results of penetration tests do you know?
- 6) What methods to estimate the fracture toughness from the results of penetration tests do you know?
- 7) How is the fracture energy E^{SP} of the penetration test defined?
- 8) How is the fracture strain ε_f of the penetration test defined ?



References

- [1] CEN WORKSHOP AGREEMENT “Small Punch Test Method for Metallic Materials” CWA 15627:2007 D/E/F, December 2007.
- [2] MATOCHA, K.: Hodnocení mechanických vlastností konstrukčních ocelí pomocí penetračních testů. Monografie. Vydala VŠB- TU Ostrava & MATERIÁLOVÝ A METALURGICKÝ VÝZKUM s.r.o., 2010, obálka a tisk GEP ARTS s.r.o., ISBN 978-80-248-2223-5.
- [3] Conference proceedings of the 1st International Conference SSTT „Determination of Mechanical Properties of Materials by Small Punch and other Miniature Testing Techniques, August 31 to September 2, 2010, ISSN 0018-8069, ISBN 978-80-254-7994-0.
- [4] Conference proceedings of the 2nd International Conference SSTT „Determination of Mechanical properties of Materials by Small Punch and other Miniature Testing Techniques“. October 2 to 4, 2012, Ostrava, Czech Rep., ISBN 978-80-260-0079-2.